Damage Tolerance of 3D Woven Composites with Weft Binders

A thesis submitted to The University of Manchester for the degree of

Doctor in Philosophy

In the Faculty of Engineering and Physical Sciences

2014

Mubeen Arshad

School of Materials

The University of Manchester

Table of Contents

2

List of Figures

List of Tables

List of Abbreviations

UD	Uni-directional
2D	Two dimensional
3D	Three dimensional
LTL	Layer-to-layer
A.I	Angle interlock
TAI	Twill angle interlock
MAI	Modified angle interlock
UTS	Ultimate tensile strength
F.V.F/V.F	Fibre volume fraction
$\sigma_{nor(vf)}$	Normalised stress with respect to fibre volume fraction
$F.V.F_{av(LD)}$	Average fibre volume fraction of all the structures parallel to loading direction
$F.V.F_{(LD)}$	V.F of individual structure parallel to loading direction
F.V.F	Fibre volume fraction
OHT	Open hole tension
OHC	Open hole compression
σ_n	Notch stress
σ_{un}	Unnotch stress
Stuffer	Straight yarn along the length of the fabric
Filler	Straight yarn across the width of the fabric

Abstract

3D woven composites, due to the presence of through-thickness fibre bridging, have the potential to improve damage tolerance and at the same time to reduce the manufacturing costs. However, the ability to withstand damage depends on weave architecture as well as the geometry of individual tows. A substantial amount of research has been performed to understand in-plane properties as well as the performance of 3D woven composites exposed to impact loads, but there is limited research on the damage tolerance and notch sensitivity of 3D weaves and no work is reported on the damage tolerance of 3D weaves with a weft binding pattern.

In view of the recent interest in 3D woven composites, the influence of weft binder on the tensile, open hole tensile, impact resistance and subsequent residual compressive strength properties and failure mechanisms of 3D woven composites was investigated against equivalent UD cross-ply laminate. Four different 3D woven architectures; layer-to-layer, angle interlocked, twill angle interlock and modified angle interlock structures were produced under identical weaving conditions. All the above mentioned tests were performed in both the warp and weft directions on 3D woven and UD cross-ply laminates.

Stress concentration and yarn waviness due to through-thickness reinforcement led to lower mechanical properties compared with the UD cross-ply laminate. However, improved in-plane and damage tolerance properties of 3D woven composites under tensile loads were achieved by modifying the weave architecture. The influence of the weave architecture and binder yarn orientation on the notch insensitivity and damage tolerance of 3D woven composites was less significant for compressive loads. Despite the lower undamaged compression strength of 3D woven structures, their residual compressive strength was found to be superior to their equivalent UD cross-ply laminates. The lower rate of strength reduction in the 3D woven fabrics laminates was attributed to a crack bridging mechanism, effectively inhibiting delamination propagation.

Declaration

No portion of the work referred to in the thesis has been submitted in support of an application for another degree or qualification of this or any other university or other institute of learning;

Copyright Statement

and/or Reproductions described in it may take place is available in the

University IP Policy (see

http://documents.manchester.ac.uk/DocuInfo.aspx?DocID=487), in any relevant

Thesis restriction declarations deposited in the University Library, The

University Library's regulations (see

http://www.manchester.ac.uk/library/aboutus/regulations) and in The

University's policy on Presentation of Theses.

Dedicated to my husband and son

Shakeel and Afan Arshad

Acknowledgements

First of all, I am very much grateful to Almighty Lord the compassionate and the most Merciful.

I would like to pay my gratitude to my supervisors, Professor. Prasad Potluri and Professor Constantinos Soutis for their support and valuable guidance throughout my work.

I highly appreciate the help I received from all my colleagues particularly Dhaval Patel without whom I would have had a much harder time. I would like to thank the staff of North West Composite Centre and The Department of Textiles, University of Manchester; specifically Dr. Alan Nesbitt, Mr Bill Godwin, Mr Chris Cowan and Mr Thomas kerr for their assistance and advice in my experimental work.

Special thanks to QinetiQ for their financial support to carry out this research programme.

I would like to express my greatest appreciation to all my friends, my parents, my husband and my lovely son for their prayers, love and support.

1 Introduction

1.1 Background

Textile reinforced composites have been used successfully for decades in many sectors such as aeronautics, space, sporting goods, marine, automotive, ground transportation and off-shore industries. The existence of these materials in such areas is because of their high levels of stiffness and strength that can be optimized for specific loading conditions as well as their low density, high-specific energy absorption behaviour and excellent fatigue performance [1, 2].

In recent years, a rapid growth in advanced composites has been driven by civil aircraft programs such as the Boeing 787, Airbus A350XWB and the Bombardier C series. A significant volume of production is now used in wind turbine blades and the automotive industry. Traditional methods of composite manufacturing based on manual prepreg lay-up and autoclave curing are expensive and a big impediment to high volume production [3, 4]. While automated tape laying and fibre placement processes are addressing throughput issues, the composite industry is seriously looking at dry fibre preforms in conjunction with resin infusion techniques. 3D woven preforms are particularly attractive because of their reduced part count and low manufacturing cost, as well as their ability to create near-net shapes as well as the presence of through-thickness reinforcement [5, 6].

In addition to the manufacturing costs and production rates, damage tolerance has become a major issue for the composite industry. Resin toughening and through-thickness reinforcement are the general approaches used to improve damage tolerance; but the use of through-thickness reinforcement is considered to be the most effective method [7, 8]. The through-thickness fibres can be inserted using a variety of textile

processes, including 3D weaving, stitching, knitting and braiding or by the use of specialist techniques such as pinning and z-anchoring. Weaving and braiding are the most promising technologies for manufacturing 3D textile structural composites [9], while 3D weaving is the textile process that is capable of producing the highest volume production at the fastest rate. 3D woven composites have superior through-thickness properties compared to 2D laminate, for example, improved impact damage tolerance, high interlaminar fracture toughness and reduced notch sensitivity [10-14]. The development of new effective methods to produce more complex and thick woven preforms for composites has raised high expectations in the military and aerospace industries [15].

1.2 Problem definition

Damage resistance and damage tolerance are important issues in the service environment for airframes and other high performance engineering structures. In order to improve the above stated composite problems, a high level of through- thickness and interlaminar strength is required. 3D woven composites impart superior impact resistance and damage tolerance properties compared to 2D laminate.

The practical utilization of 3D woven composites to structural components requires the understanding and characterization of a number of mechanical properties. A substantial amount of experimental and theoretical work has been performed to understand the in-plane properties as well as the performance of 3D woven composites exposed to impact and ballistic loads. However, the use and influence of weft binder on the in-plane, as well as the damage tolerance properties of different 3D woven composites has not yet been explored.

1.3 Aims and objectives

The primary aim of this research is to optimize 3D weave architecture for improved damage tolerance while providing good in-plane properties. In addition to this, the effect of weave modification (modification in both binder path and binder float length) is also studied.

For this purpose the following objectives have been set:

- Design and fabrication of four different weft bound 3D woven structures, ie: layer-to-layer (LTL), angle interlock (AI), twill angle interlock (TAI), modified angle interlock (MAI)

- Determine the influence of binder architecture on strength and stiffness properties of 3D woven and UD cross-ply composites in both the warp and weft direction under tension.

- Analysis of the local strain distribution using the Digital Image Correlation (DIC) technique

- Investigation of notch sensitivity of 3D woven composites to a circular hole under uni-axial tension and compression.

- Understanding of the influence of weave architecture on impact resistance and damage tolerance of 3D woven composites impacted at different energy levels.

1.4 Research outline

After the introduction given in Chapter 1, the literature survey is presented in Chapter 2, and this is divided into four sections. The first section deals with different classes of textile preforms and their fabrication effect on mechanical properties classification. In the second section, damage tolerance as well as the impact testing of different reinforcement systems is described in detailed. This also covers damage mechanisms under drop-weight impact testing, and the effect of test parameters on the subsequent

damage mechanism. The third and fourth sections are about the effect of reinforcement architecture on impact damage and residual compressive strength properties. They describe the importance and drawbacks of uni-directional and 2D woven composites, as well as the effect of interlaminar properties of 3D woven composites on impact resistance and damage tolerance.

In Chapter 3, the design and production of 3D woven structures and unidirectional cross-ply fabric is discussed. The weave design, 3D preform manufacturing, unidirectional cross-ply fabrication, preform specifications, consolidation and volume fraction processes are described in detail.

Chapter 4 describes the behaviour of 3D woven and UD cross-ply composites under uni-axial tension. First, a brief review of previous investigations is conducted on the tensile properties of 3D woven structures. Then, the effect of the weft binder for strength and stiffness properties is measured in both the warp and weft direction. Video extensometer and digital image correlation (DIC) techniques are used to analyse and measure global and local strain distribution. Finally, data on fracture mechanisms and localized strain analysis are represented.

Chapter 5 studies the notch sensitivity of 3D woven composites in tension; outlining the experimental procedure, specimen geometry, stress distribution and fracture mechanism of 3D woven composites in comparison to UD cross-ply laminate.

Chapter 6 describes the impact and compression-after-impact properties of 3D woven composites in comparison to UD cross-ply laminate. Low velocity impact tests were

performed on the laminates at various energy levels (5J, 10J, 15J, 20J, 25J, 30J), with the energy absorption then calculated for these impact energies. Similarly, the effect of incident energy on contact force and specimen deformation is discussed. Afterwards, a CAI (compression after impact) test, ultrasonic C-scanning and electron microscopy are used to evaluate the damage resistance and tolerance of these materials. A comparison of residual compressive strength properties for open hole and low velocity impact tests is also represented in this chapter.

The conclusions of the research are summarized in Chapter 7. Recommendations for future work are also listed.

2 Literature Review

2.1 Introduction

Fibre-reinforced composite materials are used extensively in the aerospace industry because of their high specific strength and stiffness, superior corrosion resistance and improved fatigue properties. More specifically, unidirectional carbon and glass fibre reinforced plastics are attractive materials for primary aircraft structures. Performance in a structural application may be optimized by tailoring the orientation of the resin pre-impregnated fibre sheet (prepeg) prior to fabrication [16, 17]. However the use of these unidirectional prepreg sheets can be compromised different loading conditions such as impact, machining or lightning, due to low interlaminar performance. Various concepts have been proposed to improve the interlaminar strength or damage tolerance properties of structural composites. These include: Interleafing, matrix toughening, high strain fibres, yarn hybridization and the use of 3D fabrics [8].

Fabrics that are three-dimensional (3D) were introduced to produce structural composites capable of withstanding multidirectional stresses. These fabrics are produced by a variety of textile processes such as weaving, braiding, knitting or stitching. Weaving is one of the most promising technologies for manufacturing three-dimensional near net-shape preforms. With this technique, the desired mechanical properties can be achieved by arranging the fibres along the length, width and thickness of the fabric. The significant improvement in interlaminar shear strength is the greatest advantage gained by the arrangement of through-thickness yarn [11, 18, 19].

The fibre architecture of the composite and its influence on impact resistance and residual compressive strength, i.e. damage tolerance in compression, is now discussed.

2.2 Textile preforms and their properties

Textile preforms may vary on the basis of fibre orientation, entanglement and geometry. Indeed, the architecture of a textile preform can vary from a simple planar sheet to a complex 3D net-shape depending on the requirement of the end user. For the proposed study, structural preforms can be classified into three categories: unidirectional, planar (2D) and fully integrated (3D). Each preform class can be further divided on the basis of structural geometry; for example, for woven fabrics, these may include plain or satin weave etc.

2.2.1 Unidirectional system

This continuous unidirectional filament system has the highest level of fibre continuity and linearity, and consequently has the highest level of mechanical properties along the fibre/ loading direction. It is suitable for angle ply lay-ups and filament wound structures [20].

The unidirectional fibres are commercially available in the form of prepreg tape in which fibres are collimated to create a tape (Figure 2.1) and then wound onto spools. The resin is heated to reduce the viscosity and disperse over the fibres to hold them together. Unidirectional prepreg tape provides the possibility of tailoring the composite properties in the desired direction [21]. Figure 2.2 shows both uni- and multidirectional lay-ups. However these laminated structures have low interlaminar strength and poor toughness when subjected to out-of-plane loading. This low toughness can be partially improved by modifying the matrix system, although this modification limits the application of these materials in a hot/wet environment [8].

Figure 2.1 Prepreg tape [22]
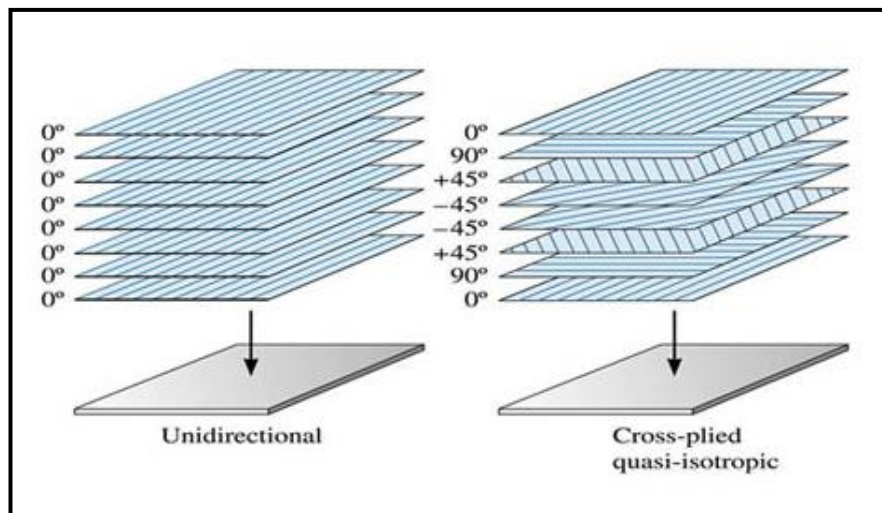
Figure 2.2 Uni- and multi-directional lay-ups [23]

2.2.2 Planar 2D fabrics

The interlaced planar and interloped system still provides continuous fibres, but with reduced mechanical properties due to fibre crimping. Two-dimensional fabric preforms are produced using textile technologies such as weaving, knitting and braiding [24]. Only woven fabrics will be discussed here.

2.2.2.1 2D woven fabrics

Woven fabrics are manufactured on a loom by interlacing two sets of yarns, warp (0 ° direction) and weft (90 ° direction) at right angles to each other [25]. They provide

superior mechanical properties in the warp and weft direction to composites when compared to knitted and braided structures due to better fibre alignment and higher fibre volume fraction [6]. Woven fabrics are used mostly in high performance applications, and may be classified by the pattern of interlacing they contain, for example, plain, satin, twill etc. The plain weave is the simplest weave pattern, and is shown in Figure 2.3a. It has the highest interlacement point as the weft yarn alternately goes over and under the successive warp yarns. Other weave patterns, such as a satin weave, may be produced by reducing the interlacement and increasing the length of straight yarn segments (known as 'floats').The selection of a weave style depends on the composite manufacturing process as well as the final mechanical properties. The weave type affects the dimensional stability and drapability of the fabric over complex shapes; for example, satin weaves exhibit good drapability [26]. Woven fabrics may also be prepregged in a similar fashion to unidirectional tapes.
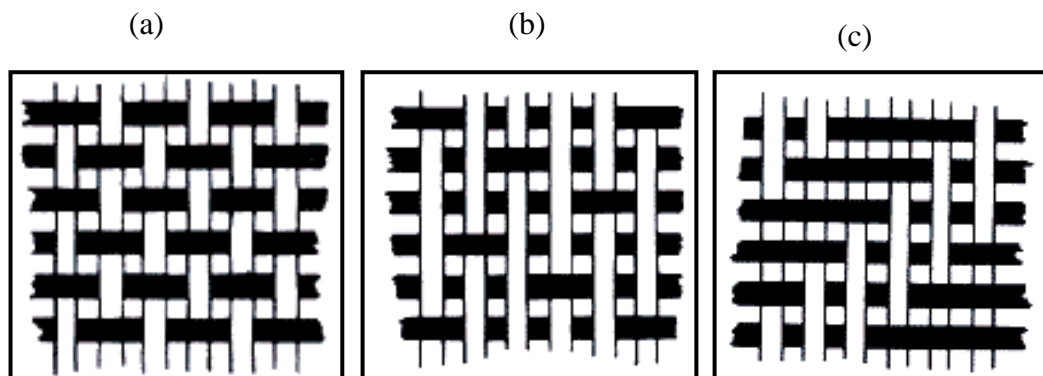
Figure 2.3 Woven fabric styles (a) schematic of plain weave (b) schematic of five-harness satin weave (c) schematic of 3/3 twill weave [27]

Two-dimensional woven fabrics improve the interlaminar failure and toughness problem associated with continuous filament systems in composites through fibre bridging. However the lack of through-thickness reinforcement leads to poor delamination resistance [1].

2.2.3 Fully integrated 3D fabrics

In 3D fabrics, the fibres are oriented in various in-plane and out-of-plane directions. The presence of in-plane multiaxial and through-thickness reinforcement provides strength and delamination resistance, as well as better resistance to crack propagation and greater notch insensitivity as compared to 2D laminates. 3D structural preforms are made using the textile processing techniques of weaving, knitting, braiding or stitching.

2.2.3.1 3D woven fabrics

It was 1972 when weaving was first used to produce 3D woven carbon-carbon composites for brake components of jet aircraft. This 3D woven composite showed some desirable properties for aircraft brakes, namely high specific strength and stiffness properties as well as excellent resistance to thermal deterioration [28]. However, research and development of 3D woven composites remained low until 1980, when interest developed in 3D woven fabric for composites, as cost effective and damage resistant components became necessary in the aerospace industry [29].

A 3D woven preform is formed of warp (0 ° direction) and weft (90 ° direction) stuffers that are bound together by a series of warp binders. By varying the binding pattern, different 3D woven structures are produced. The performance of woven preforms depends on the orientation of the binding patterns which determine the fibre architecture [30]. On the basis of the binding pattern, 3D woven structures are classified as shown in Figure 2.4.

The two major classes of 3D woven fabrics are orthogonal interlock woven fabrics and angle interlock woven fabrics. They are further divided according to the interlacing pattern of binders as shown in Figure 2.5.
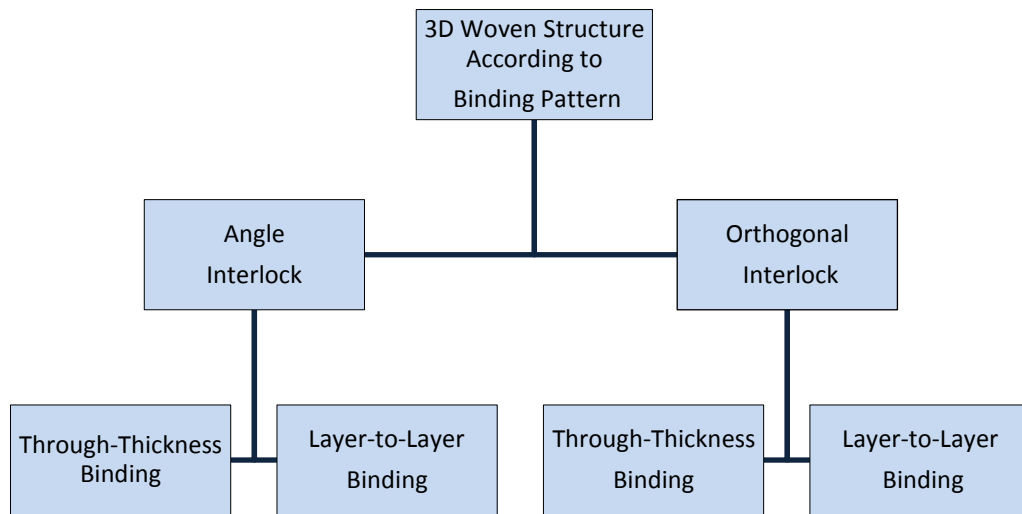
Figure 2.4 Classification of 3D woven structures according to binding pattern
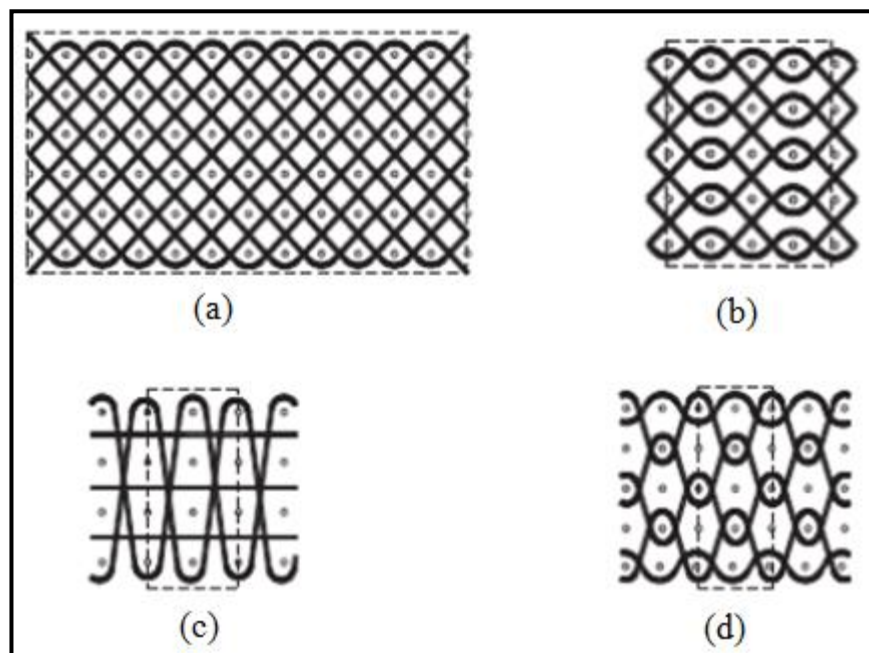
Figure 2.5 Various binding patterns (a) Angle Interlock/through-thickness binding (b) Angle Interlock/layer-to-layer binding (c) Orthogonal interlock/through-thickness binding (d) Orthogonal Interlock /layer-to-layer binding [31]

➢ **Angle interlock woven fabrics**

The z-direction (binder) fibres go through the entire thickness of the woven structure (through-the-thickness angle interlock), or weave one or more layers of weft yarns

(layer-to-layer angle interlock). The binder yarn may be of the same filament count as the warp and weft yarn or a finer yarn can be used as it allows the tight packing of warp and weft fibres. A large number of 3-D woven structures can be developed by changing the weaving pattern, the number of layers, the yarn type and count, etc.

> **Orthogonal woven fabric**

In orthogonal interlock woven fabrics, z-direction fibres are pulled through the warp and weft yarns, intersecting the layers at a 90 ° angle. The yarns are interlaced uniformly in each of the three directions to provide quasi-isotropic properties or an unbalanced amount in each direction when anisotropic properties are required. The orthogonal through-the-thickness weave forms a multi-layered preform in which the binding yarn travels from the top to the bottom of the preform, holding all the layers together; whereas in an orthogonal layer-to-layer structure the binding yarn travels from one layer to the adjacent layer, and then returns back. A set of warp weaves holds all the layers of the preform together. The orthogonally woven 3-D preforms generally have a smaller geometrical repeating unit cell than angle interlock performs [32, 33].

The performance of 3D woven structures is determined by the binding pattern. Under the same conditions, an angle interlock possess better pliability and distortion capability, whereas orthogonal interlock binding provides a greater fibre volume fraction, especially in the thickness direction[34].

With the great flexibility of weaving, 3D fabrics can be made close to near net-shape with substantial thickness and with additional yarns in the through-thickness direction, which makes them cost effective and delamination resistant when compared to traditional 2D materials. These integrally-woven 3D structures give composites that are less notch-sensitive and exhibit high strain, in both compression and tension. 3D

weaving produces fabric with reinforcement in the z-axis, which acts as a reinforcing yarn producing high composite strain in both compression and tension.

3-D woven fabrics are manufactured on a conventional 2D weaving machine with necessary modifications, and some degree of crimp or fibre damage is unavoidable during the building of a 3D fabric structure. However, a number of specialised looms have been developed to produce almost crimp free 3D woven performs [15].

A 3D woven preform can be fabricated into a composite material using different consolidation processes, such as resin transfer moulding (RTM) and resin film infusion etc. 3D woven composites are used in industrial and medical applications as well as those aimed at the aerospace industry. The stiffener in the Joint Strike Fighter is a more recent successful application of 3D woven composites in aerospace structures [33, 35].

In general, 3D woven fabrics have great potential to produce cost effective, complex and near net-shapes, as well as impact and damage resistant composites. However the influences of weaving parameters on mechanical properties are still not well understood.

2.3 Damage tolerance and impact testing

2.3.1 Damage tolerance

Damage tolerance is the ability of a structure to contain representative weakening defects under representative loading and environment without suffering excessive reduction in residual strength for some stipulated period of service.

Damage tolerance of fibre reinforced composites becomes an issue, as they may suffer damage during their manufacturing, assembly, maintenance or service life, caused by accidental blows, occasional overload and misuse. Such damage may not be detected in a routine visual inspection of the component [36].

Metals can easily cope with such damage as they have the inherent ability to yield. This is especially true of impact damage to metals, which is easily detected as the damage starts on the impacted surface. Whereas in composite laminates, low-energy impact damage is considered the most serious as it reduces the structural integrity of a structure and sometimes fractures occur [37].

The fracture process of fibrous composites depends on their damage tolerance which can be controlled by manipulating the fibre architecture. This approach does not necessarily restrict the extent of cracking, but will control the distribution of cracks and minimize their effects on the mechanical performance of the structure [38].

2.3.2   Impact testing

Although the impact phenomenon can be categorized into either low or high velocity based on the impactor velocity, a clear opinion about it does not exist. Impact at the speed range of 1-10 m/s is considered as low velocity impact while impact in the speed range > 100 m/s and >1000 m/s are termed as high and hyper-velocity testing. Cantwell and Morton [39] classify low velocity impact as < 10 m/s by considering different impact techniques, whereas Abrate [17] states that low velocity impacts occur at a speed of less than 100 m/s. Alternatively, Joshi and Sun [40] and Liu [41] characterized impact testing on the basis of the damage that occurred during impact loading. High velocity is defined as fibre breakage through penetration and low velocity by matrix cracking and delamination.

Different test methods have been developed to simulate the loading conditions to which a composite component is subject in operational service. A low velocity , high mass drop weight tester simulates the impact created by dropped tools on a structure, whereas

impact by an air gun system with a high velocity small mass projectile replicates flying debris during the take-off and landing of aeroplanes [17, 38, 39].

Low velocity impacts are expected to occur during the manufacturing process and during the life of a structure. Low velocity impact on a composite material can be replicated by using the Charpy, Izod, and drop weight impact fixtures. The Charpy and Izod are classified as destructive test methods, and provide some failure modes that were not observed on operational structures under low impact loading; whereas drop weight impact does not cause the complete destruction of the test specimen and the residual energy can be determined when required [39].

The drop weight impact test is a common method to investigate the impact resistance of composite materials – in which drops masses with different energies are dropped on the same set of specimens supported on a horizontal plane. The impact event does not cause complete destruction of the test specimen and allows one to evaluate progressive degradation and damage tolerance with increasing impact energies. Impact energy can be varied, either by changing the mass or changing the height of the drop. Different variables such as impact force, impact energy, deflection, rebound velocity and the acceleration of the projectile are recorded during the test.

In fibre reinforced composites, impact damage is a combination of four major failure modes:

1) Matrix cracking - where cracking occurs parallel to the fibres due to tension, compression and shear stress concentration.

2) Delamination - produced by stiffness mismatch at the interface.

3) Fibre breakage - in tension, fibre breakage and in compression, fibre buckling.

4) Perforation - where the impactor is perforated through the impacted plate [37]

Impact damage and the subsequent tolerance of a composite structure is influenced by test conditions (striker mass and velocity and structural support) and laminate properties (thickness, fibre/matrix interface, stiffness and the lay-up sequence). All these parameters determine the mode and geometry of the damage zone [17].

2.3.2.1 Impact damage and test conditions

The influence of indenter/projectile shape and mass has been investigated by a number of researchers [42-44], with Siow and Shim and Yang and Cantwell finding that the damage threshold varied with the projectile, with smaller diameter projectiles producing a large delamination area and fibre breakage in comparison to a large diameter projectile. Lee observed that flat and semi-spherical impactors exhibit similar failure mechanism and energy dissipation, although the internal damage caused by the flat impactor is comparatively less.

The damage response of a composite plate subjected to impact velocity has been studied by different researchers [45-47]; observing that at high impact velocity the damage zone is perforated and the damage area highly localised in the impacted zone as the available energy is dissipated over a small zone at the point of contact. Whereas at low impact velocity the damage mode is delamination where the projectile induces global damage, with the incident energy of the projectile absorbed by the whole structure as presented schematically in Figure 2.6.

 In low velocity impact, damage is more severe, in on study [48] causing compression strength loss from 58% at the barely visible threshold to 73% at the easily visible threshold of carbon/epoxy composites.
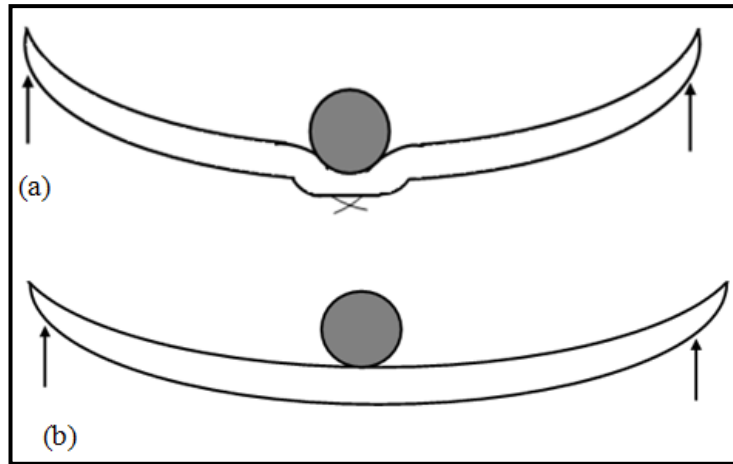
Figure 2.6 Schematic representation of the impact response under (a) high velocity impact loading (b) low velocity impact loading.[49]

2.3.2.2 Impact damage and laminate properties

The effect of target stiffness [50], geometry [49] and stacking sequence [51, 52] was studied by different researchers, who observed that the above parameters control the mode of failure in laminated composites; while Robinson and Davies [53] suggest that damage extent in composites varies according to the magnitude of the impact energy. The effect of stacking sequence or fibre architecture and thickness will be discussed in detail in the next section.

As low velocity impact damage is strongly dependent on impactor shape, mass, velocity and laminate thickness, Shim and Yang formulated a simple model to identify the effect of the above parameters on impact damage and residual strength properties. In the model they introduce a "damage severity parameter (Q)" and experimental data confirmed that residual strength properties are linearly dependent on Q, which is a function of impact energy, impactor radius and laminate thickness [54]

2.4 Effect of reinforcement architecture on impact damage

In regard to the type of the fibre and matrix, reinforcing fibre architecture is one of the main factors for determining the mechanical performance of a composite. Composite

structures with optimum properties under different loading conditions can be designed by the proper placement of fibres in the required loading direction [12].

2.4.1 Unidirectional composites

Impact damage in laminated composites is very complex and is initiated in the form of matrix cracking and delamination. The impact and damage response may be global (structural), local (contact) or both, depending on test and laminate characteristics [55]. At low impact velocity the whole structure (target) responds to the impact loading. Therefore the structural geometry of the target determines its impact response and elastic energy absorbing capability. The energy absorption of a target increases by increasing its beam size [49, 56]. Conversely, high impact loading induces more localized target responses, while geometrical parameters (length and width) have little or no influence on the high impact response of a material [57].

Cantwell and Morton investigated the influence of specimen geometry on the initiation and propagation of damage in carbon fibre composites [46, 50]. They observed that the flexural stiffness of a target changes the mode of fracture by varying specimen thickness. In long and thin targets, low impact energy damage is initiated at large distances from the impactor. The large tensile stresses generated due to the flexure of a beam initiate a failure (or crack) at the lower fibre/matrix interface. This matrix crack extends upward to form a plane of delamination at the lowest interface. The delamination planes extend through a series of cracks propagating upward and away from the plane of impact as shown in Figure 2.7b. Whereas in short and thick targets, damage occurs in the uppermost ply by the large contact stresses generated around the point of impact. These shear cracks cause delamination at the interface and diverge outward in a conical shape from the area of contact. The change of the impact area

during the penetration process changes the location of shear stresses, resulting in multiple shear cracks. Which extend parallel to each other as shown schematically in Figure 2.7a.
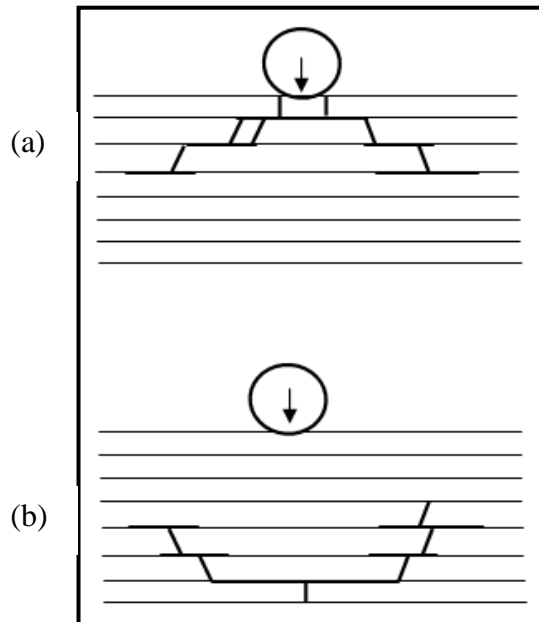
Figure 2.7 Schematic representation of damage progression due to (a) contact stresses (b) flexural stresses [50]

The subsequent damage development depends on the ability of a structure to absorb energy and the energy absorption mechanism is dependent on the ply orientation and constitutive material properties [58, 59].

Hong and Liu [45, 60] studied the effect of stacking sequence on the impact resistance of tape laminates, observing that both the initiation and extent of delamination is determined by the stacking sequence. According to bending mismatch stiffness theory, the delamination area increases as the ply orientation angle increases. Larger delamination was predicted and observed for a mismatch angle of 90 ° and no delamination was found at the ply interface of the same orientation.

In term of delamination area and residual strength, it was observed [51] that the material with 0 ° fibres in the outermost layers suffer matrix cracking and delamination which

40

effectively detach the (load bearing) outer layer. However, matrix cracking in the specimen with 45º fibres on the outside had little or no effect on the residual strength . Mili and Necib [52] analysed the stacking sequence in a cross-ply laminate in terms of the central deflection of the laminate, determining that the impact force and deflection are functions of impact velocity. Morton and Godwin [51] and Strait [61] and his colleagues suggest that the effect of the stacking sequence on energy absorption is less prominent in toughened resin systems as compared to normal matrix systems.

Typically, the first load drop on force-time or force-deflection curves is considered the damage initiation in the form of delamination [62]. However, matrix cracking cannot be detected by examining force-time curves as these occur at high frequencies and do not result in large load drops [63].

2.4.2   2D woven composites

For this composite system, quantitative comparative research has been carried out to understand some of the interlaminar failure problems that are associated with uni-directional, cross-ply or quasi-isotropic lay-ups under low velocity impact. Here, the main interest are 2D woven fabric laminates subjected to low velocity impact. Early studies [64-66] on the use of woven fabric show that woven fabric composites confine the damage area by suppressing the fibre splitting failure mode as shown in Figure 2.8. They also were able to identify that the use of $\pm$ 45º woven plies with non-woven not only reduce the extent of damage, but also improve the residual strength properties by suppressing the initiation of delamination. The nature of damage in woven composite laminates is similar to that of the UD prepreg tape composites. Under impact loading, damage initiated in the form of matrix cracks can lead to delamination when these cracks extend to the interface of the two layers [67]. Matrix cracks can be initiated as

tensile cracking on the back surface of the laminates or appear as compressive buckling close to the front surface [66]. Besides delamination, localised fibre fracture is a common mode of failure in woven fabric laminates. The fibre interlacement creates an area of stress concentration at the cross over point and fibres fail more easily at that point when compared to UD or cross-ply tape laminates [43].
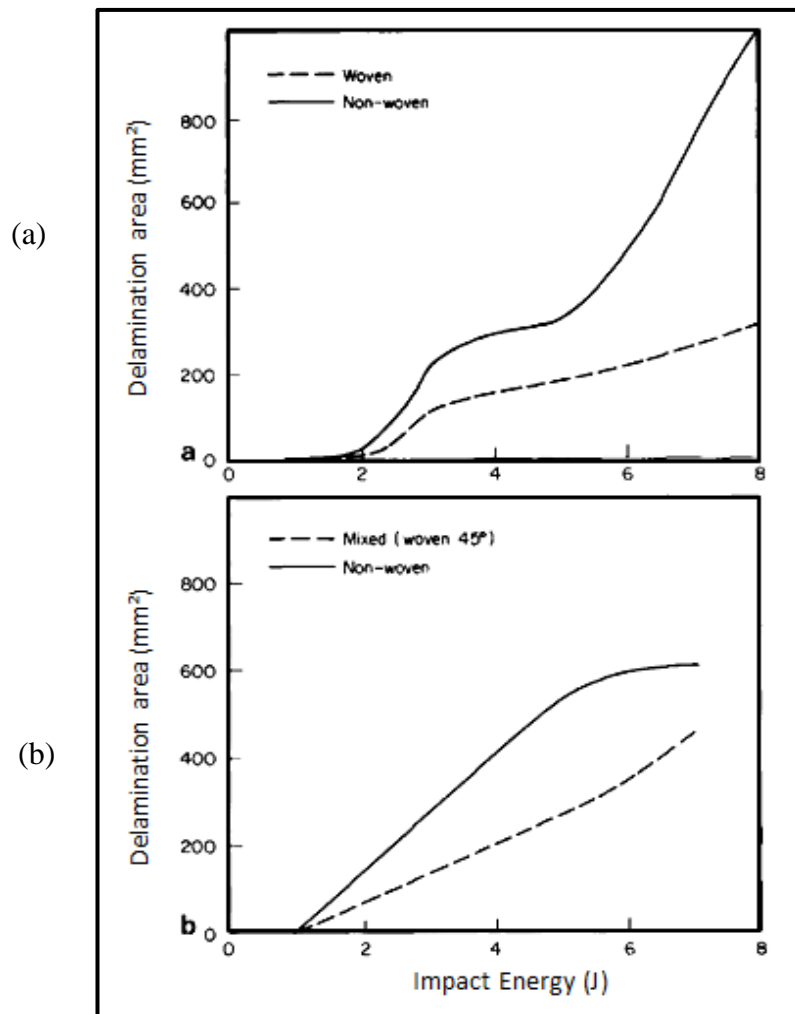
Figure 2.8 Damage area vs impact energy of woven and non-woven laminates from drop-weight impact (a) (0,90) and (±45) laminates (b) (0, ±45) laminates [66]

Failure during an impact event can be interpreted by the load-time-energy curves obtained by an instrumented impact tester. First Ko and Hatman [68] and then Chou [69] were able to relate the load-time curve response to the fracture process that occurs in a woven laminate, mentioning that this response depends on the weave architecture.

Chou identified an incipient damage point in the initial part of the curve. The incipient damage point (IDP) was considered as the first sudden load drop in the initial part of the load-time or load-deflection curves as a result of internal delamination. Afterwards, a comprehensive study was performed on woven carbon/epoxy composites to understand the effects of several impact parameters such as the incipient impact energy for damage initiation, the delamination area and the threshold energy for strength reduction and it was found that the effect of these parameters were consistent with the previous findings [70, 71].
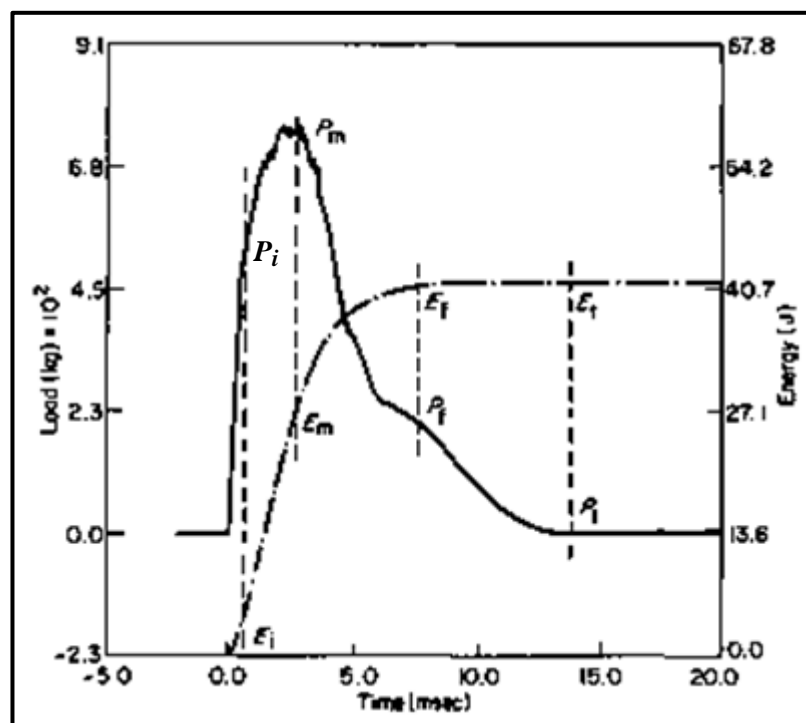
Figure 2.9 A typical load/energy vs time curve with the characteristic points of an impact event (Pi & Ei = Incipient damage load and energy , Pm & Em= Maximum damage load and energy , Pf & Ef= load and enegy at failure point Incipient energy Pt & Et= total load and energy)[70]

The load-time-energy curves in Figure 2.9 represent the different impact parameters where Pi and Pm represent the incipient damage load and maximum damage load respectively. Here Pi is the minimum load required to initiate damage in the form of delamination or fibre/matrix interface, while Pm is the peak load that a laminate can tolerate before encountering any major damage [70, 72, 73].

43

Davies and Zhou [74, 75] suggest that impact force and incident kinetic energy maps can be used to identify damage initiation without examining any impacted specimens. An energy profile method was proposed to identify the penetration and perforation threshold of woven composites, while the load–deflection curve, energy profile curves and the images of damaged specimens were used to reconstruct the damage process of the woven composites [76, 77].

Curtis and Bishop [66] and Shim [43] noted that the threshold energy for the initiation of damage is similar for both woven and prepreg tape composites but the damage appears more contained (smaller) in a woven material. This is because the interlacement of fibres prevents extensive crack propagation in woven fabric laminate. The extent of the damage and the energy absorption capability of woven laminates depend on the weaving. Atas and Liu [76] observe that woven composites with smaller weaving angles (angle between the interlacing yarn) have more energy absorption capability than those with larger weaving angles, as the low crimp and more polarized fibre orientation can be attributed to lower bending stiffness, resulting in a large deflection, fibre pull out and extended damage zone.

The effect of stacking sequence [78] and hybridization [79-81] on the energy absorption of woven composites was investigated, and it was observed that damage initiation and delamination threshold load are matrix controlled events, dependent on laminate thickness, whereas the maximum load and energy absorption capability of a laminate depends both on stacking sequence and laminate thickness. In particular the energy absorption increases with laminate thickness and is improved by the presence of 45° plies [78]. Under low velocity impact, Jang and Rohchoon [79] and Hosur and Jeelani [80] studied the effect of hybridization in Aramid/glass and carbon/S2 glass composites,

respectively. They observed that the addition of a glass fabric layer not only restricted the delamination but also delayed the damage initiation process. The absorbed energy and delamination area are dependent on the position of the glass layer in the composite. Most of the benefit could be attained by placing the S2 glass plies near the top and bottom surfaces of a laminate[81].

2.4.3   3D woven composites

Laminated composites have low interlaminar fracture toughness and are prone to delamination when subjected to a concentration of interlaminar stresses. These interlaminar stresses occur during manufacturing as well as under impact damage. The situation can be improved by introducing through-thickness reinforcement. One effective approach to enhance the delamination resistance and damage tolerance is weaving, where fibre tows are woven together in a 3D architecture to create one preform. The outstanding damage resistance of 3D woven composites is due to their high level of delamination resistance [82].

The main parameters governing impact tolerances are the amount of energy that can be absorbed in the fracture process before tensile and shear delamination, crack initiation and propagation. During the fracture process of 3D woven composites, the through-thickness reinforcement not only improves the delamination by increasing interlaminar fracture toughness, but is also responsible for crack arresting and deviating [13]. Figure 2.10 shows the energy absorption of 2D and 3D woven composites under impact. In Ko. and David's [68] study of the impact behaviour of E-glass/epoxy composites reinforced by 3D orthogonally woven and 2D biaxial woven fabric, it could be concluded that the impact resistance of composites is characterizable in terms of damage area and damage initiation as well as propagation energy. With the visual observations of specimens

these parameters can be used to assess the impact behaviour of composites. It was observed that 3D woven composites have less damage area than 2D woven composites, while the damage initiation point was also close to the composites maximum load as shown in Figure 2.11.
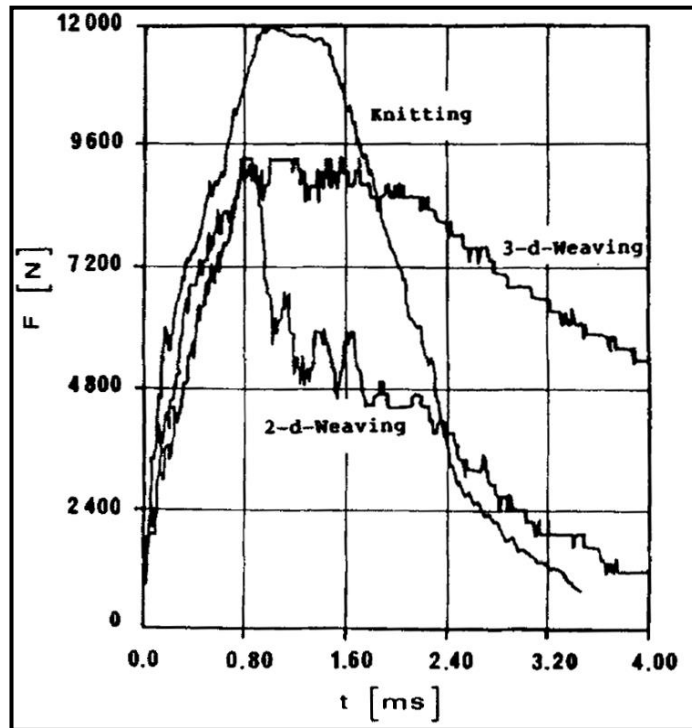
Figure 2.10 Impact energy absorption of textile composite [12]
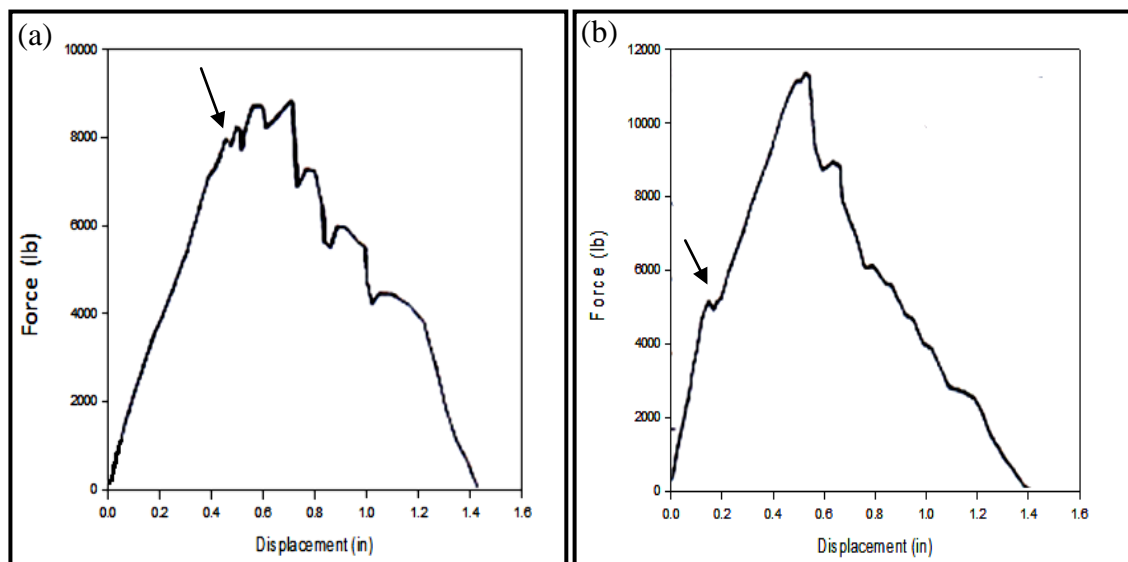
Figure 2.11 Impact response of 3D and 2D woven composites (a) 3D orthogonally woven (b) 2D Plain woven (arrows represent the incipient damage points in 3D and 2D woven composites) [68]

Barndt and Drechsler [12] and Mohamed [83] observed that under comparable test conditions, the through-thickness yarn (z fibres) in a 3D woven structure suppresses delamination and absorbs significantly more impact energy than 2D woven laminates. This reduced sensitivity to delamination also leads to an improvement in residual compression strength after impact. The fracture behaviour of 3D composites also demonstrates that through-thickness fibres hinder the propagation of delamination although the fibre damage during manufacturing process may reduce the strength and fracture resistance of a component [84].

Baucom and Zikry's [85, 86] investigation of the effect of reinforcement geometry (2D and 3D woven composites) on damage progression and perforation failure, showed that in the 2D woven laminates damage appears in the form of delamination and fibre breakage on both the rear and front surfaces of the specimens. In 3D orthogonally woven composites the spread of radial damage appeared larger on the rear surface of the specimen, with damage progressing in the form of the straining and fracture of the through-thickness z-yarns. On the front surface only, fibre debonding and matrix cracking was observed. The 3D woven composites also absorb more energy though the frictional sliding of surface weft tow through the z-yarn crimps. The impact induced deformation was also analysed through the use of Finite Element (FE) analysis. The deformation was similar to quasi-static bending and failure was predicted due to fibre damage at the backside of the target plate [87].

For 3D orthogonal hybrid woven composites, Luo [88] and Lv [89] tested composite specimens with hemispherical-ended and flat-ended steel rods. The energy absorption and damage mechanism were both dependent on the loading rate. Under low rate impact loading, composite failure occurred due to excessive tensile and compressive stresses

created by the bending moment. At higher impact loading the damage appeared in the form of matrix cracking, fibre breakage and fibre pull-out. It was observed that the through-thickness reinforcement prevented delamination. However, Walter [90] found that during high velocity ballistic loading, delamination was the dominant failure mode accompanied by fibre breakage and matrix failure. Although z-yarn assists in reducing delamination during the initial penetration, the effect of z-fibre reinforcement was negligible at much higher velocities.

The influence of binder volume fraction and the location of binder yarn were studied during impact for 3D woven carbon fibre composites [91]. Specimens with low binder volume fraction had a high damage area when compared to specimens with a high binder volume fraction Similarly, impacts to the edge of the binder were deeper than impacts to the middle of the binder. So binder location under the impactor had a direct influence on impact depth [92].

In Padak and Alagirusamy's [93] study of the effect of yarn interlacement on impact behaviour, they used the interlacement index to represent the interlacement points and observed that the impact strength of a material increases linearly with the interlacement index. The yarn interlacement produces binding points which transmit the impact load from one fibre to other. More interlacement in the preform is able to reduce fibre failure in the composite, which is due to a better distribution of the load within the multilayer structure through the interlacement points; whereas a comparison of different fibre architectures showed that impact/damage resistance (the ability of a material to absorb impact energy with minimal damage) and damage tolerance (the residual strength of the material following impact damage) properties of 3D woven composites are superior to UD laminates and 2D non-crimp fabrics [14].
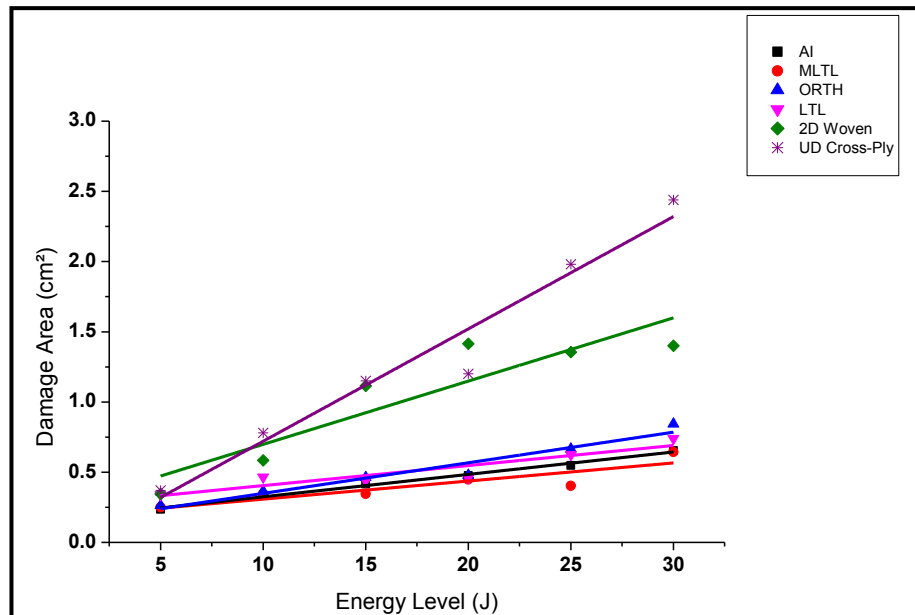
Figure 2.12 Damage area vs impact energy [94]

(Al= Angle Interlock, MLTL =Modified Layer-to-layer, ORTH= Orthogonal,
LTL= Layer-to-layer)

Potluri et al [94] compared the impact resistance of 3D woven composites at different energy levels in comparison to 2D woven and UD cross-ply laminates. 3D weaves exhibited a significantly lower damage area and higher damage resistance when compared to 2D woven and UD cross-ply laminates, as represented in Figure 2.12. It can be seen that the damage area increases linearly with the impact energy. He also found that in 3D woven composites the damage appears highly localized and spread in the thickness direction.

2.5 The effect of reinforcement architecture on post-impact compression behaviour

The term 'damage tolerance' is typically associated with the residual strength of the target material following impact. In-plane compression is believed to be the critical loading mode for impact-damaged specimens, as the strength reduction is largest under this type of loading. Therefore, a widely accepted characteristic of damage tolerance is obtained using the compression-after-impact (CAI) test. This characteristic is called

compressive-strength-after-impact (CSAI) or residual compressive strength.

The in-plane compression properties of different material systems following the impact damage states (which were discussed earlier) are discussed in the following sections.

2.5.1 Unidirectional composites

One major concern with laminated composites is their low post-impact compressive strength which is the main weakness in terms of residual properties. The reduction in compressive strength is due to delamination which leads to increased buckling instability [66, 95].

Post-impact compression failure is controlled by sub-laminate buckling, which depends on delamination area, damage location and layer sequence [96].The delamination area is influenced by both stacking sequence and damage/delamination initiation energy. The delamination initiation energy is increased by placing $\pm$ 45 surface plies and the presence of these on the surface is able to protect the load bearing 0° plies against damage induced by impact. Consequently, the composites with $\pm$ 45 surface plies show superior impact resistance and improved residual strength [51, 97]. A similar effect was observed for high strain carbon composites in comparison to standard high-strength carbon laminate. It was also shown that the compressive strength of a composite is mainly determined by a stability criterion, independent of material strengths and dependent only on the width of the delamination zone and the ply stiffness [98]. Whereas Mehmet et al [99] found that residual compressive strength (CAI strength) of laminate with (0/90) lay-up is higher than laminates with (0/90/$\pm$45) lay-up; therefore for higher CAI, top and bottom composite plies should be oriented in the loading direction.

Ghelli and Minak [100] showed that the residual compression strength and fracture behaviour of laminates is influenced by the lay-up as well as the specimen geometry. They observed that in small specimens the stacking sequence has little effect on residual compressive strength. However, in large specimens compressive strength and damage behaviour depend on the orientation of the fibres in the external layer. A gradual failure with longitudinal splitting and global buckling occurred when the fibres in the external layer are parallel to the loading direction. However, when the fibres are perpendicular to the loading direction the delamination extended in the transverse direction and a sudden catastrophic fracture occurred. Demutus and Deo [48] observed that loss/damage in compressive strength after low velocity impact is higher than the damage created by drilled holes and that a structure without the appropriate damage tolerant design may fail due to invisible internal damage occurring without any visible sign of external surface damage.

In general, residual compressive strength is plotted against impact energy to determine the influence of impact damage to the specimen under compressive loading. The residual compressive strength of non-woven laminates decreases with increased impact energy, while the drop in strength is significant even for very loe-energy impact [64, 101].

2.5.2   2D woven composites

The residual compressive strength of woven fabric laminates is equivalent or superior to uni-directional (UD) prepreg tape, in both percentage and absolute terms, when compared on the basis of incident impact energy. This is despite the fact that the undamaged compressive strength of woven fabric laminate are lower than the UD laminates. This improvement in compression after impact strength of woven fabric

laminates is due to limited shear cracking and constrained delamination, and also dependent on weave architecture and stacking sequence [38, 66, 102].

Curtis and Bishop [66] suggested that the use of woven ± 45° fabric with non-woven 0° is a serious contender for high performance applications, offering improved impact and residual strength properties (Figure 2.13). The woven fabric oriented at ±45° to the loading direction could be used as a substitute for non-woven material with an improved residual strength after impact. It was also found that residual strength properties of (0/90) laminates are more degraded than (0/90, ±45, 0/90) laminates due to a flexural stress miss-match. The retention in residual compressive strength is more than residual bending stress at the same impact energy, as energy and residual strength decreases with the increase of impact energy [54].
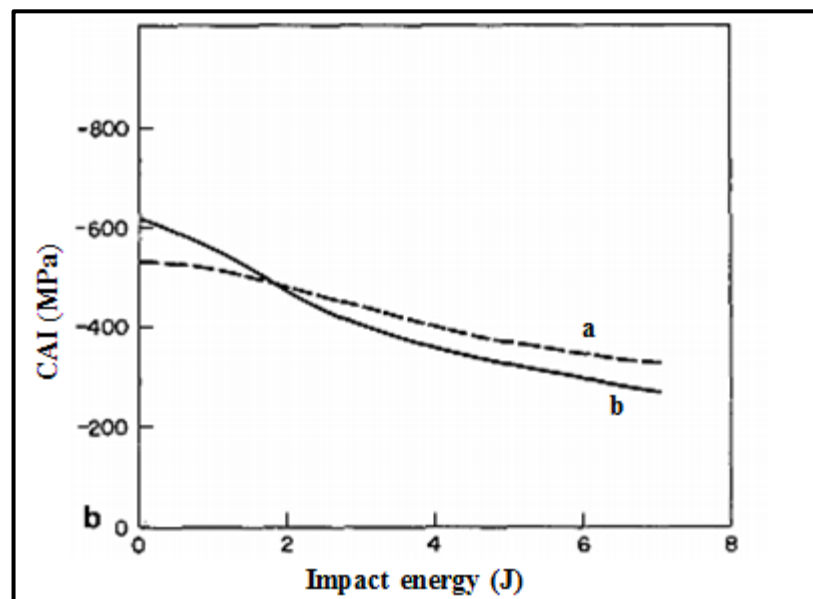
Figure 2.13 The effect of impact damage on compression after impact strength (CAI) of mixed woven and non-woven (± 45) laminates: (a) mixed woven ± 45 with non-woven 0° laminate (b) non-woven laminate [66]

Ghasemi and Parvizi [70] observed that woven fabric composites confine the damage area by suppressing the fibre splitting failure mode (which usually occurs on the back of unidirectional composites) during impact, which in turn improves the residual

compression strength of woven composites. The failure mechanism of the post-impact compressed specimen was a shear mode accompanied by the kinking of fibres. The specimen sheared at an angle of 45º-60º with respect to the direction of the applied load. The authors also observed a tough resin system further improved the residual compression strength by limiting delamination during impact.

Zou and Davies' [74, 75] investigation of the residual compressive strength of thick woven fabric laminates observed that residual compressive strength reduces rapidly with the increase of impact damage; this is due to extensive delamination, as delamination divides the laminate into two or more sub-laminates. This multiple delamination degrades the local flexural stiffness of an impacted panel which consequently fails in compression with kink band formation at a significantly lower load compared to an un-impacted panel. It was suggested that damage force and incident kinetic energy maps may be used to identify the damage initiation, although care should be taken in using these maps for damage tolerance assessment.

The experimental and theoretical results of Shim et al [54] verified that the residual mechanical properties of laminates are linearly dependent on damage severity parameter Q, where Q is a function of impact energy, impactor tip radius and laminate thickness.

2.5.3   3D Woven composites

The compression after impact strength of a composite laminate is a primary function of undamaged compression strength. The undamaged compression strength is controlled by fibre architecture, fibre volume fraction and geometrical defects such as crimp, damage to the fibres, and manufacturing defects etc. Under a uniaxial compressive load, 3D woven composites fail by kink band formation in the primary load bearing yarns. Each kink band is confined to a single aligned tow and does not spread catastrophically

into neighbouring tows. Kink band formation is influenced by initial stuffer misalignment, stuffer buckling, lateral loads imposed by binder yarn, delamination and the buckling of layers of stuffers (straight yarns along the length of the fabric) and fillers (straight yarns across the width of the fabric), plus the debonding of individual stuffers. The initial misalignment and geometrical flaws tend to lower the compressive strength but cause the damage to be spatially distributed, resulting in a high strain to failure [10, 103]. It was observed that kinking reduced the load carrying capability in the outer layer yarns, resulting in a 20-35% decrease in compressive strength and stiffness of 3D orthogonally woven composites. The critical load required for kinking decreased with an increase of the misalignment angle [104].

The effect of fabric structure [14, 105], fabric compaction [106] and yarn crimp [107] in compression has been studied by different researchers. All of them observe that composites fail in shear, with local yarn buckling and the formation of kink bands. However, the damage zone depends on the amount of yarn distortion and varies from structure to structure.

The compressive strength of 3D woven structures can be improved upon, degraded or remain unchanged by through-thickness (z-binder) reinforcement [12, 104]. Through-thickness yarn does not entirely eliminate delamination during an impact event but it does suppress both delamination growth (by bridging the delamination crack) and buckling under subsequent compressive loads, as well as increase interlaminar fracture toughness. With delamination suppressed, kink band formation (kinking) is the ultimate failure mechanism [13, 19].

3D woven composites limit delamination significantly by absorbing more energy and thus possess higher residual compression strength than their respective 2D laminates at

the same impact energy, despite having undamaged strength less than that of the 2D materials. The high damage tolerance and energy absorption capability of 3D woven structures is strongly influenced by the architecture and amount of the through-thickness reinforcement as shown in Figure 2.14. Improved residual strength properties can be achieved by using hybrid yarn techniques [12, 83].

Potluri et al [94] showed the residual compressive strength properties of 3D woven structures in comparison to 2D woven and UD cross-ply laminates. The rate of change for residual compressive strength with respect to impact energy for the 3D woven composites, is similar to the UD cross-ply laminate. Also, the 3D woven composites have a critical damage width below which there appears no apparent degradation to the compression strength. It can also be seen that a finer through-thickness reinforcement improves residual compressive strength by minimising in-plane yarn distortion [92].
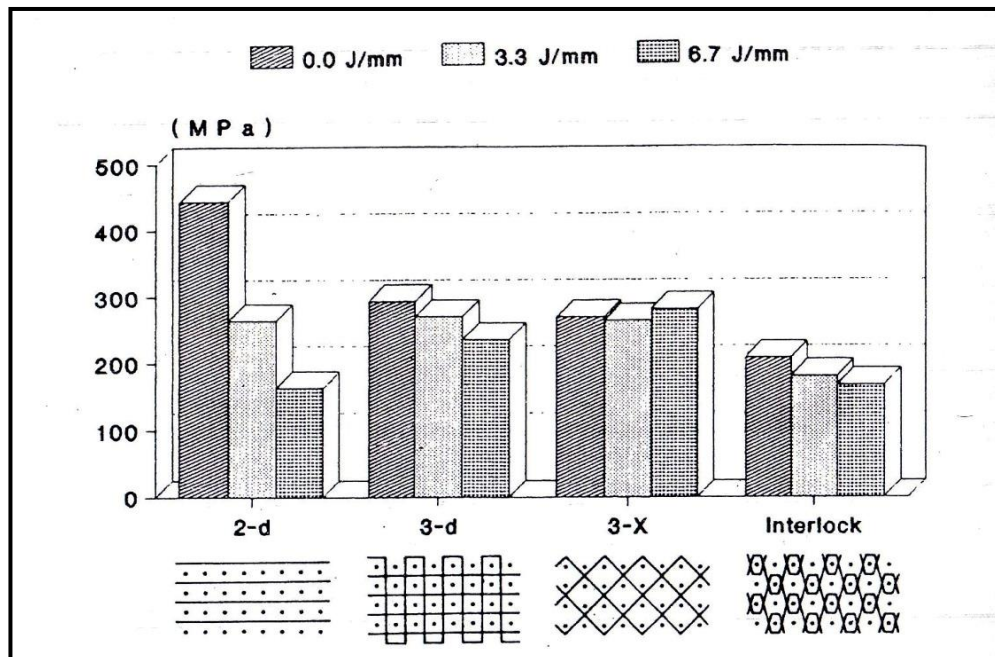
Figure 2.14 Compression after impact strength of 3D woven composites at different energy levels [8]

The compressive failure of 3D woven composites is caused by the same kinking phenomenon as the 2D laminates, but the failure mechanism is more complex [103].

The variation in the weave architecture could change the dispersion and orientation of kink band failure. There is limited data on the residual compressive properties of different 3D woven structures, and therefore, further studies are required to understand the effect of different 3D woven architecture on impact resistance and damage tolerance in comparison to UD laminates.

2.6 Summary

Damage resistance and damage tolerance are important issues in high performance engineering structures. The damage sustained by a composite during impact and other forms of loading is a function of its fibre architecture. This literature survey highlights the effect of fibre architecture on the impact resistance and residual compressive properties of different preform systems. It also highlights the delamination problem associated with unidirectional and 2D woven laminates as well as the potential of 3D woven composites at improving delamination resistance and interlaminar properties. Compared with unidirectional and 2D woven composites, limited research has been conducted to study the impact and post-impact compression behaviour of 3D woven composites, especially under different energy levels when compared to UD laminates. It also needs to be highlighted that in previous studies the binder yarn is always in the warp direction and the effect of weft bound 3D woven structures on in-plane as well as out-of-plane properties has not yet been explored.

3 Manufacturing of preforms and composites

3.1 Introduction

Textile structural composites are a class of advanced composites that utilize fibre preforms for primary and secondary load-bearing applications. Textile structures are used in composites because they are light weight, strong, have manufacturing flexibility, integrity and toughness. Textile structures manufactured to acquire desired shapes are called preforms. On the basis of degree of reinforcement in the thickness direction, textile preforms are categorized as two-dimensional (2D) and three-dimensional (3D). In 2D preforms, fibres are aligned along the x-direction or the horizontal axis, and across the y-direction or vertical axis, of the material; while in the 3D preforms, fibres are aligned with the through-thickness as well, i.e. in all directions (X, Y and Z) [1, 29].

The use of textiles in composite components has progressed from a simple 2D fabric lay-up to very complicated near net-shape 3D preforms. These 3D preforms can be manufactured by weaving, braiding, knitting, stitching etc. The preform manufacturing technique is dictated by the design of the composite structural component [6, 9]. Weaving is the most widely used textile manufacturing techniques in the composite industry for the production of 2D fabric. It is a low cost fabrication method, although all of the desired properties are difficult to impart in the fabric. In the 2D weaving process, two sets of yarns are used - one set (warp yarns) is separated into layers to form an opening called a shed. Then the second set (weft yarns) is inserted one at a time through the shed (or the warp yarn layers), whereas, in the 3D weaving process, the straight weft yarns are inserted between the layers of warp yarn. The yarns parallel to the x-axis are

referred as warp yarns and they run along the fabric length, whereas weft yarns run across the width of the fabric and lie parallel to the y-axis. The warp and weft yarns lie in the x-y plane without interlacing with each other, similar to in a 0/90 laminate. These multiple layers of warp and weft yarns are bound together by a small portion of in-plane yarns which are termed 'z-binders' because they are woven through the thickness of the preform, which is designated the z-axis [108, 109]. A number of specialised looms have been developed to produce 3D woven preforms. However, 3D woven fabric can also be produced on a multi warp loom and a conventional 2D weaving machine with necessary modification [26, 110].

This chapter describes the preform and composite manufacturing process of 3D woven and UD cross-ply S2 glass fibre-reinforced composites. The conventional weaving process is used to manufacture four different types of 3D woven structures: layer-to-layer, angle interlock, twill angle interlock and modified angle interlock, whereas for UD cross-ply, a pin board is employed to place the yarns around the pins. Later in this chapter the composite manufacturing through resin infusion and fibre volume fraction of 3D woven and UD cross-ply structures is described in detail.

3.2 Manufacturing of S2 glass preforms

3.2.1 3D woven preforms

3D woven preforms can be produced on a variety of commercial weaving looms but looms equipped with Jacquard are the mostly employed because of the high degree of automation and good control. The machine shown in Figure 3.1 was employed to manufacture the S2 glass 3D woven fabrics in this research.

Figure 3.1 Rapier weaving machine equipped with Jacquard

The following 3D weaving process was used to produce the preforms:

- warp creel set-up

- warp let-off

- shedding

- weft insertion

- beating and

- take-up

Figures for the warp creel set-up and beat-up mechanism are shown in Figure 3.2 and Figure 3.3, respectively. The processes performed on loom equipped with Jacquard to manufacture woven preforms are outlined below:

Creeling The warp yarns for the production of 3D woven preform come from an individual spool that is mounted on the creel. A two-folded yarn is used in the warp direction to achieve the required thickness of the woven preform. This two-folded yarn is acquired by twisting the two warp yarns from two different packages and then

winding them onto the small spool. The amount of the twist appears to be 20 turns per metre. The warp spools hold a sufficient amount of warp yarn for weaving

Let-off At the start of the weaving process the warp yarns are drawn off the spools towards the shedding mechanism.
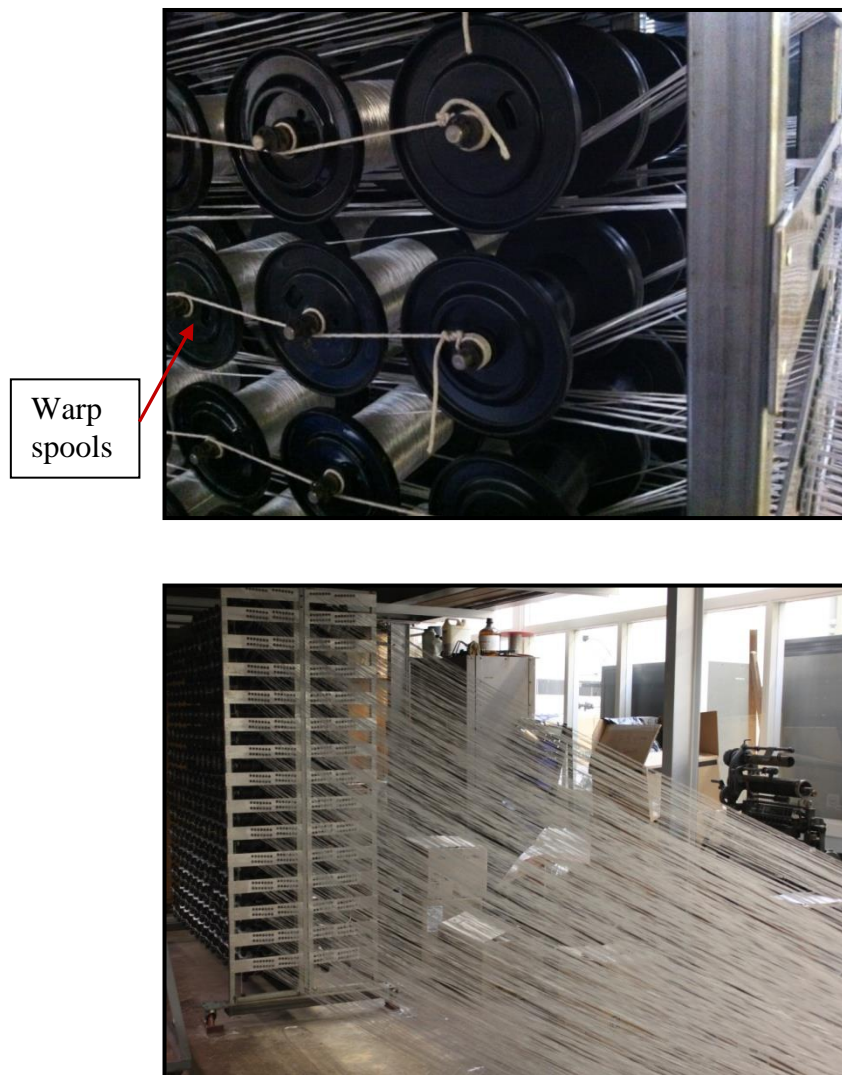
Warp
spools

Figure 3.2 Warp yarn spools and let-off stage

Shedding During this stage the warp yarns are drawn through the eyes of the heald wires that control the vertical displacement of the yarns during weaving. Each layer of the warp yarn is raised or lowered according to the weave pattern to form a gap, known as a shed, for the weft insertion.

Weft insertion A rapier is used to insert the weft stuffer between the warp layers. Weft yarns are then inserted at an angle of 90 degree to the warp yarns. Binder yarns are also inserted in the weft direction to hold the multiple layers of warp and weft stuffer.

Beating A comb like device called a reed is used to push the newly inserted weft stuffer and binder into the fabric. Beating is done after each weft insertion.

Fabric take-up The 3D woven fabric is wound onto a roller so that the weaving process can be repeated. Now the fabric is ready to be processed into a composite form.
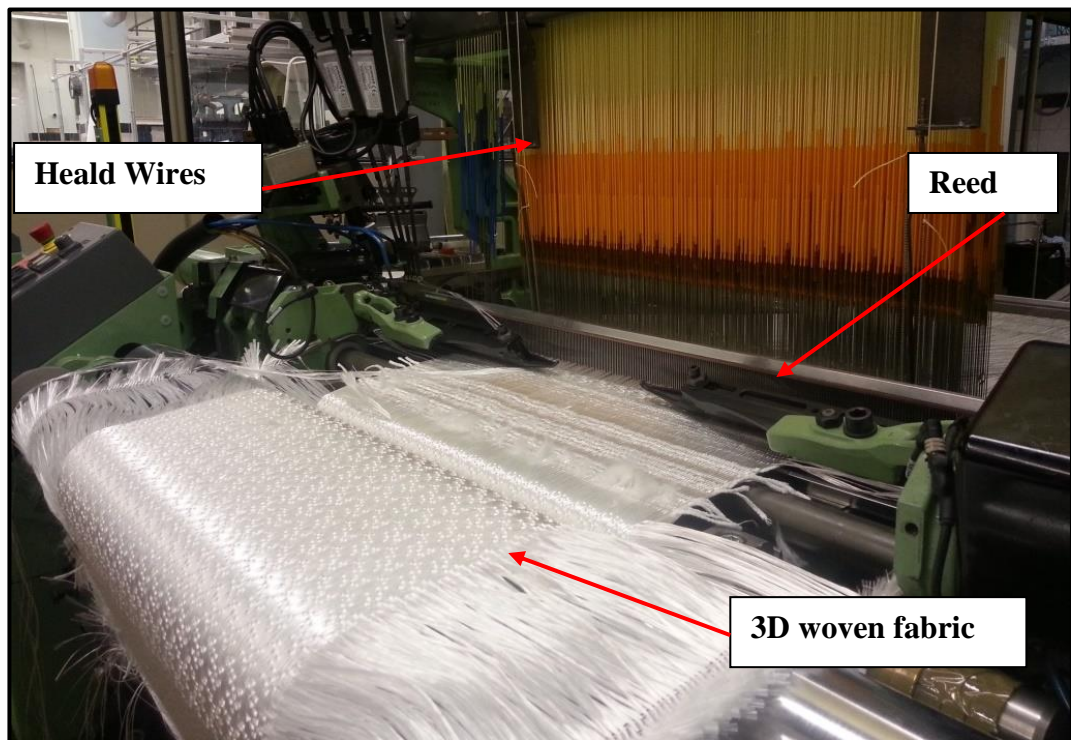
Figure 3.3 Beat-up mechanism and weft guides

3.2.1.1 Structural selection of 3D woven composites

The performance of 3D woven preforms is dependent on the fabric architecture which is determined by the binding pattern. Different combinations of 3D woven preforms can be produced given the variation of the binding pattern. They can be classified into angle interlock and orthogonal interlock according to the binder orientation, or through-the-thickness and layer-to-layer if the penetration depth of binders is involved (Figure 2.5).

For the proposed study, angle interlock structures with through-thickness and layer-to-layer binding were manufactured and named as:

- Layer-to-layer (LTL): In the LTL structure, the binder goes through half of the thickness of the preform and then returns back. After every two binders in this structure, three layers of weft stuffers (straight yarns at 90°) are inserted sequentially between the four layers of warp yarn as depicted in Figure 3.4. All the 3D weave modals were produced by the Autodesk inventor software.

- Angle Interlock (AI): In AI structures, the binder goes all the way through-the-thickness and then returns back. According to the binding pattern, shown in Figure 3.5, one binder yarn is inserted after every three layers of weft stuffer.

- Twill Angle Interlock (TAI): TAI is the replicate of the angle interlock; the only difference is the binder yarn that passes over two warp yarns before passing through the thickness of the fabric and repeating the pattern. The front and perspective view of the binder path is shown in Figure 3.6.

- Modified Angle Interlock (MAI): MAI consist of two layers of weft stuffers in between the top and bottom layers of the warp yarns; instead of using the third stuffer in the middle layer, the binder path is modified in such a way that it passes over two warp yarns at the top and bottom to give a straight portion in the middle of the structure (Figure 3.7). The purpose of this modification is to improve the damage resistance properties by providing an extra interlacement point in the middle of structure as well as by placing the binders next to each other. Another objective is to reduce the steepness of its through-thickness angle. In this structure, after every fourth binder two layers of weft stuffers (as mentioned above) are inserted between the top and bottom layers of the warp yarns.
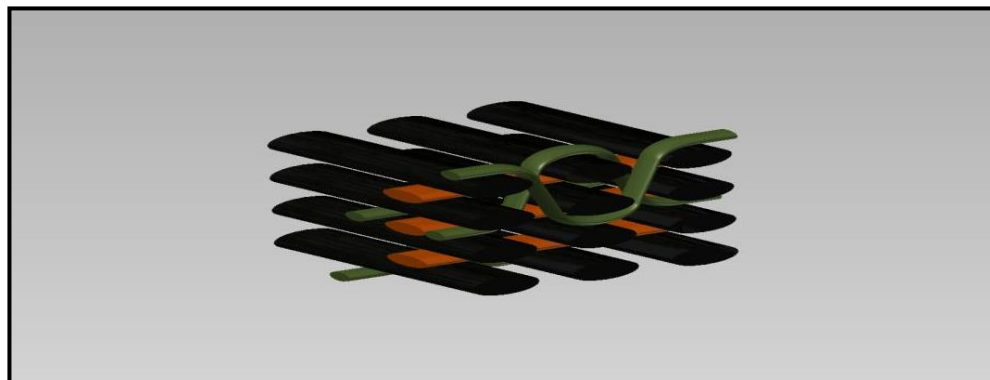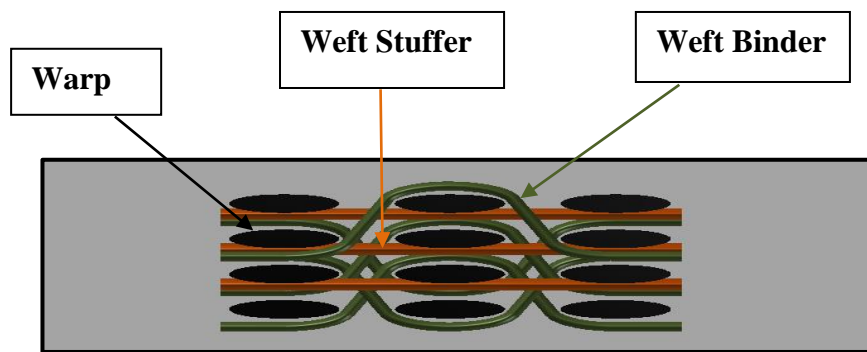
Figure 3.4 Layer-to-layer (front and perspective view)
(Binder yarn goes through half of the thickness of the preform and the returns back)
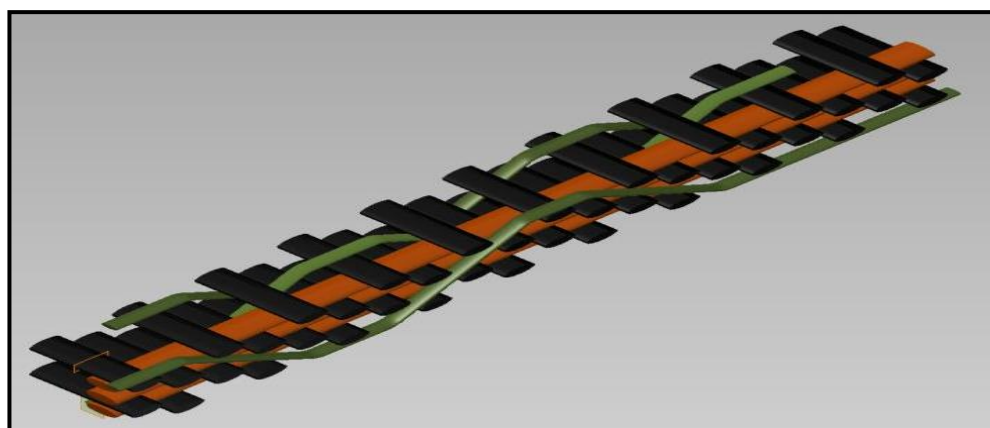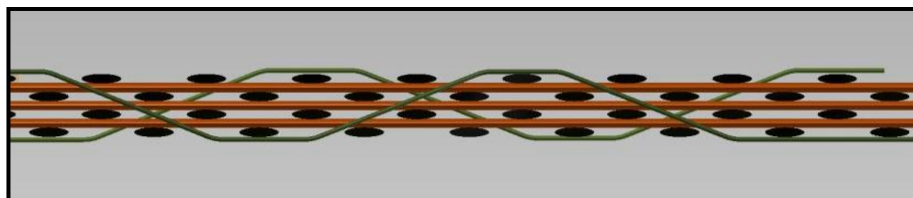
Figure 3.5 Angle Interlock (front and perspective view)
(Binder yarn goes all the way through-the-thickness and then returns back)
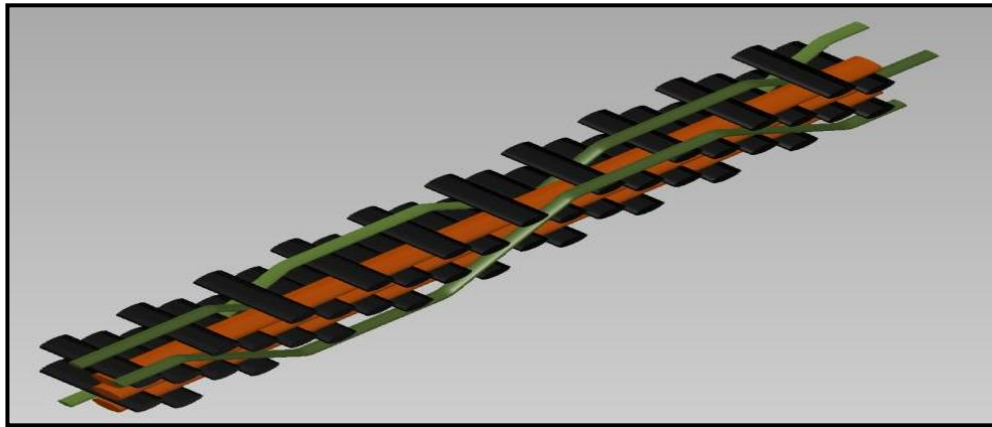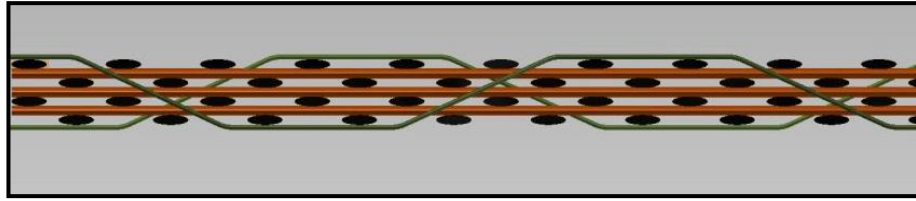
Figure 3.6 Twill Angle Interlock (front and perspective view)
(Passage of the binder is the replicate of AI structure but the binder yarn passes over two warp yarn before passing through the thickness of the fabric and then returns back)
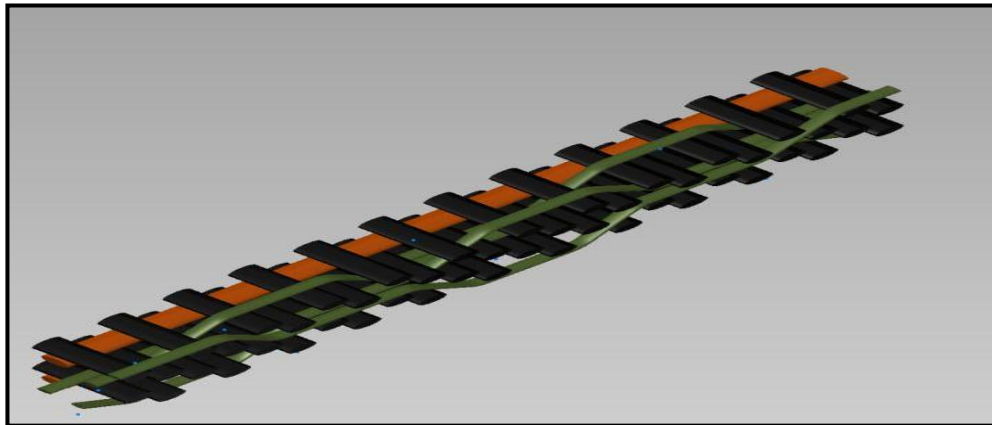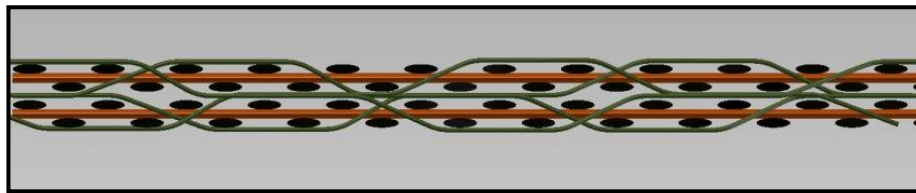
Figure 3.7 Modified Angle Interlock (front and perspective view)
(Binder path is modified in such a way that it passes over two warp yarns at the top and bottom as well as gives a straight portion in the middle of the structure)

(Warp yarns (black) =Straight yarns along the length of the fabric , Weft stuffer (Orange)= Straight yarns across the width of the fabric, Weft Binder = Yarns which are binding straight warp and weft yarns together) (Autodesk Inventor software was used to produce all the 3D weave modals)

All structures consist of 4 layers of warp (fibres parallel to weaving direction or at 0º) and 3 layers of weft stuffer (fibres transverse to weaving direction or at 90º), which are held together by the binders (through-thickness fibres) inserted in the weft direction at regular intervals. The binder path is shown in Figure 3.4 to Figure 3.7. For the warp and weft stuffer, a two-folded yarn with a 1360 Tex was used, whereas for the binder a single yarn with a 680 Tex was used. A twist of 20 turns/metre was introduced to the two-folded yarn for better cohesion and handling in the fabric formation process. The preform specifications for all the structures are presented in Table 3.1.

3.2.2 UD cross-ply preform manufacturing

In addition to comparing the properties of 3D woven structures with some benchmarking material, a UD cross-ply (0º/90º) preform with 4 layers of 0º and 3 layers of 90º yarns was also produced with a similar density. A pin board shown in Figure 3.8 was employed to place the yarns around the pins, with a two-folded yarn with 1360 Tex being inserted in both directions. The specifications of this are also presented in Table 3.1.
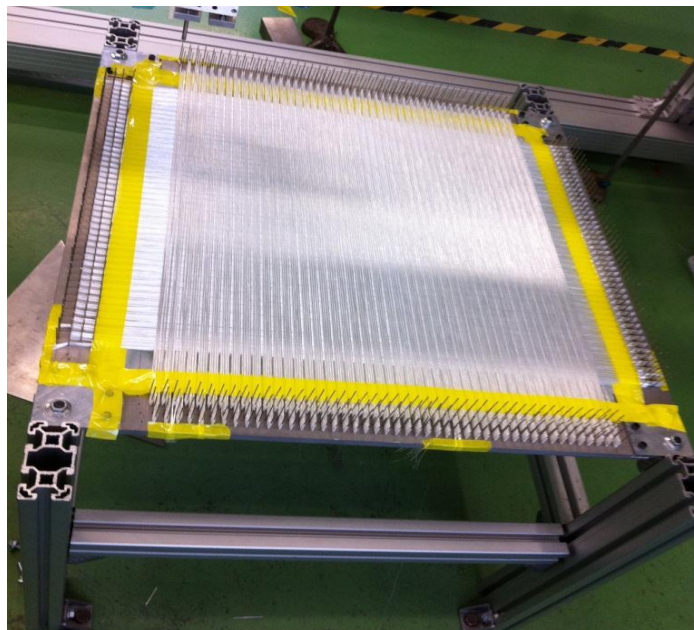
Figure 3.8 Tool for UD tow placement

Table 3.1: Preform specifications

Preform Structure	Layer-to-Layer	Angle Interlock	Twill Angle Interlock	Modified Angle Interlock	UD Cross-Ply
Ends/cm	4.05	3.95	4.225	4	4
Picks/cm	2.2	2.8	3.06	1.75	4
Binders/cm	4.5	3	3.7	7.6	
Total Ends/ Layers/cm	16.2	15.8	16.9	16	16
Total Picks/ Layers/cm	6.6	8.4	9.2	3.5	12
Warp & Weft Stuffer Count	1360	1360	1360	1360	1360
Warp Layers	4	4	4	4	4
Weft Layers	3	3	3	2	3
Binder Count	680	680	680	680	
Fabric Area Density (g/m²)	3414	3572	3559	3339	3808
Warp Crimp (%)	1.108	1.231	0.612	0.55	-
Weft Crimp %	0.59	0.66	0.56	0.55	-
Binder Crimp (%)	1.313	1.58	1.267	1.619	-

3.3   Composite manufacturing

The vacuum bag infusion process was used to make the composite using the 3D woven structures. The schematic diagram and finished product of the bagging process is depicted in Figure 3.9 and Figure 3.10. The main reason for the selection of the vacuum bag infusion process was the ease of the setting up time and the low cost of the process.

Vacuum Bagging

Vacuum bagging was performed over a polished aluminium mould, sized at 50x50 cm. The mould was cleaned and coated with 3 layers of Frekote release agent, with an interval of five minutes, then left to dry at room temperature.

The required amount of pre-cut fabric measuring 40x40 cm was placed onto the mould. A sheet of peel ply measuring 50x41cm was draped over the top. To help with uniform resin flow, a spiral tube was fixed onto the peel ply on each side of the mould. One side of the spiral tube was sealed with the tacky tape while the other side was connected to a plastic tube to act as resin inlet on one side and as an outlet on the other side. These spiral tubes were then covered with the peel ply to facilitate their removal once the laminate had cured. For better resin distribution across the preform, a sheet of infusion mesh was placed under the spiral tube and over the peel ply. The length of the mesh was 2 cm shorter than the end of the fabric. Tacky tape was stuck on all four sides of the mould, while a sheet of bagging material was placed over the tacky tape to seal the mould. At the exit tube, a small vacuum bag filled with breather fabric was connected as a resin trap to absorb the excess resin and prevent it from flowing into the vacuum pump (Figure 3.10). The inlet tube was sealed and a vacuum of -30 in.Hg was pulled out and left overnight to check for any leakage. A bi-functional epoxy resin (LY564) and the hardener (XB3486) supplied by Huntsman were used to manufacture the

laminates. A weight proportion of 100:34 was used for mixing the epoxy resin and the hardener according to their datasheet. At the same time it was degassed to remove any excess air trapped in the resin during mixing. Degassing was performed in a vacuum oven for at least 75minutes at 25^0C. The resin was infused at room temperature until it flowed through the medium and began to saturate the preform. The infusion process was stopped when the fabric was fully wetted, and the resin flowed up the exit pipe. Finally, the whole assembly was moved into an oven for curing at 80^0C for eight hours. After curing, the laminate composite was demoulded and cut into test pieces accordingly.
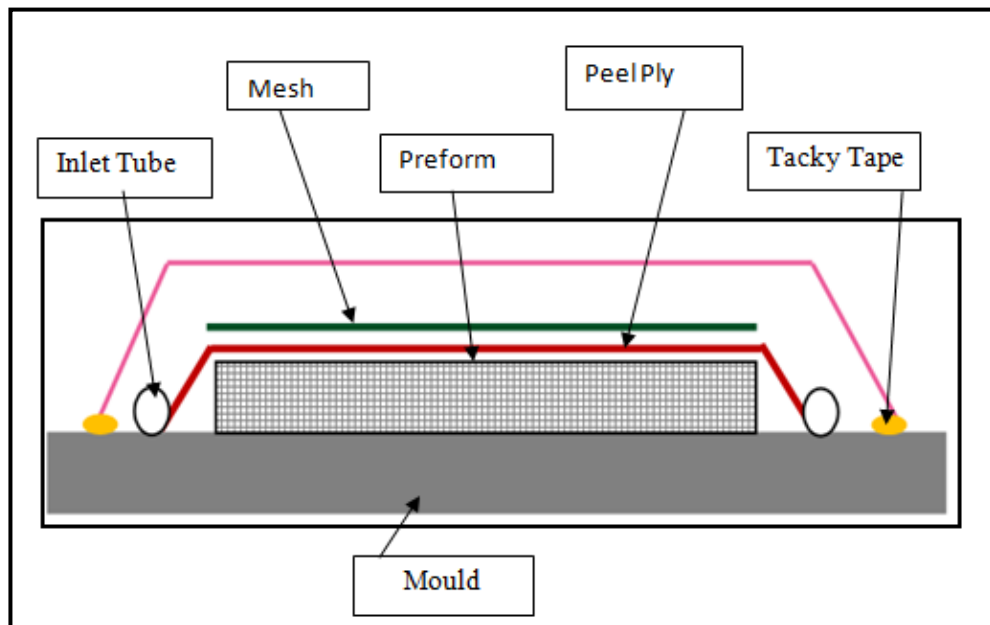
Figure 3.9 Schematic diagram of vacuum bagging
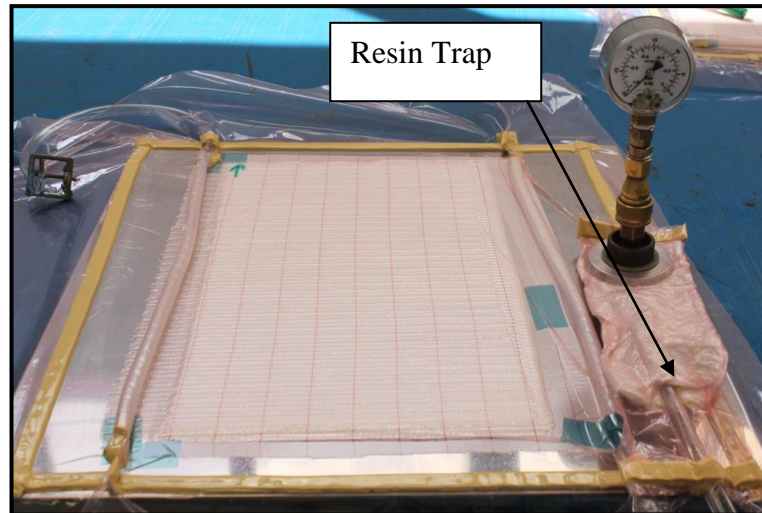
Figure 3.10 Vacuum bagging

3.4 Fibre volume fraction determination

A fibre volume fraction test was performed to determine the amount of fibres in each direction for 3D woven and UD cross-ply laminates after consolidation. All the 3D woven glass fibre reinforced composites were tested to measure their density (ASTM D 792-86) and subsequently had their resin burnt off (ASTM D 2584-68) to determine their fibre volume fraction [111, 112].

Table 3.2 and Table 3.3 provides the details of the cured laminate thickness and total fibre volume fraction constituted by all fibres, whereas Table 3.3 lists the volume fraction of each constituent, ie. warp, weft stuffer and weft binder. To calculate the volume fraction of yarns in each, a specimen of 3x3cm was cut and its density and weight fraction was measured by using the same method as mentioned above. After burning off the entire resin warp, the weft and binder yarns were carefully separated from the specimen and weighted separately to find out their weight fraction, then from those fibre volume fractions were calculated.

Table 3.2: V.F (%) and laminate thickness

Structure	Nominal Thickness (mm)	Volume Fraction (%)
Layer to Layer	3.08	51.24 ± 0.746
Angle Interlock	3.03	50.35 ± 0.257
Twill Angle Interlock	3.05	48.17 ± 0.284
Modified Angle Interlock	2.54	51.20 ± 0.385
UD Cross-Ply	3.50	45.93 ± 0.431

Table 3.3: Yarn volume fraction

Structure	Volume Fraction (%)		
	Warp	Weft Stuffer	Weft Binder
Layer to Layer	32.87 ± 0.202	13.62 ± 0.318	4.74 ± 0.159
Angle Interlock	31.21 ± 0.258	15.83 ± 0.357	3.05 ± 0.328
Twill Angle Interlock	28.87 ± 0.783	15.08 ± 0.896	3.28 ± 0.293
Modified Angle Interlock	34.16 ± 0.045	8.06 ± 0.912	8.44 ± 0.777

3.5   Conclusion

The four different 3D weave architectures and UD cross-ply were produced to study the influence of weft binder on mechanical properties, as well as to make a comparison with the UD cross-ply. The 2D weaving process was used to fabricate 3D woven preforms named as: layer-to-layer, angle interlock, twill angle interlock and modified angle interlock, whereas for UD cross-ply, a pin-board was employed to place the yarns around the pins. Both 3D woven as well as UD laminates were prepared using the resin infusion process. The fibre volume fraction for 3D woven and UD cross-ply laminates

after consolidation was determined through the resin burn-off method. The yarn to composite manufacturing process is highlighted in this chapter. The effect of weave architecture on the tensile properties of 3D woven composites and their comparison with UD cross-ply laminate are discussed in detail in the next chapter.

4 Tensile properties of 3D woven weft bound structures

4.1 Introduction

3D woven composites generally have superior through-thickness mechanical properties when compared with traditional 2D laminates. This through-thickness reinforcement increases interlaminar fracture toughness and limits the delamination and damage propagation that occurs after impact. However, the through-thickness reinforcement also reduces the in-plane fibre volume fraction and consequently the respective planar properties [12, 13].

Comprehensive research has been performed on the tensile properties of 3D woven composites with orthogonal, layer-to-layer and angle interlock structures made of carbon, glass or Kevlar [10, 12, 69, 105, 113-119]. It has been found that through-thickness reinforcement may either improve (due to higher fibre volume fraction) or degrade (due to crimp and lower fibre volume fraction along the loading direction) the elastic modulus and strength of 3D composites by up to 20%, compared to the equivalent 2D laminate [19, 69, 113, 120, 121]. The reduced mechanical performance is due to crimping and misalignment of the in-plane fibres by the insertion of z-binders during weaving [2, 10, 113, 121, 122]. The in-plane fibre waviness causes tensile deformation of 3D woven composites at relatively lower stress values than for 2D laminates. This deformation or softening effect can reduce stiffness by 20-50%, depending on the type of the composites and can be observed in the form of kinking in the stress-strain curve of 3D woven composites [116, 121]. In some materials the binder yarn crimp and the irregularity of the in-plane tows enhanced the frictional resistance between yarns and caused the ultimate tensile failure in the form of z-binder debonding and tow pull-out [115]. In addition, fibre damage occurring during the weaving process

not only degrades the tensile strength of the load bearing tows, but may also increase fibre waviness and the pinching of surface tow at the binder cross-over point. Upon consolidation, the pinching and waviness of in-plane fibres creates localised resin-rich areas [121, 122]. However a change in the binder architecture also affects the arrangement and size of the resin-rich areas in composites [114].

Recently, different strain mapping techniques have been utilized to study progressive damage, and the strain distribution of 3D woven composites in tension has been studied by Quinn [117] and Lomov [123-125]. Quinn highlighted that crimp due to binder tows creates resin-rich areas at the binder cross-over and reduces the efficiency of the structures, as well as initiating the crack formation. Lomov used Digital Image Correlation (DIC), Acoustic Emission (AE) and Finite Element (FE) modelling techniques to study and compare the meso-scale strain of a textile composite. DIC and AE techniques were also used to study the progressive local tensile behaviour of non-crimp 3D orthogonal weave in comparison to 2D woven laminates. It was found that the through-thickness yarn (in 3D woven composites) delays the growth and size of the transverse crack as well as prevent the extensive debonding and splitting of yarns at the final failure in comparison to 2D woven laminates [126, 127].

Mostly, however, it was the influence of the binder yarn on the 3D woven structures in the warp direction that was studied, therefore understanding the influence of the weft binder on tensile properties and failure mechanism still needs to be explored. The primary objective of this chapter is to evaluate the tensile properties and failure mechanism of weft-bound 3D woven composites with strain mapping diagrams. For this study, four different 3D woven and UD cross-ply laminates were manufactured and tested, with tests performed in both the warp and weft direction. DIC was used to

analyze the damage and strain behaviour of the 3D woven composites during tensile loading.

4.2 Tensile testing

Tensile testing was performed on the 3D woven layer-to-layer (LTL), angle interlock (AI), twill angle interlock (TAI), modified angle interlock (MAI) as well as on UD cross-ply laminates in both the warp and weft direction. Schematic diagrams of weave structures are represented in Figure 3.4 to Figure 3.7.

4.2.1 Preparation of the test specimen

All the specimens for tensile testing were cut and tested in both the warp and weft direction. First, the test specimens and end tabs were cut using a rotary diamond cutter, sand blasted and then washed under running water. End tabs were dried at room temperature for 24 hours and attached to tensile coupons, according to the ASTM standard D3039. The end tabs were glass fibre epoxy woven fabric composites with square edges. The tabs were bonded using Araldite 2011 and cure to cure overnight at room temperature. For Araldite 2011 the ratio of the resin and hardener was 50:50 by volume.

Tensile testing was carried out according to ASTM standard D3039, on specimens 250 mm long and 25 mm wide. All the tests were performed in both the warp and weft directions and the gauge length was 150 mm. A video extensometer and DIC were used to calculate the strain measurement; both are non-contact strain-measuring devices. An Instron 5982 R2680 testing machine was used to perform the test.

4.2.1.1 Strain measurement using the video extensometer

A video extensometer measures deformation by tracking the movement of two attached markers (spots or lines). This deformation is monitored with the help of a digital video camera and converted into strain values by dedicated software.

Prior to the tensile test, all the tabbed specimens were marked using a stencil in the longitudinal and transverse directions in the active gauge length at a distance of 25 mm and 10 mm from the centre to measure the axial and transverse strain, respectively, as shown in Figure 4.1a and Figure 4.1c. A minimum of five specimens were tested for each sample type and average strength, modulus and strain to failure were evaluated.

4.2.1.2 Surface strain measurement using DIC

DIC is a non-contact method for measuring whole-field displacements. This technique consists of capturing consecutive images with a digital camera during the deformation period to evaluate the change in surface characteristics of a specimen while it is subject to incremental loads.

DIC test was performed on one specimen from each sample style (weave style) to analyse the strain mapping. Before the actual test, the specimens were painted with a white spray followed by a black speckle pattern over the surface of the white paint. The painted specimen and testing equipment is shown in Figure 4.1b and Figure 4.1d, respectively. To capture the full-field strain behaviour a region of interest of approximately 100 mm x 25 mm was identified. After taking the initial/reference image of the specimen, subsequent images were captured (1 image/2kN) over the defined speckle pattern until the specimen failed. At the end of the tensile test a strain distribution map was created with Istra4D software. This was done by correlating all the pixels of the initial image before loading and any deformed images just before the final

failure of the composite specimen. Further, the average and local strain at different points were computed across the previously defined area with the help of the same software. To analyze the progressive strain behaviour of different weave architectures the local strain at three different load levels was calculated along the loading direction. These loads were 50%, 75% and 95% of the failure load.

(a)

(b)

(c)   **(d)**
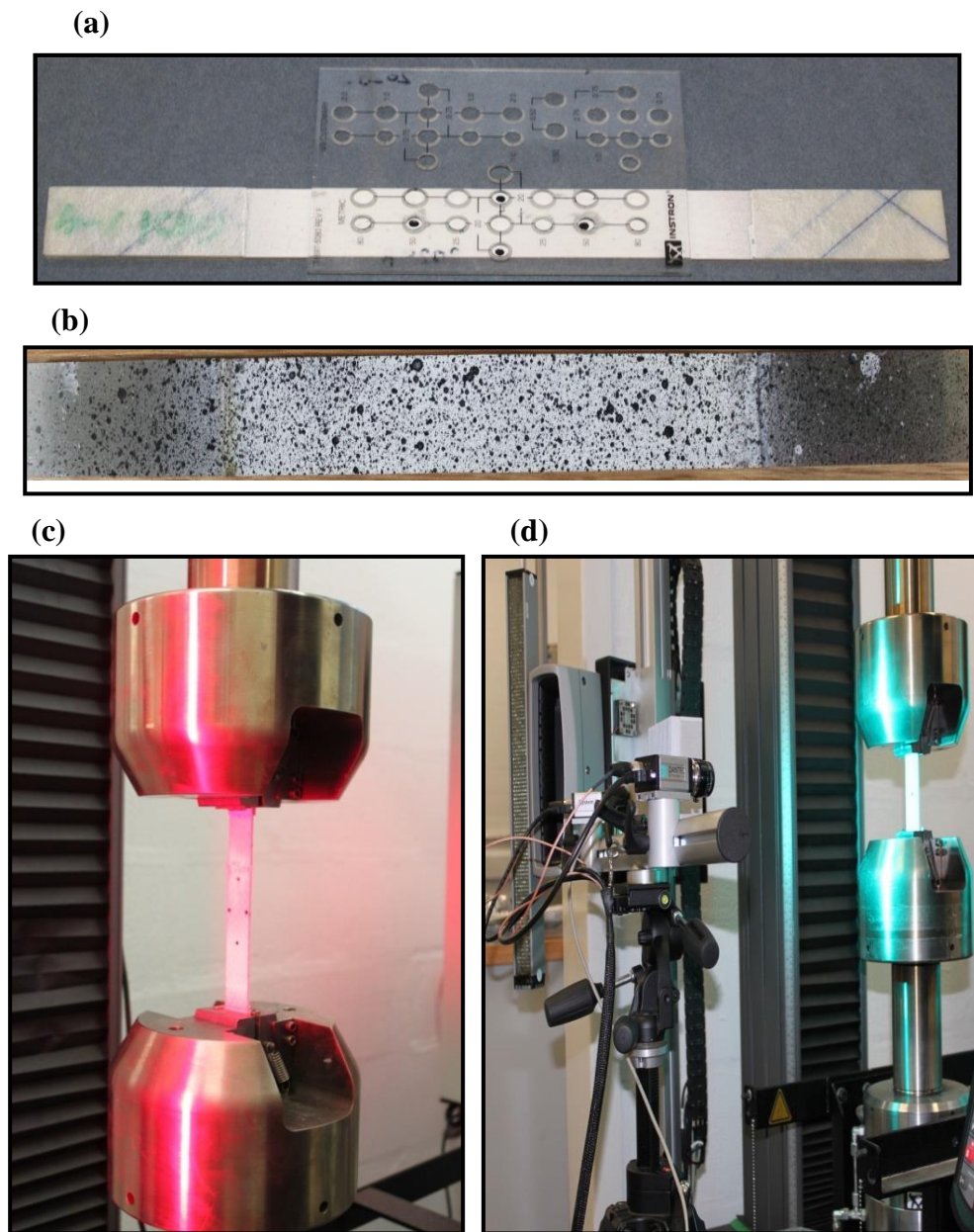
Figure 4.1 Tensile testing (a) Video Extensometer specimen (b) Digital Image Correlation specimen (c) Testing with VE (d) Testing with DIC

4.3   Results and Discussion

The results of the tensile test on UD cross-ply and four different 3D woven composites, tested in both the warp and weft directions are summarised in Table 4.2,Table 4.3 and Table 4.4. Representative load-extension and stress-strain curves are shown in Figure 4.2 and Figure 4.3. The elastic modulus was measured in the warp and the weft direction within a strain range of 0.1% - 0.3%. To make a meaningful comparison the modulus and strength values are normalised in each direction because all the composites have different volume fraction in both (warp and weft) direction. The modulus and strength data were normalised to an average volume fraction of 31% and 18.4% in the warp and weft direction, respectively. The average values were then calculated by averaging the volume fraction of all the structures in the representative direction. Normalised strength and normalised modulus in each direction is calculated according to the following equations

$$\sigma_{nor(vf)} = \sigma * F.V.F_{av(LD)} / F.V.F_{(LD)} \qquad (1)$$

$$E_{nor(vf)} = E * F.V.F_{av(LD)} / F.V.F_{(LD)} \qquad (2)$$

Where,

$\sigma_{nor(vf)} =$ Normalised stress with respect to fibre volume fraction

$\sigma =$ Ultimate tensile strength

$F.V.F_{av(LD)} =$ Average fibre volume fraction of all the structures parallel to loading direction

$F.V.F_{(LD)} =$ Fibre volume fraction of individual structure parallel to loading direction

Figure 4.4 and Figure 4.5 are the graphical representations of the original and normalised values of ultimate tensile stress and modulus in both warp and weft directions.
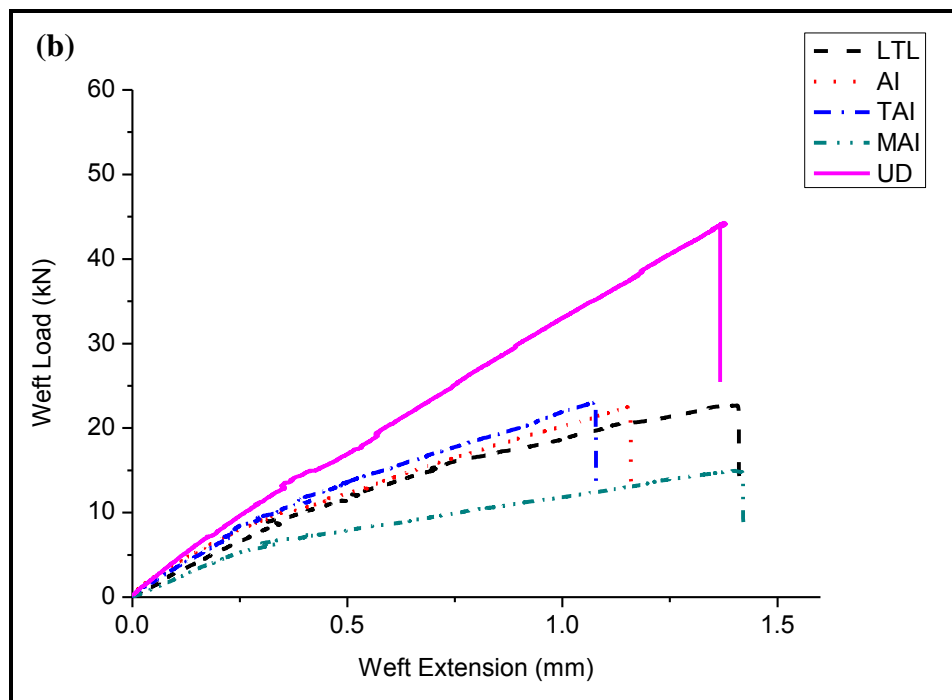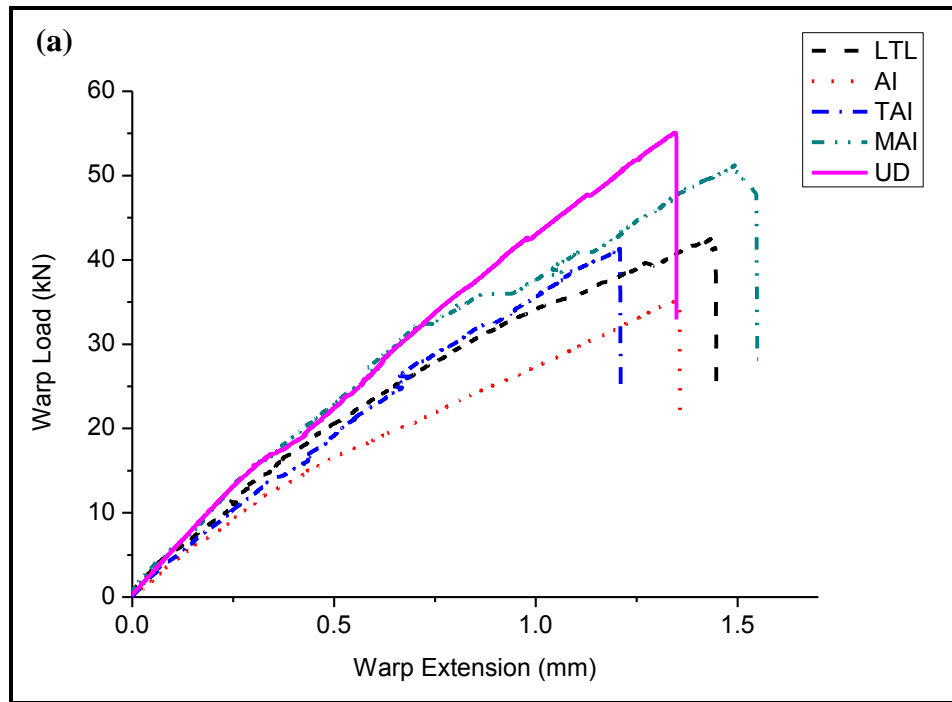
Figure 4.2 Load-extension curves (a) Warp direction (b) Weft direction

4.3.1 Tensile properties

Warp stress-strain curves (Figure 4.3a) showed that the stiffness of the composite decreases with the increase of the strain due to the composite yielding. This yielding effect is more prominent in the A.I structure after a strain of 0.7%, while the curves of

the LTL, TAI and MAI structures showed a series of jagged peaks on the stress strain curve. It is assumed that under tensile load, stress redistribution due to straightening of the warp yarns beneath the binder yarns appears in the form of yielding and a series of jagged peaks on the stress-strain curves. These jagged peaks are more prominent in the MAI structure and a possible reason may be the combined influence of the complicated weave structure and the higher number of binder yarns per unit area. The schematic diagram (Figure 3.7) of the weave structure shows that any two adjacent warp yarns are constrained by the binder yarns, while the binder yarns interlace with the warp yarns at three different points: top, middle and bottom. When the composite is stretched in the warp direction, more force is required to release/unlock the warp yarns; this effect appears on the stress-strain curve in the form of enhanced jagged peaks, in comparison to other weave architectures.

In contrast, the stress-strain curves for the 3D woven composites loaded in the weft fibre direction show more distinct features on the stress-strain curve (Figure 4.3b). The first region of the curve, up to a strain level of 0.5% is called the elastic region and is characterized by a linear increase in the curves. This region represents the initial response of the material, and is presumably damage free. At the end of this portion, the slope dropped, and the curve deviated from linearity at a strain of 0.5%. This second region is called the yielding phase and in this region the composite is softening in a linear manner until a failure occurred at a strain of 2.2-2.9%. More composite yielding can be observed in the weft direction due to the fewer number of straight yarns in the loading direction, especially in the MAI structure. Similarly, in the weft stress-strain curves the jagged peaks are not very prominent because the binder yarns lie along the loading direction, with less load required to straighten them compared to those in the warp direction specimens.

4.3.1.1   Tensile strength

The representative warp stress-strain curves show that in the warp direction (Figure 4.3a) the laminate tensile strength decreases in the following sequence: modified angle interlock, UD cross-ply layer-to-layer, twill angle interlock and angle interlock.
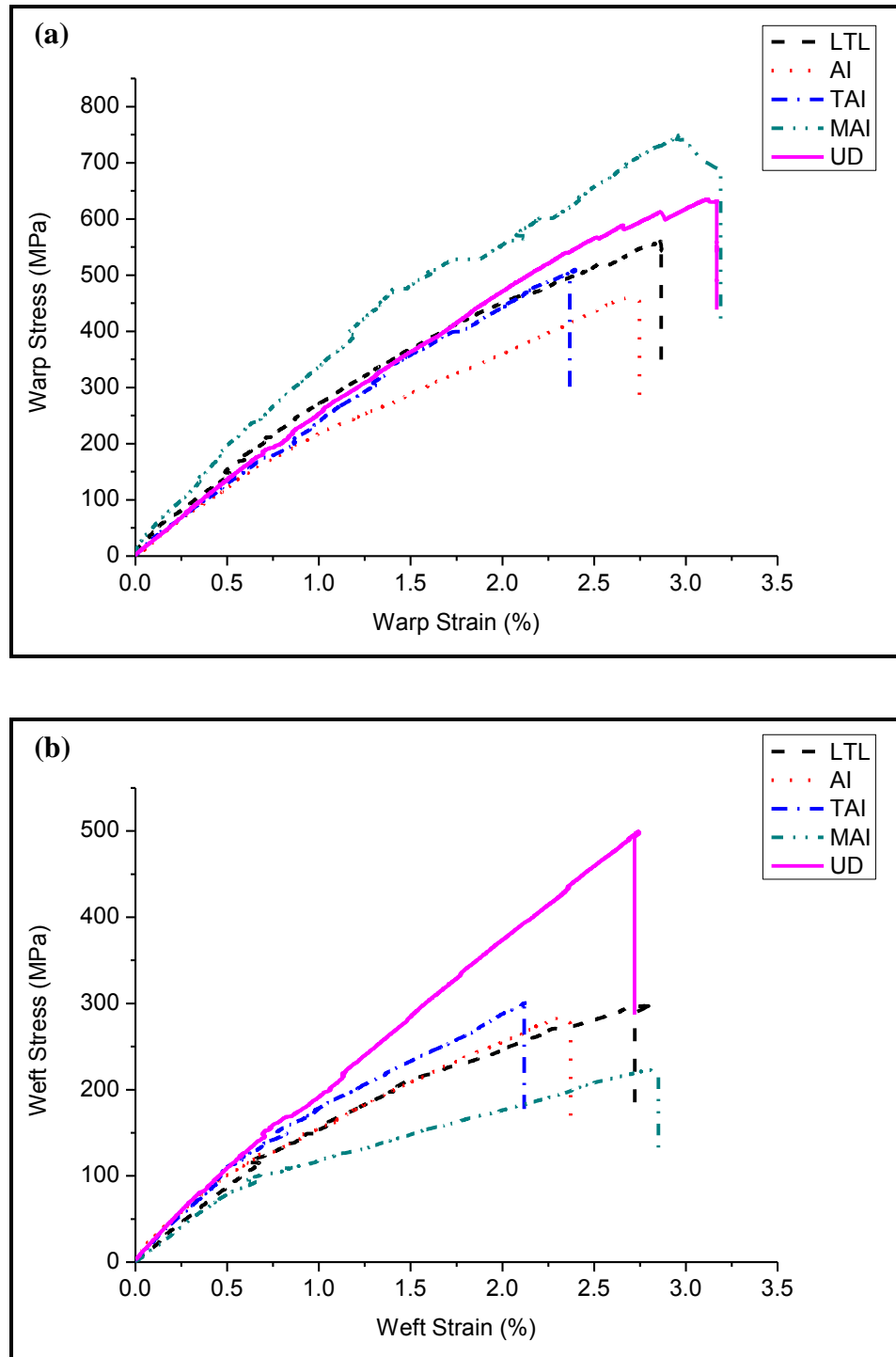
Figure 4.3 Typical Stress-strain curves (a) Warp direction (b) Weft direction

The higher strength of the MAI is because of a higher number of warp yarns along the loading direction as compared with UD and the other 3D woven structures. Due to the modification of the binder path, the MAI can accommodate more warp yarns per unit area following consolidation, although warp density on the loom appeared the same for all the 3D woven structures. This phenomenon can also be verified by the volume fraction (Table 3.3 from chapter 3) measure for all the structures in the representative direction. For the weft direction (Figure 4.3b) UD cross-ply exhibits the highest strength compared with the 3D woven composites because of a higher volume fraction of straight yarns in the loading direction. There was also a sharp decrease in the strength of 3D woven structures after the elastic region because of the fewer number of straight yarns and binder crimp, especially for the modified angle interlock where half the load bearing yarns are binders.

Tensile properties for the 3D woven and UD composites were comparable once the volume fraction of fibres in the test direction was accounted for. Experimental and normalized tensile strength values are presented in Table 4.2 and shown in the Figure 4.4. The strength values were normalized to the average volume fraction of the fibre in the representative direction. It can be observed that the UD laminate has the highest tensile strength in both warp and weft direction because the yarns along the loading direction are straight (Figure 4.17b). In the 3D woven structures, the binder yarns pass over and under the warp yarn in the thickness direction in order to hold the structure. This undulation, and the tension of the binder yarn, induces some level of crimp into the structure and crimp percentage depends on weave architecture. Therefore, of the 3D woven structures the MAI has the highest tensile strength in the warp direction and lowest in the weft direction. The modification in the MAI binder path induces less crimp into the warp yarns and gives the highest tensile strength in the warp direction

followed by TAI, LTL and AI. The % crimp values presented in Table 4.1 for the warp yarns also verify this behaviour and are calculated by using the following equation:

$$Crimp \% = E.L - O.L / O.L$$

Where, E.L = Extended length of the yarn   and   O.L = Original length of the yarn

Table 4.1: Preform Crimp

Structure	Preform Crimp %		
	Warp Crimp	Weft Crimp	Binder Crimp
Layer-to-Layer	1.108	0.59	1.313
Angle Interlock	1.231	0.66	1.58
Twill Angle Interlock	0.612	0.56	1.267
Modified Angle Interlock	0.55	0.55	1.619

Similarly, the effect of crimp factor on tensile strength can also be observed in the weft direction where TAI and LTL exhibit higher tensile strength and lower crimp values in the binder yarn. Although the crimp percentage in the binder yarns of AI and MAI is almost the same, the lower MAI strength is due mainly to the higher number of binder yarns along the loading direction.

The ultimate tensile strength of 3D woven composites is between 14-55 % and 58-87 % of ultimate tensile strength of the UD laminate in the warp and weft direction, respectively. This huge difference in the weft direction is due to the presence of binder yarns along the loading direction. Within the 3D woven structures the normalized MAI strength in the warp direction is 14%, 20% and 35% higher than TAI, LTL and AI respectively. However in the weft direction, LTL and TAI have almost the same

strength values, while for the AI and MAI, it was 5% and 31% compared to the TAI structure.
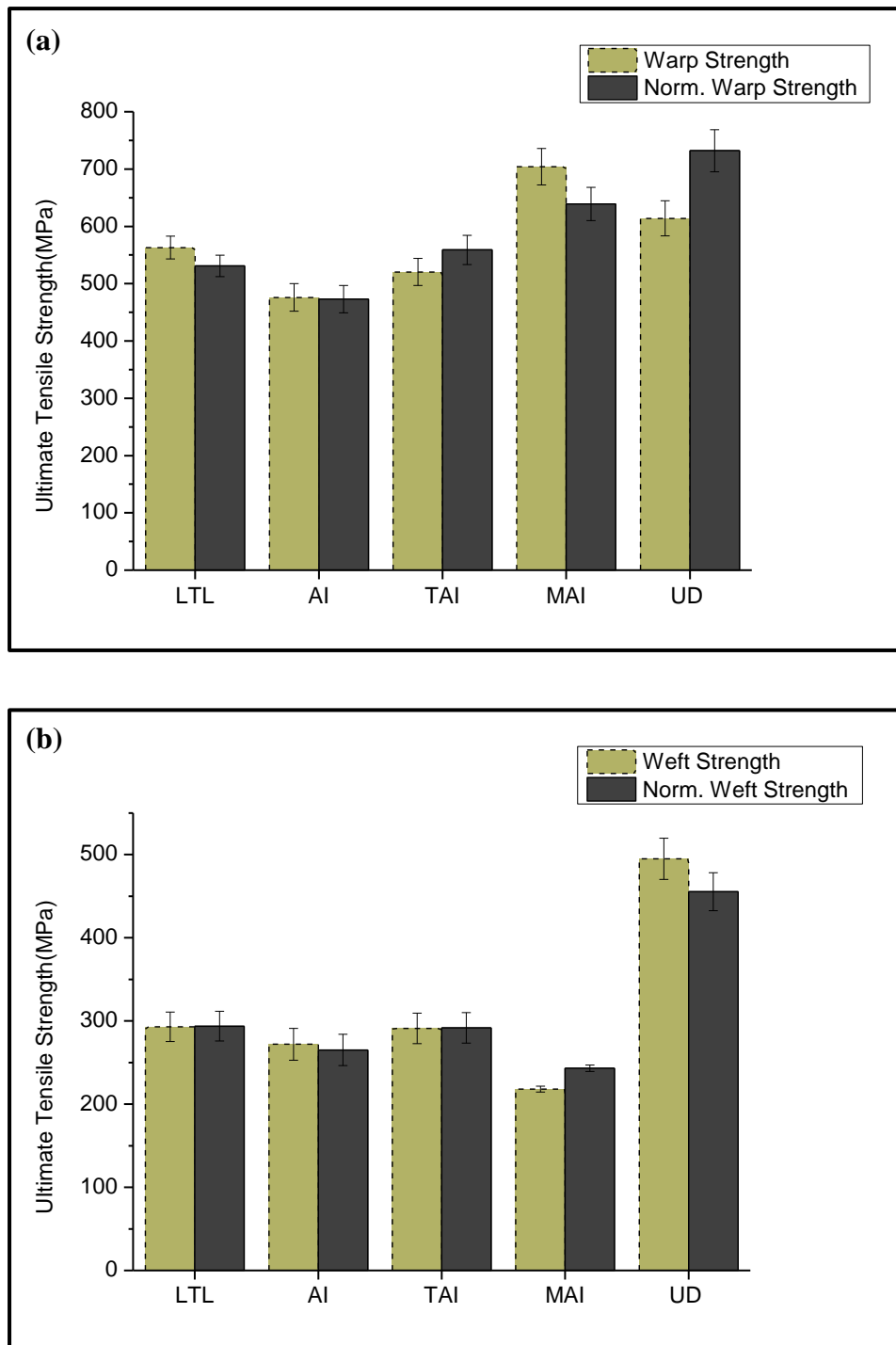
Figure 4.4 Ultimate tensile strength (a) Warp direction (b) Weft direction

Table 4.2: Ultimate Tensile Strength (MPa)

Original and Normalised data (using equation 1on page 81)

Structure	Ultimate Tensile Strength (MPa)			
	Warp		Weft	
	Original Data	Normalized Data	Original Data	Normalized Data
Layer-to-Layer	563 ± 19.71	531 ± 18.57	293 ± 17.79	293.5 ±17.84
Angle Interlock	476 ± 24.12	473 ± 23.96	272 ± 19.21	265 ±18.72
Twill Angle Interlock	520 ± 23.78	559 ± 22.53	291 ± 18.34	292 ± 18.38
Modified Angle Interlock	704 ± 31.81	639 ± 28.86	218 ± 3.58	243 ±3.99
UD Cross-Ply	614 ± 30.69	732 ± 36.59	495 ± 24.75	455 ±22.77

4.3.1.2 Tensile modulus

Figure 4.5a and Figure 4.5b show a comparison of original and normalized modulus values in the warp and weft directions, respectively. Originally, the MAI and UD had the highest values in the warp and weft directions due to a high fibre volume fraction along the loading direction. However, after normalization the UD cross-ply laminate showed the highest stiffness value in the warp direction followed by TAI, MAI, AI and LTL. The moduli of the 3D woven composites are between 10-33% of the UD laminate along the warp yarn. In the weft direction, the TAI exhibits the highest modulus followed by UD, LTL, MAI and AI. However the difference between the 3D woven composites and the UD cross-ply laminate is less significant in the weft direction as compared to the warp direction.

The combined effect of binder yarn float, crimp and yarn alignment following consolidation contributes to the modulus of the materials. A long float length in the

structure imparts a larger percentage of nominally straight fibres in the warp direction
and a reduced amount of binder yarn crimp.
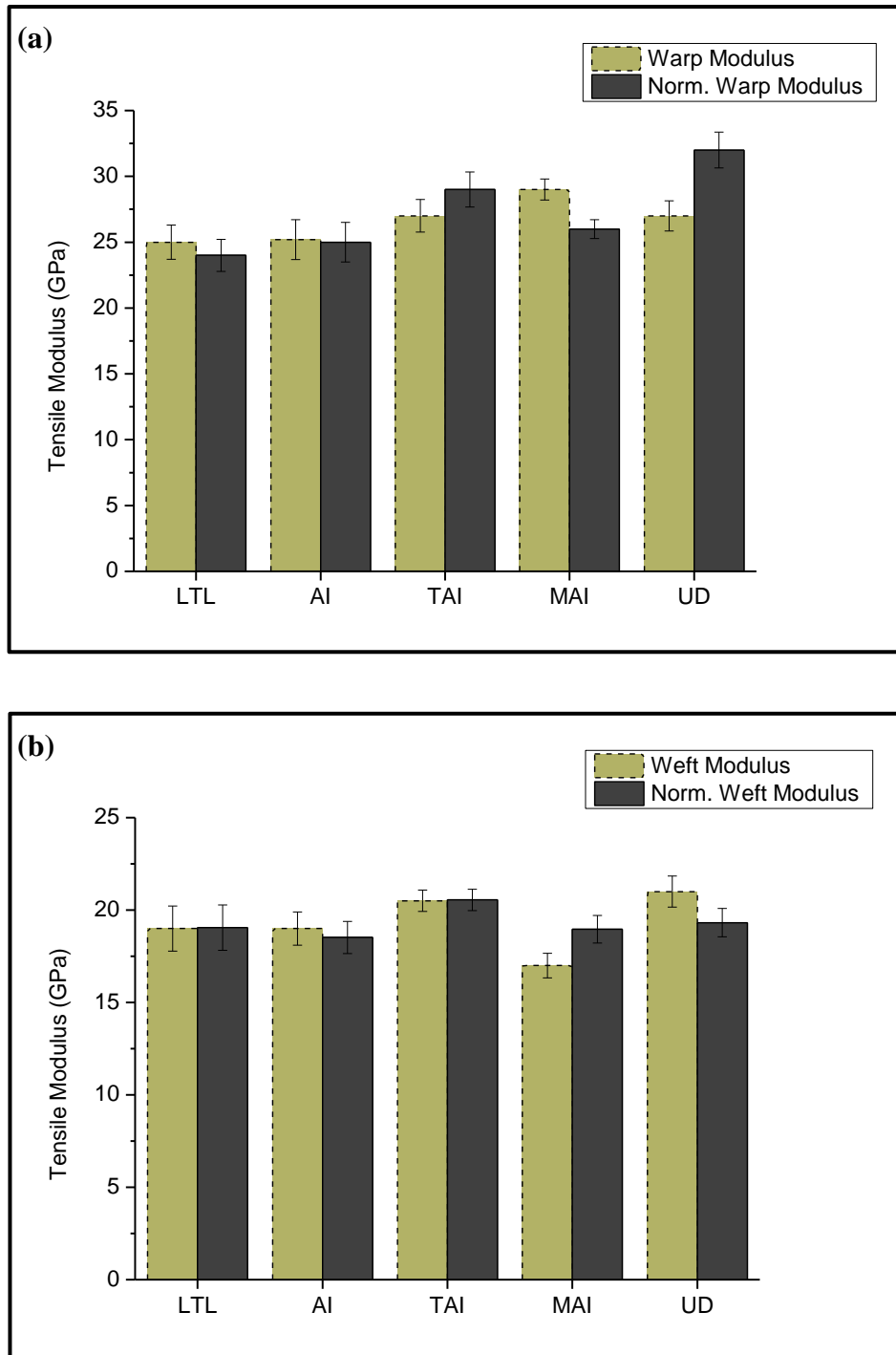
Figure 4.5 Tensile modulus (a) Warp direction (b) Weft direction

Within the 3D woven structures, TAI has the highest modulus in both the warp and weft

directions. In the warp direction, the modulus of TAI and AI are 10% and 5% higher

than MAI and LTL, respectively. The higher modulus is due to greater alignment of warp yarns along the loading direction after consolidation.

Micrographs of TAI and A.I depicted in Figure 4.13c and Figure 4.11c show that the warp yarns are more aligned with the loading direction compared to MAI and LTL shown in Figure 4.9c and Figure 4.15c. In the weft direction, LTL, AI and MAI have almost the same level of modulus, while the higher values of TAI may be attributable to the influence of a lower crimp and longer float of the binder yarn along the loading direction.

Table 4.3: Tensile Modulus (GPa)-

Original and Normalised data (using equation 2 on page 81)

Structure	Modulus (GPa)			
	Warp		Weft	
	Original Data	Normalized Data	Original Data	Normalized Data
Layer-to-Layer	25 ±1. 29	23.57 ± 1.22	19 ± 1.22	19.05 ± 1.22
Angle Interlock	25 ±1 .51	24.83 ± 1.51	19 ± 0.89	18.52± 0.87
Twill Angle Interlock	27 ±1 .23	28.98 ± 1.33	20.5 ± 0.58	20.55 ± 0.58
Modified Angle Interlock	29 ± 0.793	26.32 ± 0.72	17 ± 0.66	18.96 ± 0.71
UD Cross-Ply	27 ± 1.14	32.19 ± 1.35	21 ± 0.84	19.32 ± 0.769

4.3.1.3   Failure mechanism of 3D woven composites in tension

The failure of the specimens tested for this work occurred within the gauge length in each case. Along the warp direction, failure was preceded by delamination and the longitudinal splitting of warp yarns as shown in Figure 4.6. Longitudinal splitting before the final failure of the laminate was more extensive in MAI and covered almost

the whole of the gauge length. In AI and TAI, specimen failure occurred at an angle of around 40º-60º to the loading direction and yarn splitting was less extensive compared to MAI. In LTL the composite delamination and warp splitting fell between MAI and the two other angle interlock structures. Examination of broken specimens in the warp direction revealed that in all the 3D woven structures, warp yarns split/broke at the region where they entered or exited the binder yarn.
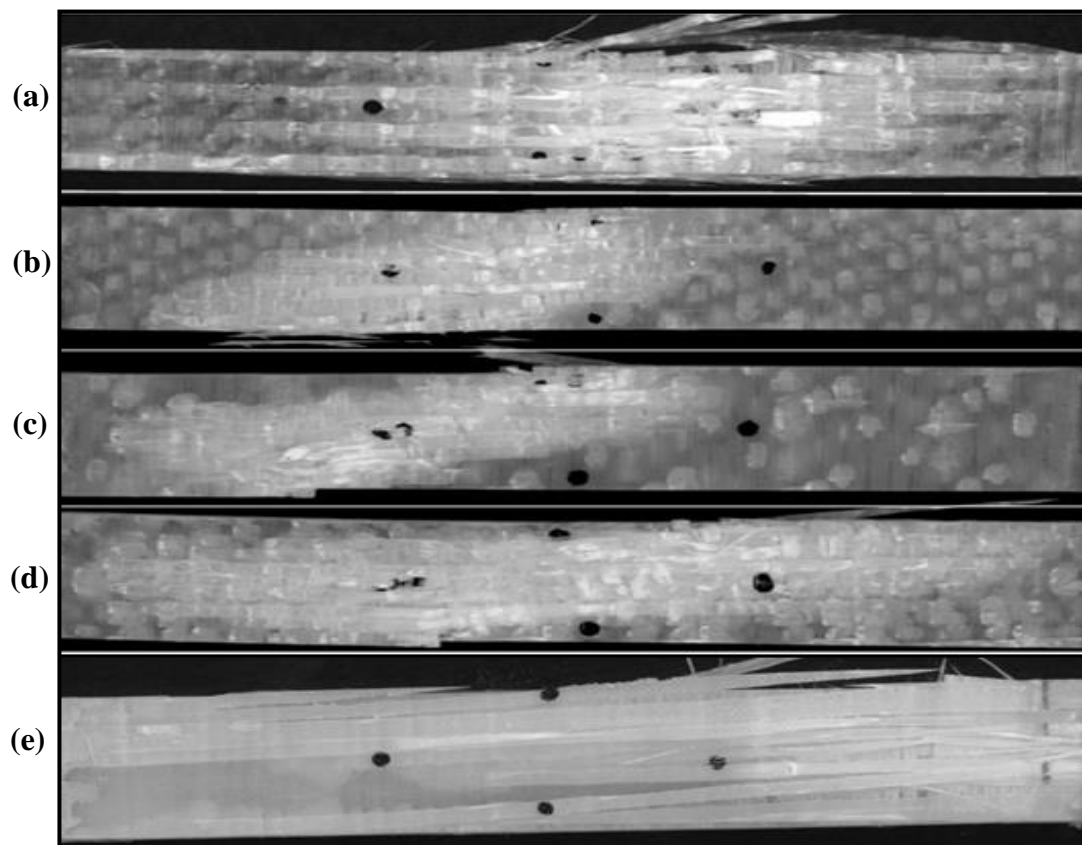
Figure 4.6 Photographs of failed specimens in warp direction (a) Layer-to-layer (b) Angle Interlock (c) Twill Angle Interlock (d) Modified Angle Interlock (e) UD Cross-Ply

There could be two reasons for this type of failure. First, during the weaving process the highly tensioned and densely packed binder yarns exerted extra pressure on the warp yarns laying beneath, and as a result the cross-over region became a natural local site for stress concentration in the preform. When the tensile load was applied, the warp yarns tried to straighten, applying a force that would be normal to the warp yarn onto the binder yarn. In response to axial loading, the binders under transverse load also exerted

normal and shear forces on the neighbouring (warp) yarn. A combination of normal and shear forces created a further concentration of stress at the cross-over point, resulting in reduced strength of the warp yarns pinched by the binder yarn; the fracture started to initiate from these points. Second during the weaving, at the interlacement (cross-over) point, the binder yarn passing through the structure of the fabric left a depression on the surface of the fabric. During resin infusion this depression filled with the resin and was subsequently cured to form a resin-rich area [128]. Under the tensile load, high localised strain brought about by deformation of the resin-rich area caused the failure. The combined effect of stress concentrated at the interlacement points and high localised strain in the resin-rich areas reduced the strength of the composite. This phenomenon was more enhanced in the AI structure when loaded along the warp yarns. In AI and TAI, the binder yarn travelled from the top to the bottom of the structure; however the sharp curve of the binder yarns in the AI structure created resin-rich areas, as well as exerting more pressure on the warp yarns beneath it, resulting in reduced structure strength. This is different to TAI, where the long binder floats were able to reduce the pinching as well as increase the amount of aligned tows in the loading direction, resulting in better strength and superior modulus properties in both warp and weft directions. In examining the effect of binder path on tensile properties, Leong [128] and Quin [117] observed that strength and stiffness can be improved by modifying the binder path. In LTL the binder angle is less steep as the binder yarn is penetrating to half the thickness of the structure, however it induces more crimp into the warp yarns. Therefore, the ultimate strength of LTL in the warp direction is 5% lower than TAI and 12% higher than A.I. However in the weft direction the LTL and TAI structures have almost the same strength due to lower binder crimp. For MAI, the binder yarn passes through the thickness direction in a step manner, helping to reduce the warp crimp as

well as resin-rich areas due to the nesting of warp yarn in adjacent layers; consequently, a superior ultimate tensile strength was achieved in the warp direction as compared to other 3D woven structures. The inferior strength and modulus of MAI in the weft direction was due to the high crimp and higher number of binder yarns along the loading direction.
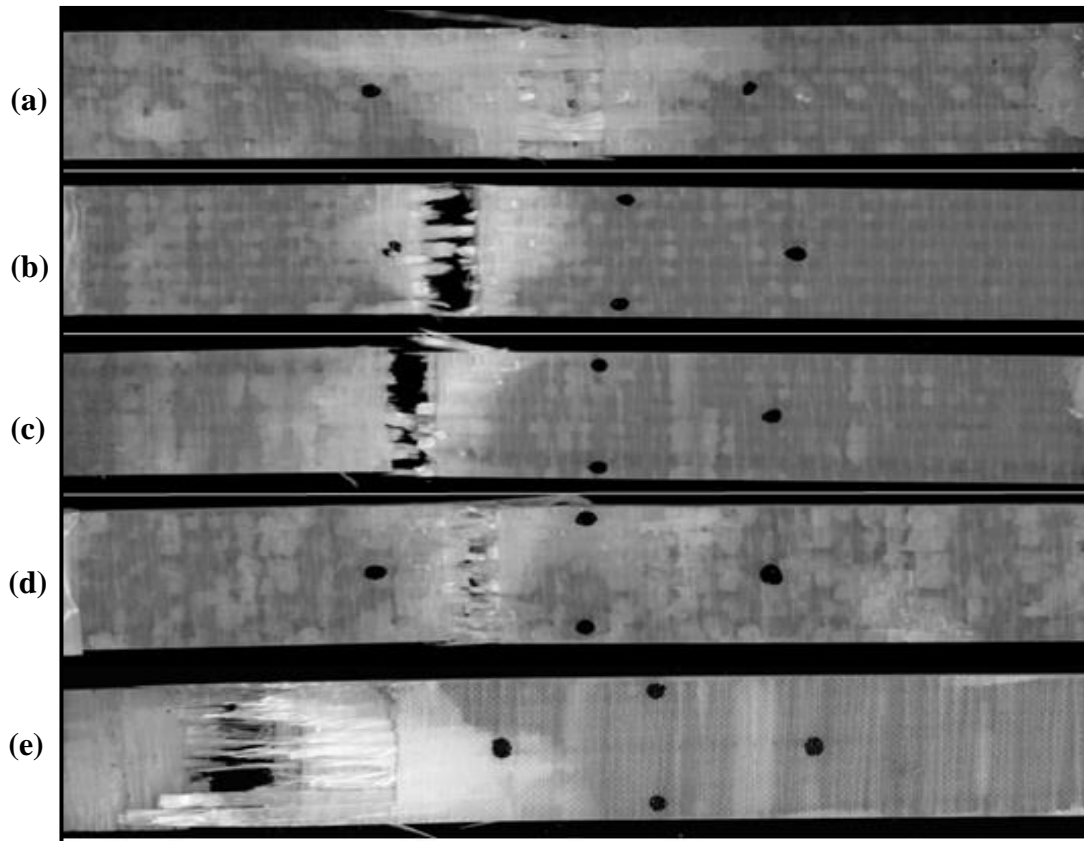
Figure 4.7 Photographs of failed specimens in weft direction (a) Layer-to-layer (b) Angle Interlock (c) Twill Angle Interlock (d) Modified Angle Interlock (e) UD Cross-Ply

In the weft direction, the failure zone was far more constrained and failure mode occurred in a straight line, at 90 degree to the loading direction as shown in Figure 4.7. Failure occurred due to failure of the binder yarns, with specimens splitting into two pieces. As the binder yarn was parallel to the loading direction, high stress and strain concentrated at the binder interlacement point led to the final failure of the specimens. The same behaviour has been observed by other researchers looking at the binder tow path in a warp bound composite [128].

The resin-rich areas due to warp and binder yarn misalignments leads to high localised strain and these localized strain points can be observed in the DIC images. A comparison of local strain and the strain to failure showed that in 3D woven composites the localised strain was significantly higher than the strain to the failure of the UD cross-ply.

4.3.2   Localized strain analysis of 3D woven composites

As discussed previously, the region of the 3D woven structure where the binder yarn enters or leaves the layers of warp yarns to accomplish the binding is a potential area of weakness in the 3D structure. The resin-rich areas and stress concentration at the binder cross-over point have been proposed as reasons for the weakness in this region of composites. To examine this, DIC was used to identify changes in deformation and strain distribution of the 3D woven composites as well as in the UD cross-ply laminate. As the 3D woven structures were made of repeating patterns, the area of strain concentration would hence be repeated over the surface of the specimens. The strain distribution was calculated for the predefined area. The average strain was calculated by selecting a polygonal area on the strain mapping diagram as shown in Figure 4.8a, whereas the local strain values were calculated along a straight line parallel to the fibre direction using different load levels (Figure 4.8b). Istra4D software was used to calculate the strain at different points. For each structure, strain maps and strain profile curves at different load level are displayed in Figure 4.9 to Figure 4.18.

Results from DIC showed that the strain distribution within the 3D woven and UD cross-ply laminates is hetrogeneous. except in the UD warp direction where it seems quite homogeneous. For 3D woven, the levels of localized strain are often higher than the strain to failure. The strain maps show the formation of the localized strain band

which are correlated with the weave structures (Figure 4.9a to Figure 4.16a). It is observable from the strain mapping diagrams that the regularity of the areas of maximum strain occured where the binder yarns interlace with the warp yarns. These areas cause locally higher levels of strain in tension. A similar phenomenon was observed by Quinn [117] and Hale [129] for strain mapping analyses of orthogonal and angle interlock structures.
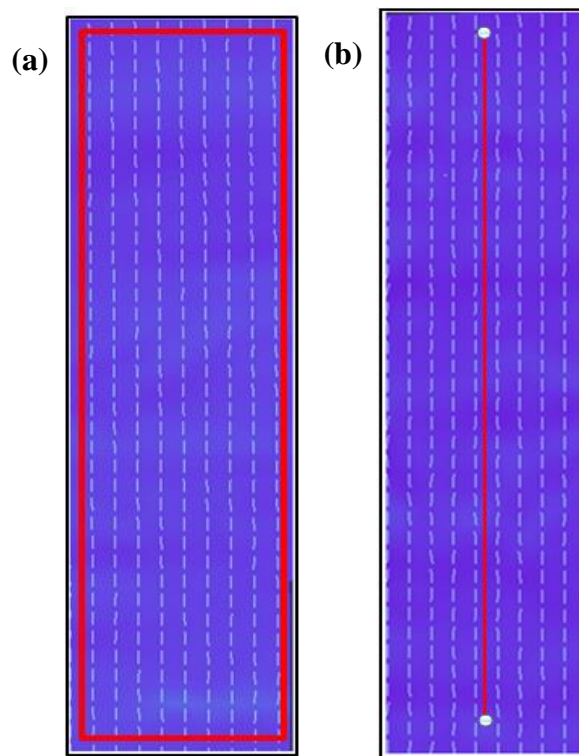
Figure 4.8 (a) Average strain calculation area (b) Local strain calculation along a line

The strain profiles of UD cross-ply laminates (Figure 4.17) show that in the warp direction, the distribution of local strain is more homogeneous up to failure and that the local strain was the same as the strain to failure because the outer layer of the fibres was along the loading direction. While in the weft direction (Figure 4.18), the local strain was higher than the strain to failure (DIC only measure the surface strain of the composites so the higher deformation means higher strain values), as the outer (sufrace) yarns were at 90 degree to the loading direction and during loading the high

deformation of suface yarn due to shear stresses between axial and transverse fibres led to high localised strain in the weft direction specimens.

The strain profiles can explain the variation in the strain along a straight line parallel to the loading axis as shown in Figure 4.8b. These local strain profiles just before fracture along the warp and the weft direction at different load levels are presented in Figure 4.9d to Figure 4.16d. A comparison of strain profiles showed that AI had the highest local strain in both the warp and weft direction which is the consequence of local stress concentrations and resin-rich areas caused by the sharp angle and pinching of the binder yarn, as mentioned previously. In the warp up to 75 % of failure load the maximum local strain in the LTL, TAI, and MAI are almost the same, and beyond 95% of failure load the MAI showed the highest localized strain until failure occured. The local strain to failure of MAI was higher than LTL and TAI in both directions.The high local strain values of MAI led to higher failure load and fibre splitting along the warp direction and localized damage along the weft direction. The localised strain of all the interlock structures is higher in the weft direction because of the greater elongation of the binder yarn along the loading direction as it travelled from the top to the bottom of the structure. Whereas in LTL, the localised strain in the weft direction is lower than the localised strain in the warp direction due to lower deformation of the binder yarn as the binder yarn penetrated to half the thickness of the structure and then returned back.

The variation in the strain profiles corresponds well to the different weave architectures. The peaks in the strain profiles represent the binder interlacement point, highlighted with the letter 'A' . These peaks occurred with the same frequency as the binder yarn interlacements points. The spacing between the two peaks depends on the distance between the two binder yarns and is coherent with the binder path in both the warp and

weft directions. These localized strain accumulations are probably the commulative result of normal and shear forces at the cross-over point, the plastic deformation of matrix and micro-damages, which eventually leads to delamination, plus splitting and specimen failure. A comparison of average strain values obtained from the video extensometer and DIC is shown in Figure 4.19 and Figure 4.20.The curves show that average strain measure from both the techniques is fairly similar. Any deviation in the curve line is due to the specimen variation as strain values obtained from videoextensometer and DIC were taken from two different specimens of the same weave structure.

Table 4.4: Tensile Strain-to-Failure

Structure	Strain-to-failure (%)			
	Warp		Weft	
	Video Extensometer	DIC	Video Extensometer	DIC
Layer-to-Layer	2.94 ± 0.114	2.94	$2.66 \pm 0 .416$	2.54
Angle Interlock	2.76 ± 0.057	2.86	2.2 ± 0.115	2.19
Twill Angle Interlock	2.56 ± 0.151	2.62	2.1 ± 0.291	2.27
Modified Angle Interlock	2.97 ± 0.166	2.91	2.8 ± 0.00	2.52
UD Cross-Ply	2.75 ± 0.173	2.71	2.75 ± 0.070	2.88
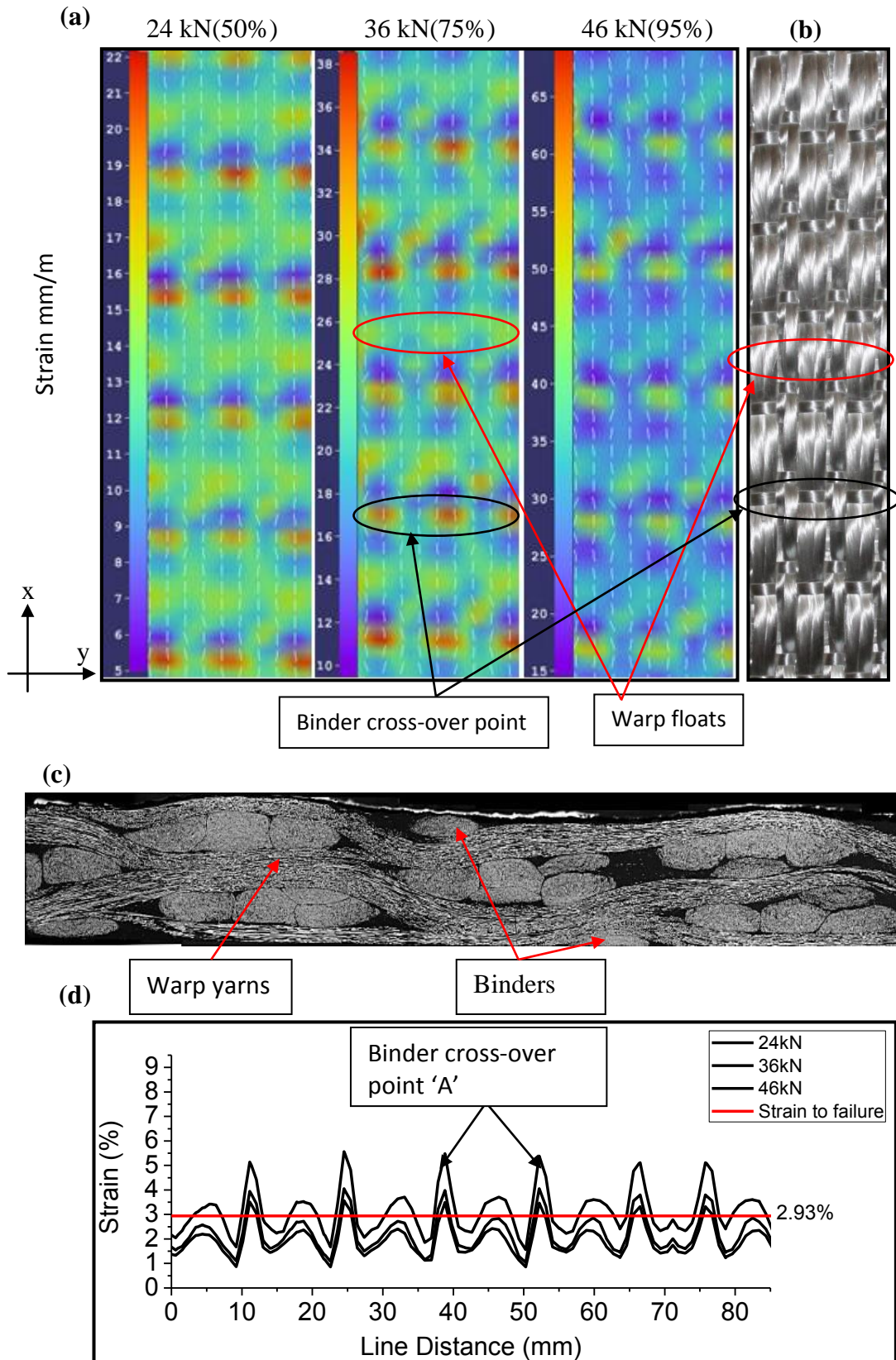
Figure 4.9 Layer-to-layer in the warp direction (a) Surface strain maps at different load levels show high strain at binder cross-over points (b) Photograph of 3D woven fabric (c) SEM image along warp yarns (d) Strain profiles showing local strain variation along a straight line at different load levels (x is the loading direction)

(Purple and orange colours represent the lowest and the highest strain values, respectively, where the maximum strain value increases with the load)
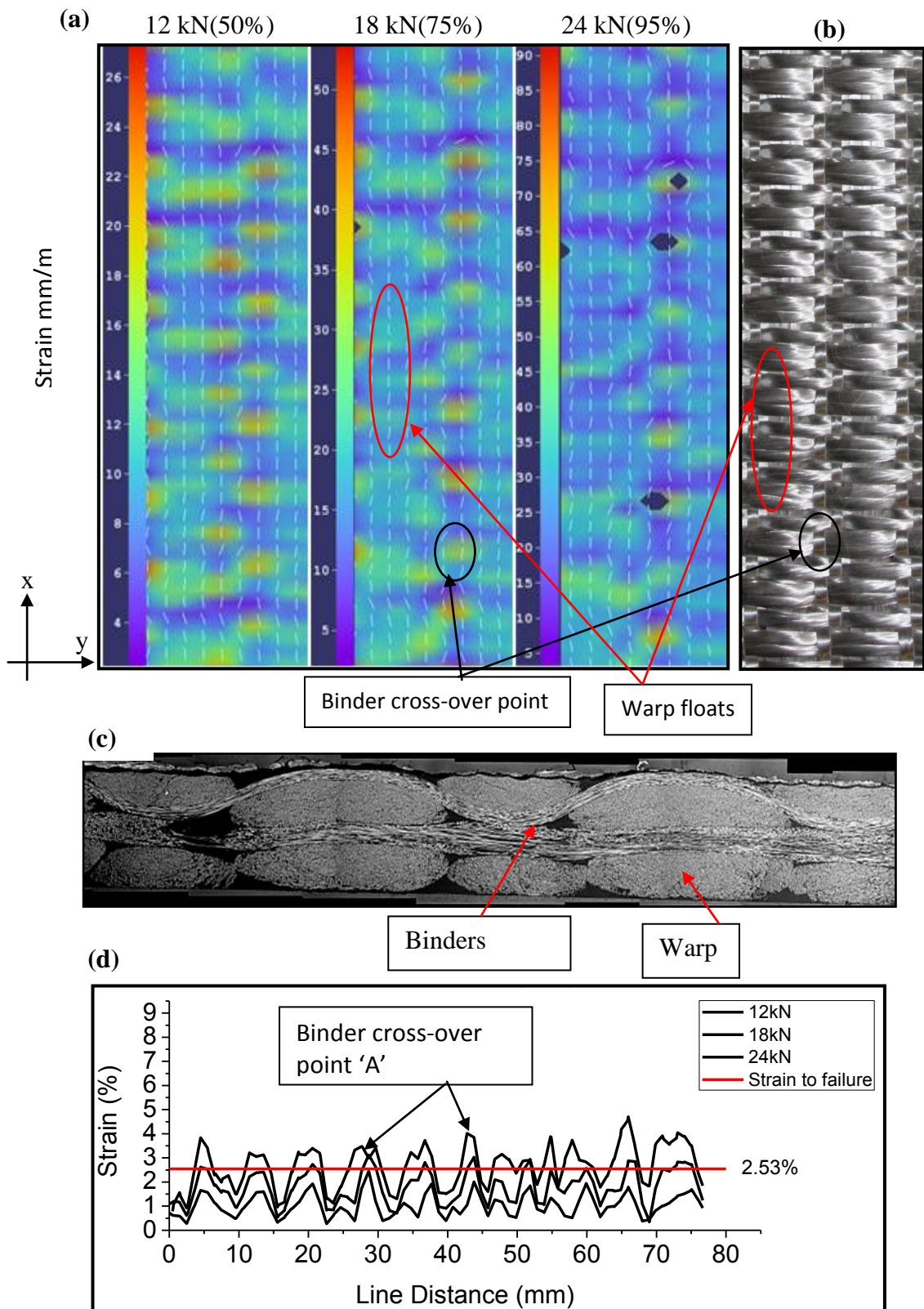
Figure 4.10 Layer-to-layer in the weft direction (a) Surface strain maps at different load levels show high strain at binder cross-over points (b) Photograph of 3D woven fabric (c) SEM image along binder yarn (d) Strain profiles showing local strain variation along a straight line at different load levels (x is the loading direction)

(Purple and orange colours represent the lowest and the highest strain values, respectively where the maximum strain value increases with the load)
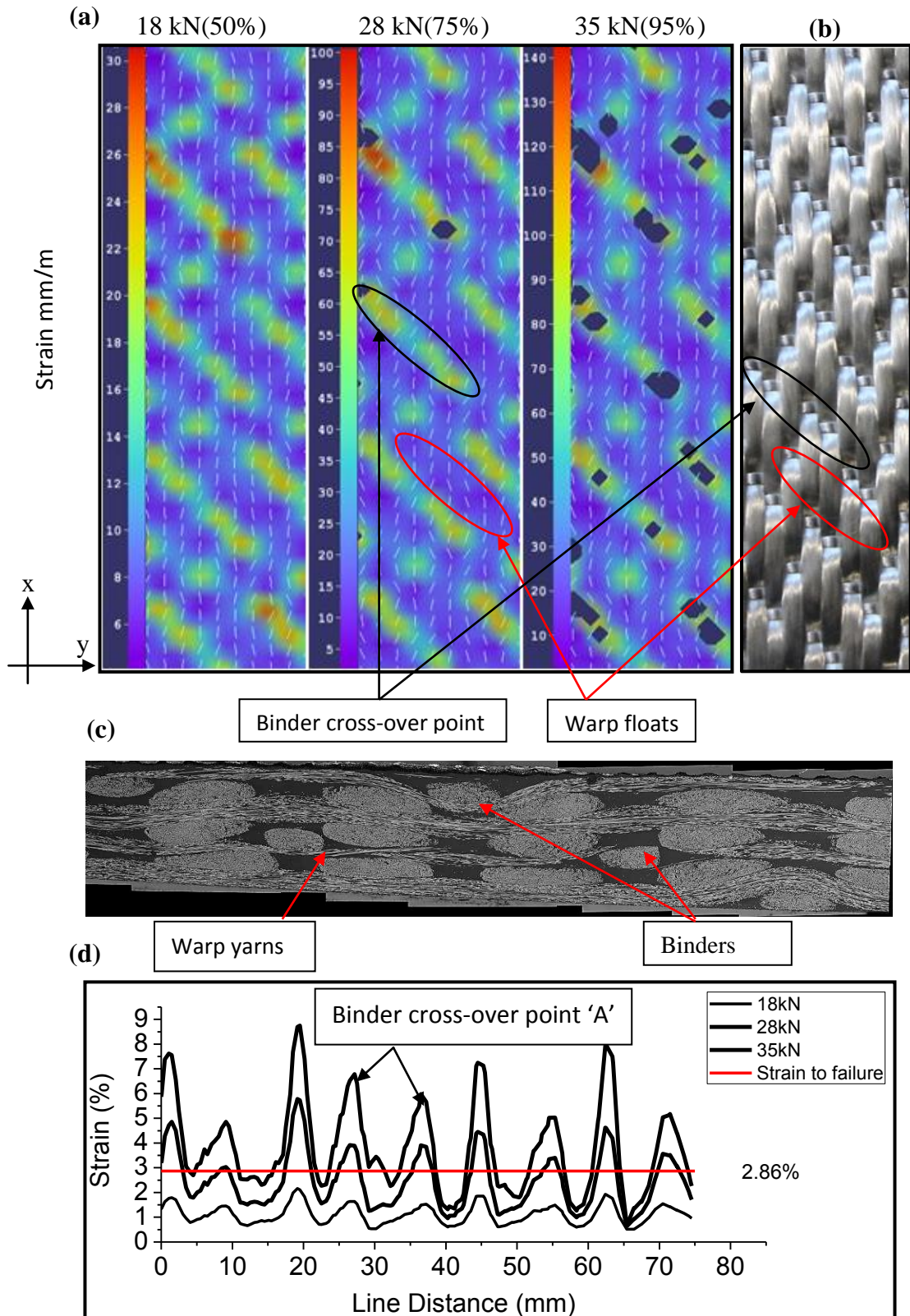
Figure 4.11 Angle interlock in the warp direction (a) Surface strain maps at different load levels show high strain at binder cross-over points (b) Photograph of 3D woven fabric (c) SEM Image along warp yarns (d) Strain profiles showing local strain variation along a straight line at different load levels (x is the loading direction)

(Purple and orange colours represent the lowest and the highest strain values, respectively where the maximum strain value increases with the load)
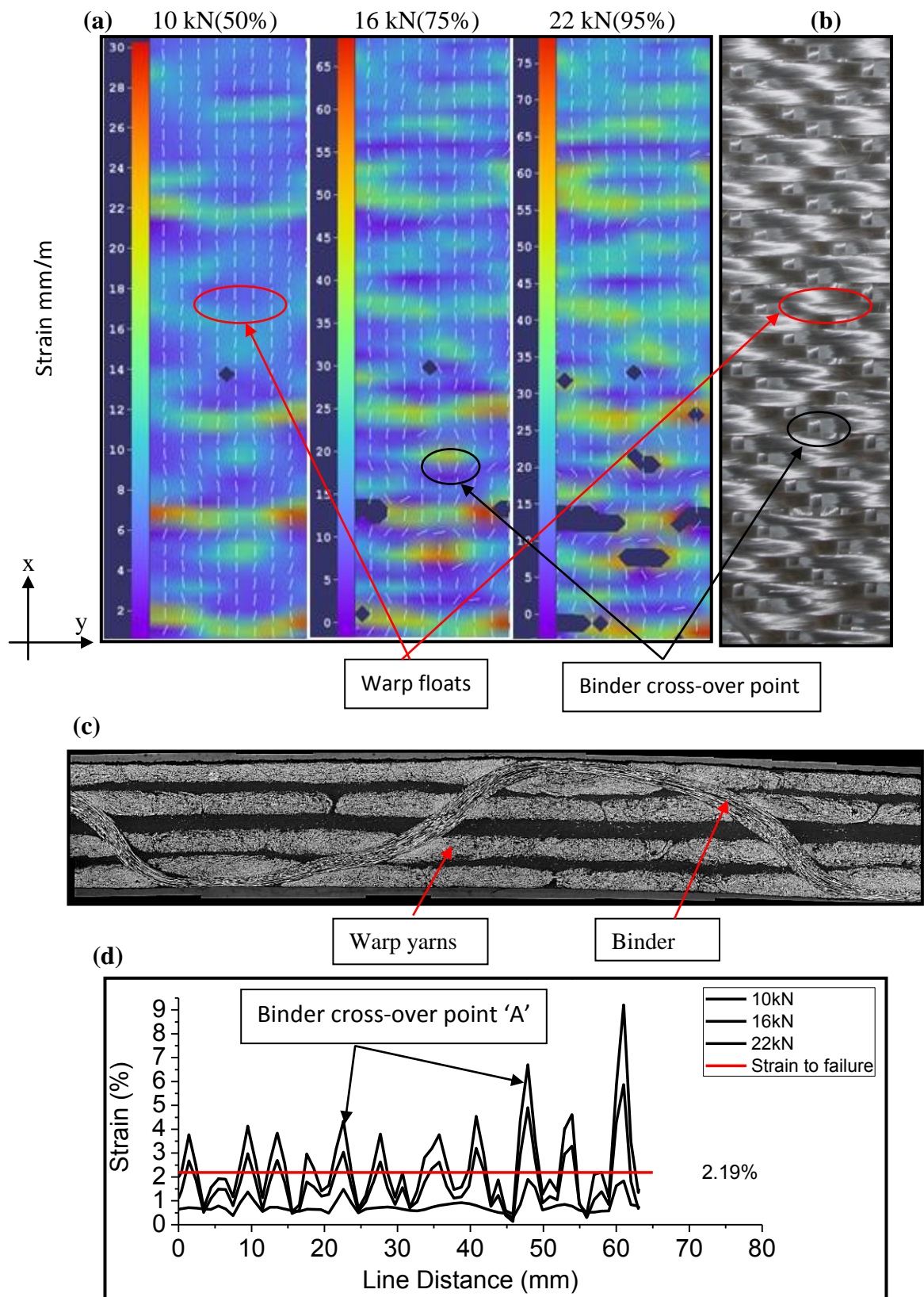
Figure 4.12 Angle interlock in the weft direction (a) Surface strain maps at different load levels show high strain at binder cross-over points (b) Photograph of 3D woven fabric (c) SEM image along binder yarn (d) Strain profiles showing local strain variation along a straight line at different load levels(x is the loading direction)

(Purple and orange colours represent the lowest and the highest strain values, respectively where the maximum strain value increases with the load)
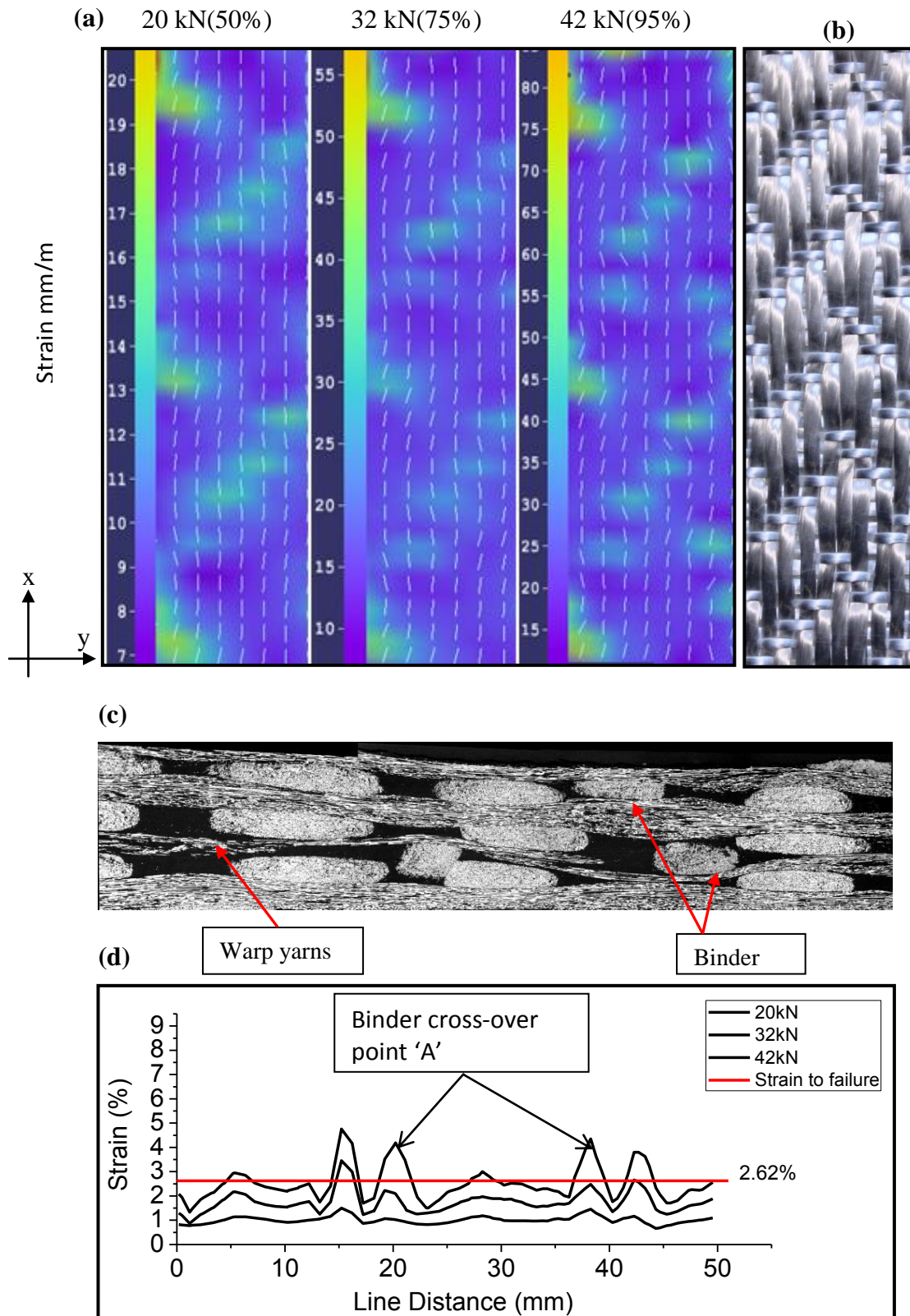
Figure 4.13 Twill Angle Interlock in the warp direction (a Surface strain maps at different load levels show high strain at binder cross-over points (b) Photograph of 3D woven fabric (c) SEM image along warp yarns (d) Strain profiles showing local strain variation along a straight line at different load levels (x is the loading direction)

(Purple and orange colours represent the lowest and the highest strain values, respectively where the maximum strain value increases with the load)
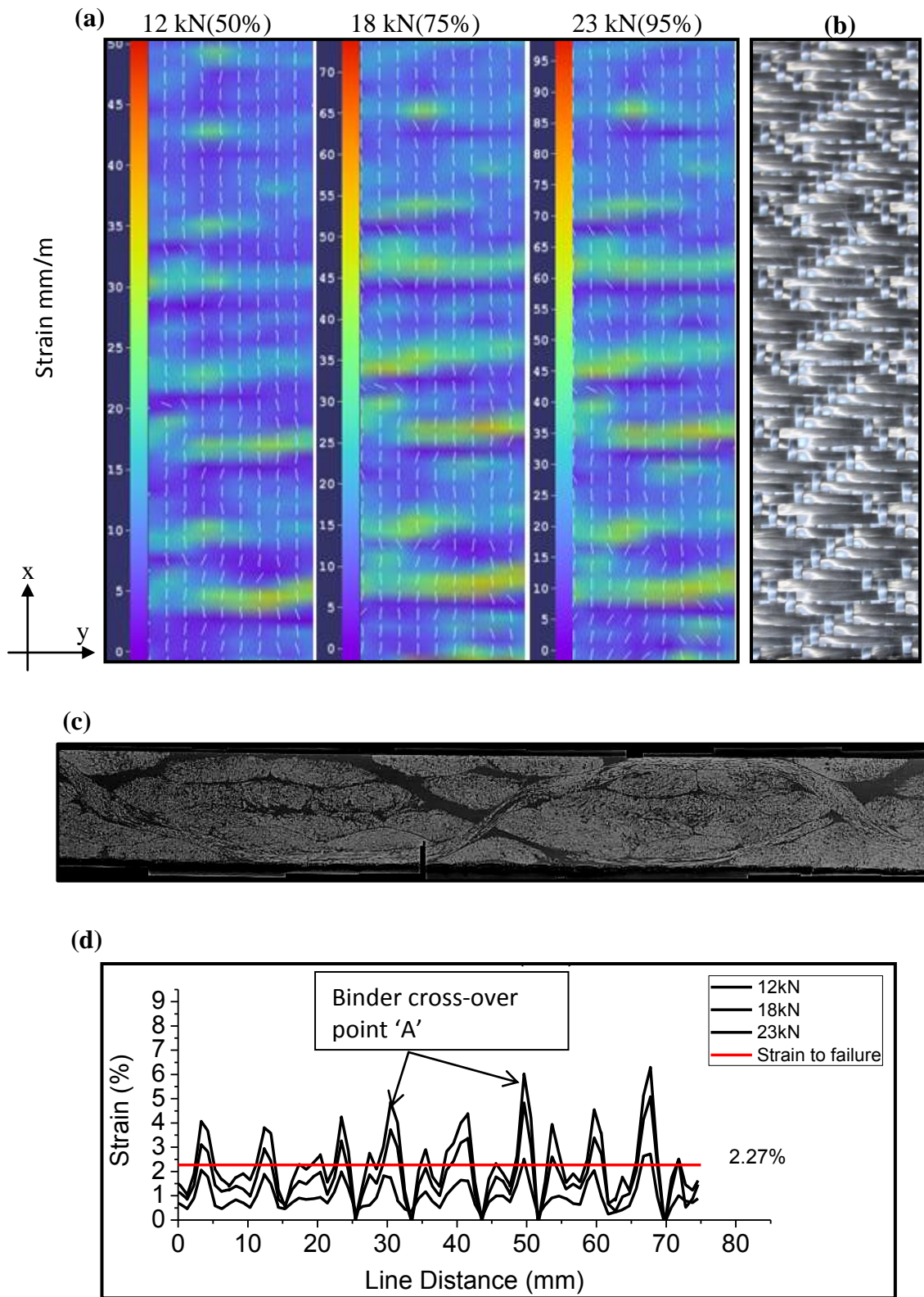
Figure 4.14 Twill angle interlock in the weft direction (a) Surface strain maps at different load levels show high strain at binder cross-over points (b) Photograph of 3D woven fabric (c) SEM image along binder yarn (d) Strain profiles showing local strain variation along a straight line at different load levels (x is the loading direction)

(Purple and orange colours represent the lowest and the highest strain values, respectively where the maximum strain value increases with the load)
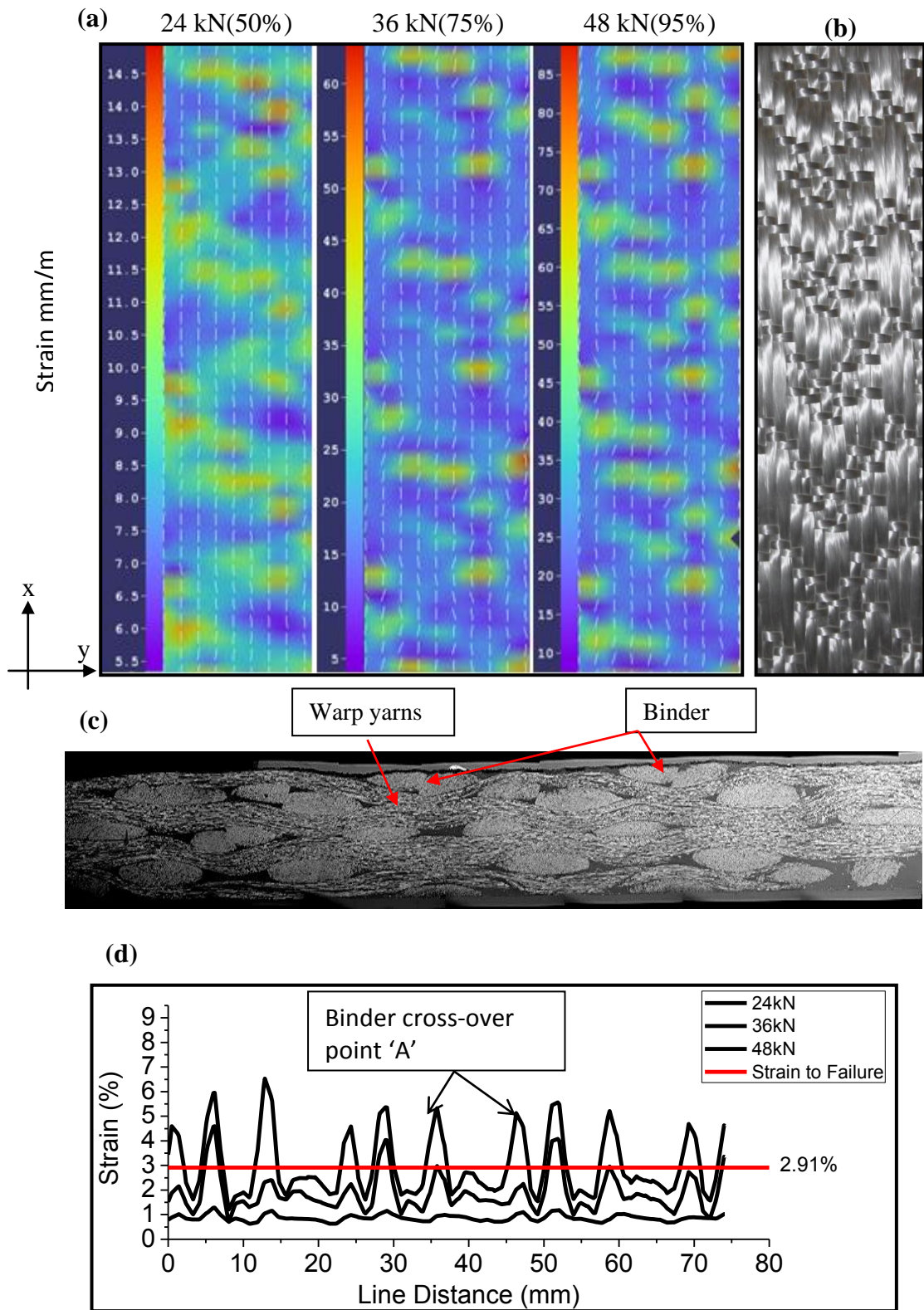
Figure 4.15 Modified angle interlock in the warp direction (a) Surface strain maps at different load levels show high strain at binder cross-over points (b) Photograph of 3D woven fabric (c)SEM image along warp yarns (d) Strain profiles showing local strain variation along a straight line at different load levels (x is the loading direction)

(Purple and orange colours represent the lowest and the highest strain values, respectively where the maximum strain value increases with the load)
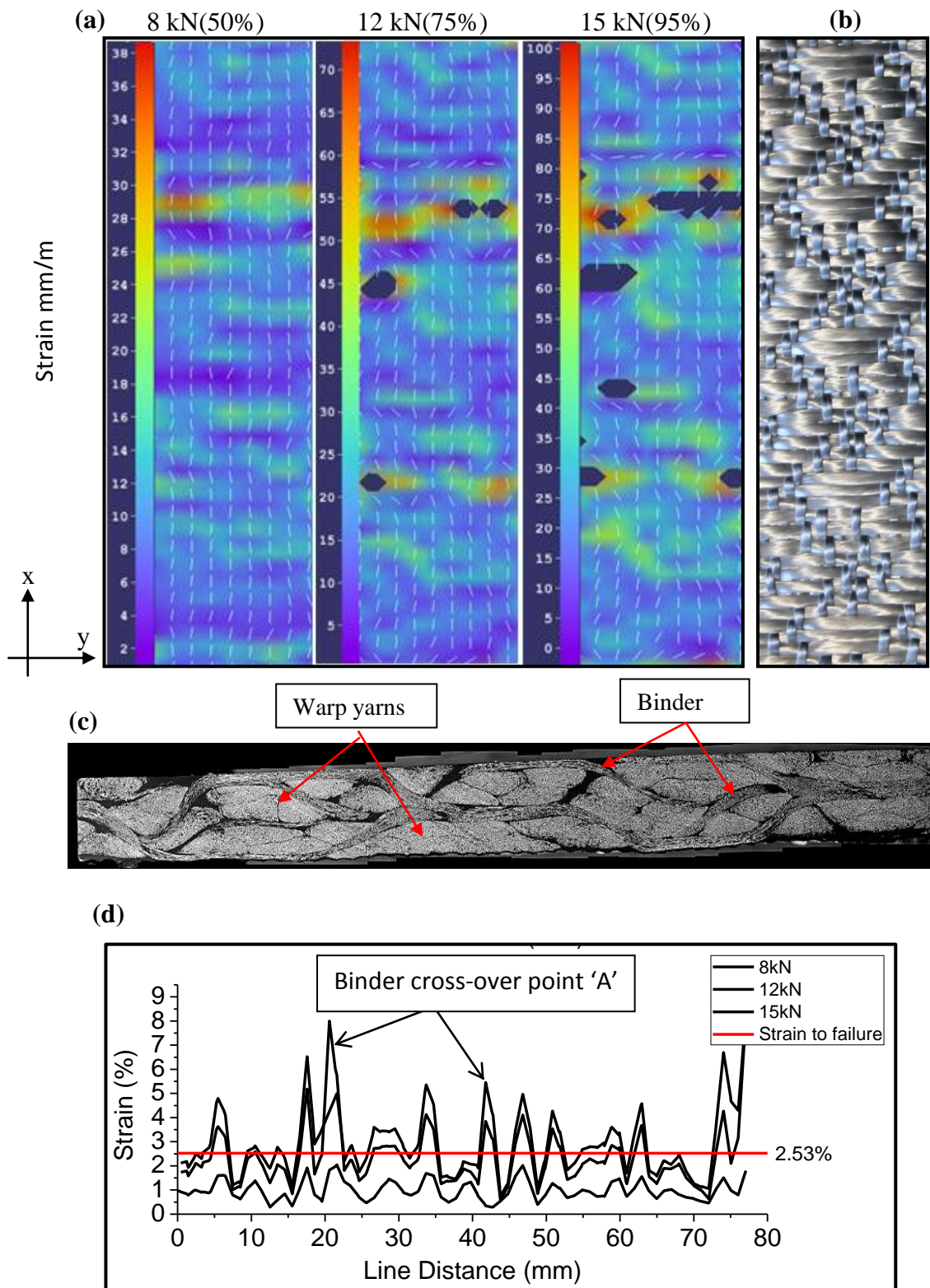
Figure 4.16 Modified angle interlock in the weft direction (a) Surface strain maps at different load levels show high strain at binder cross-over points (b) Photograph of 3D woven fabric (c) SEM image along binder yarn (d) Strain profiles showing local strain variation along a straight line at different load levels (x is the loading direction)

(Purple and orange colours represent the lowest and the highest strain values, respectively where the maximum strain value increases with the load)
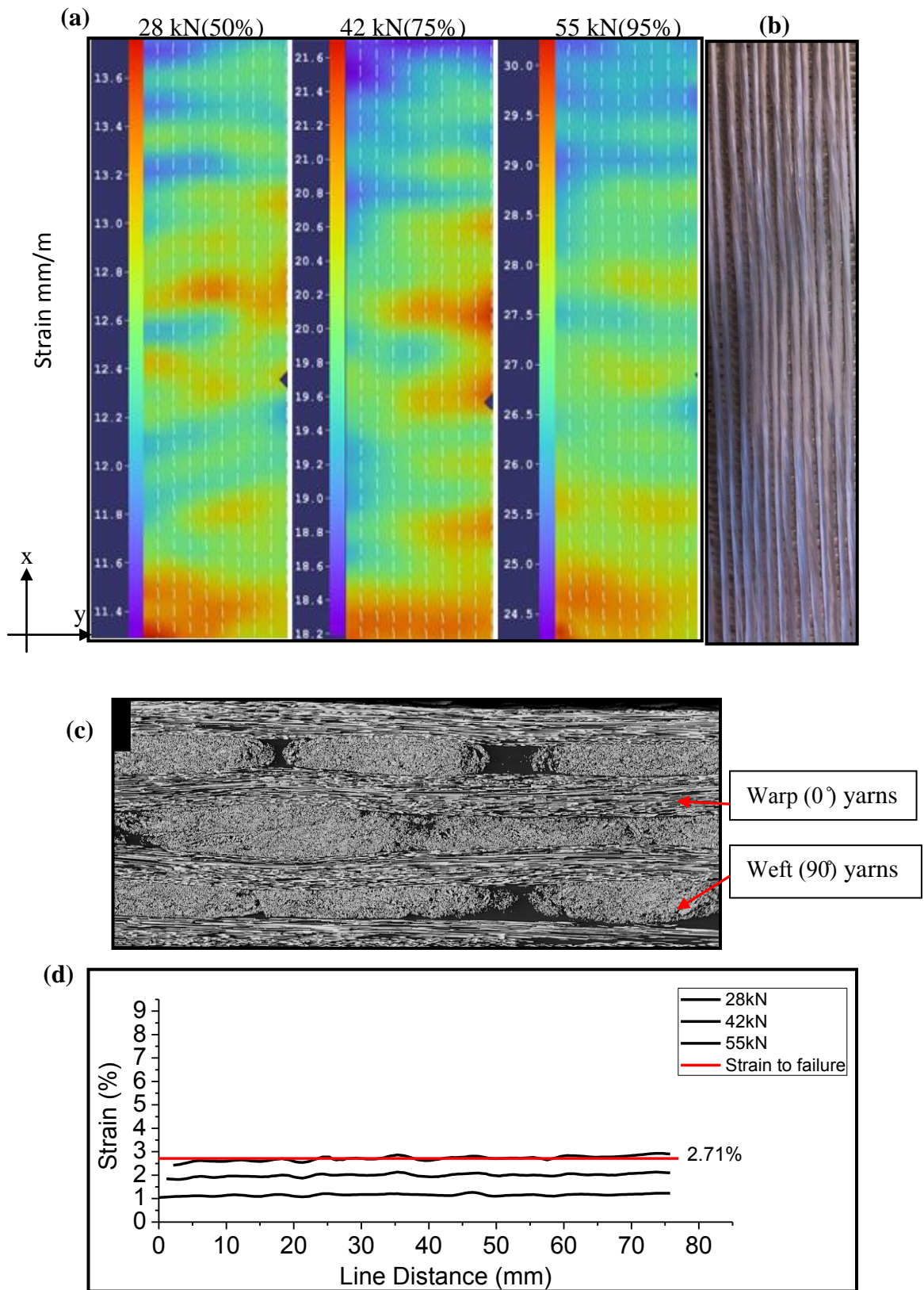
Figure 4.17 UD Cross-ply in the warp direction (a) Surface strain maps at different load levels (b) Photograph of UD cross-ply fabric (c) SEM image along warp yarns (d) Strain profiles showing local strain variation along a straight line at different load levels (x is the loading direction)

(Purple and orange colours represent the lowest and the highest strain values, respectively where the maximum strain value increases with the load)
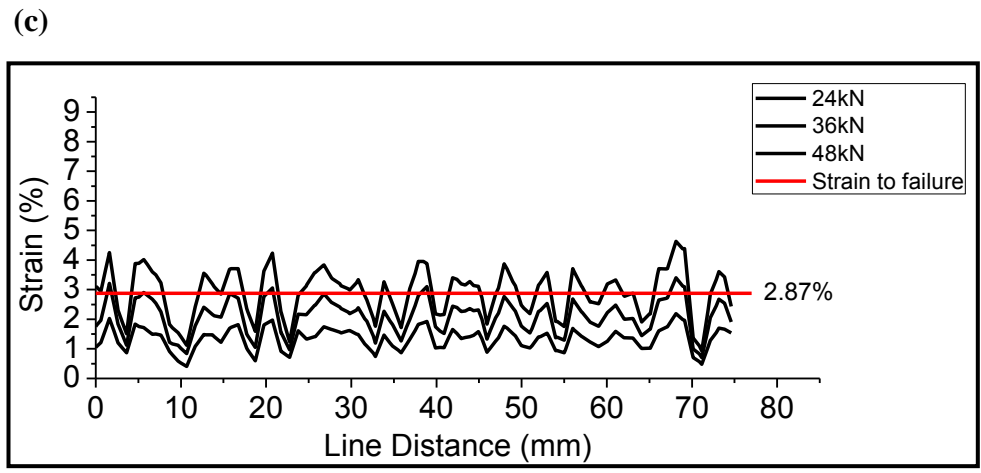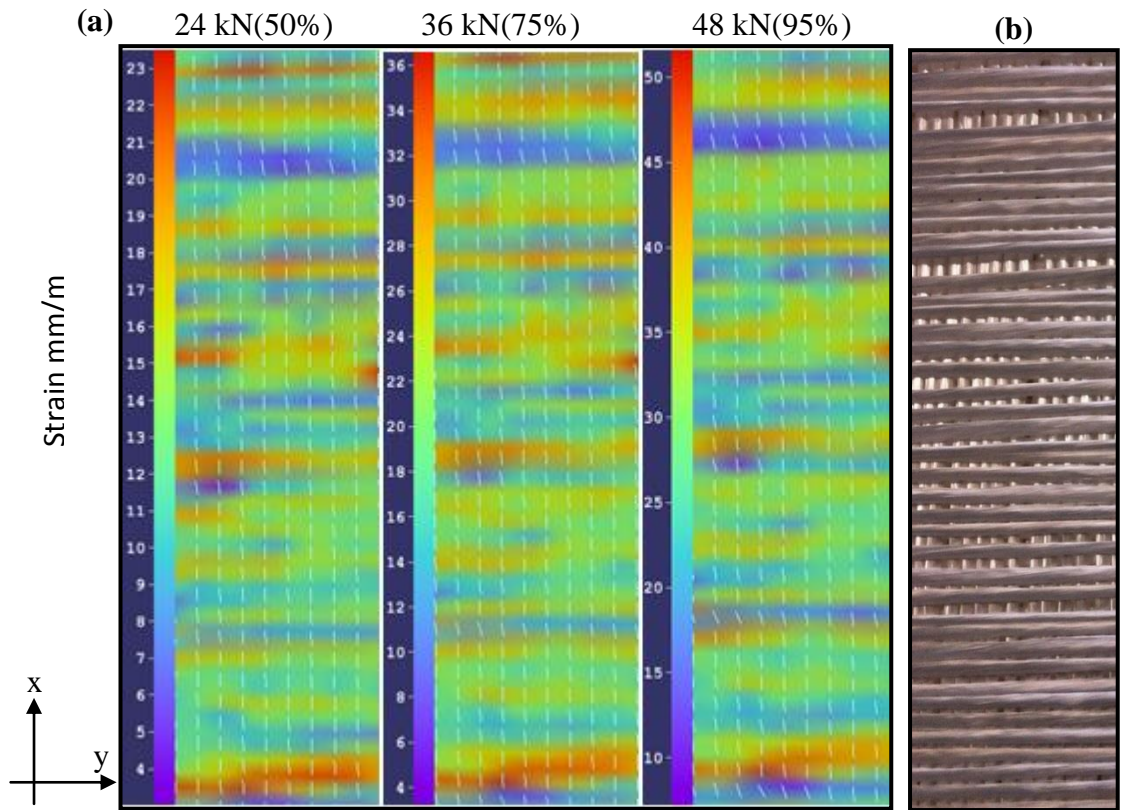
Figure 4.18 UD Cross-ply in the weft direction (a) Surface strain maps at different load levels (b) Photograph of UD cross-ply fabric (c) Strain profiles showing local strain variation along a straight line at different load levels (x is the loading direction)

(Purple and orange colours represent the lowest and the highest strain values, respectively where the maximum strain value increases with the load)
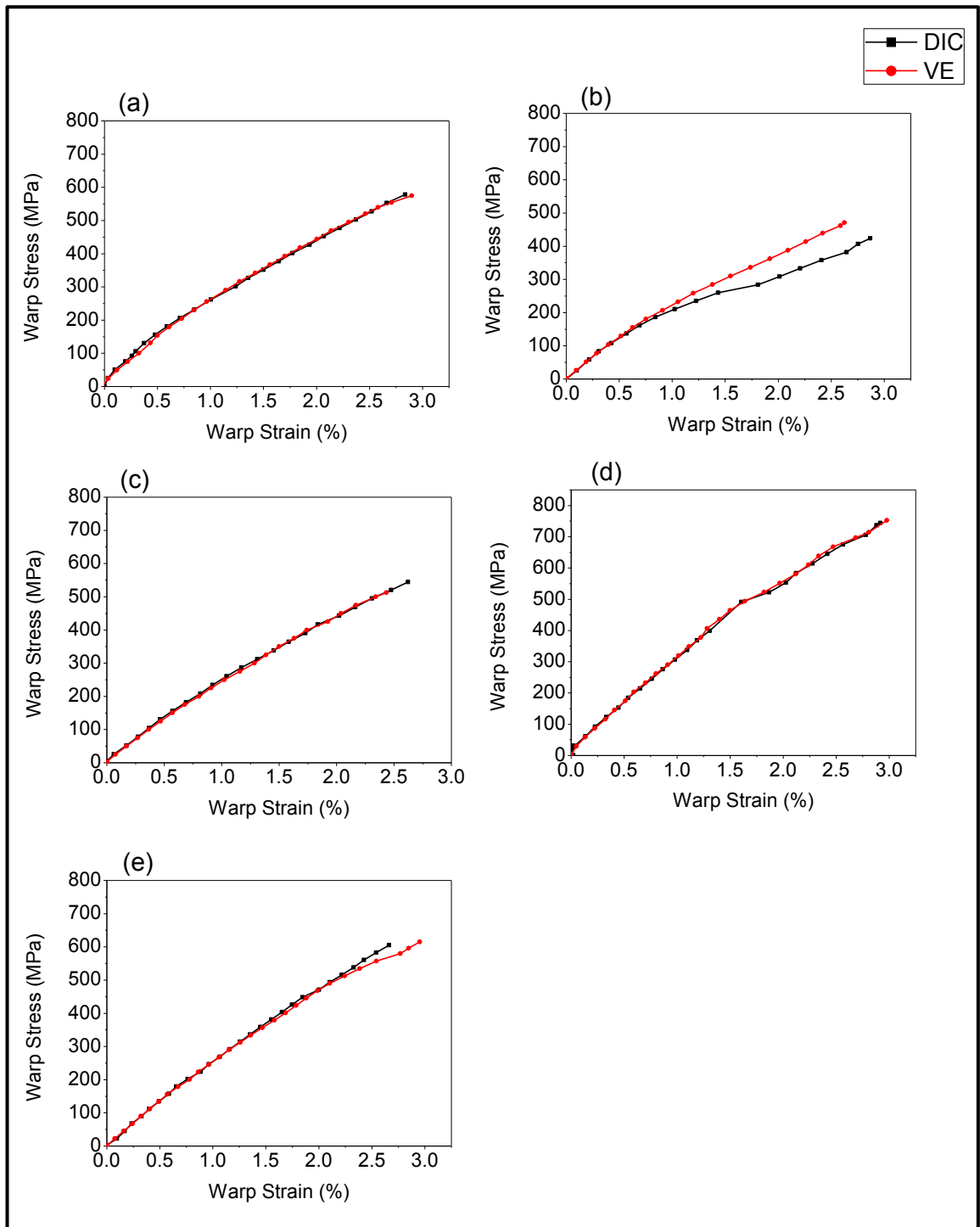
Figure 4.19 Comparison of average strain values from DIC and video extensometer in the warp direction (a) Layer-to-layer (b) Angle interlock (c) Twill angle interlock (d) Modified angle interlock (e) UD cross-ply
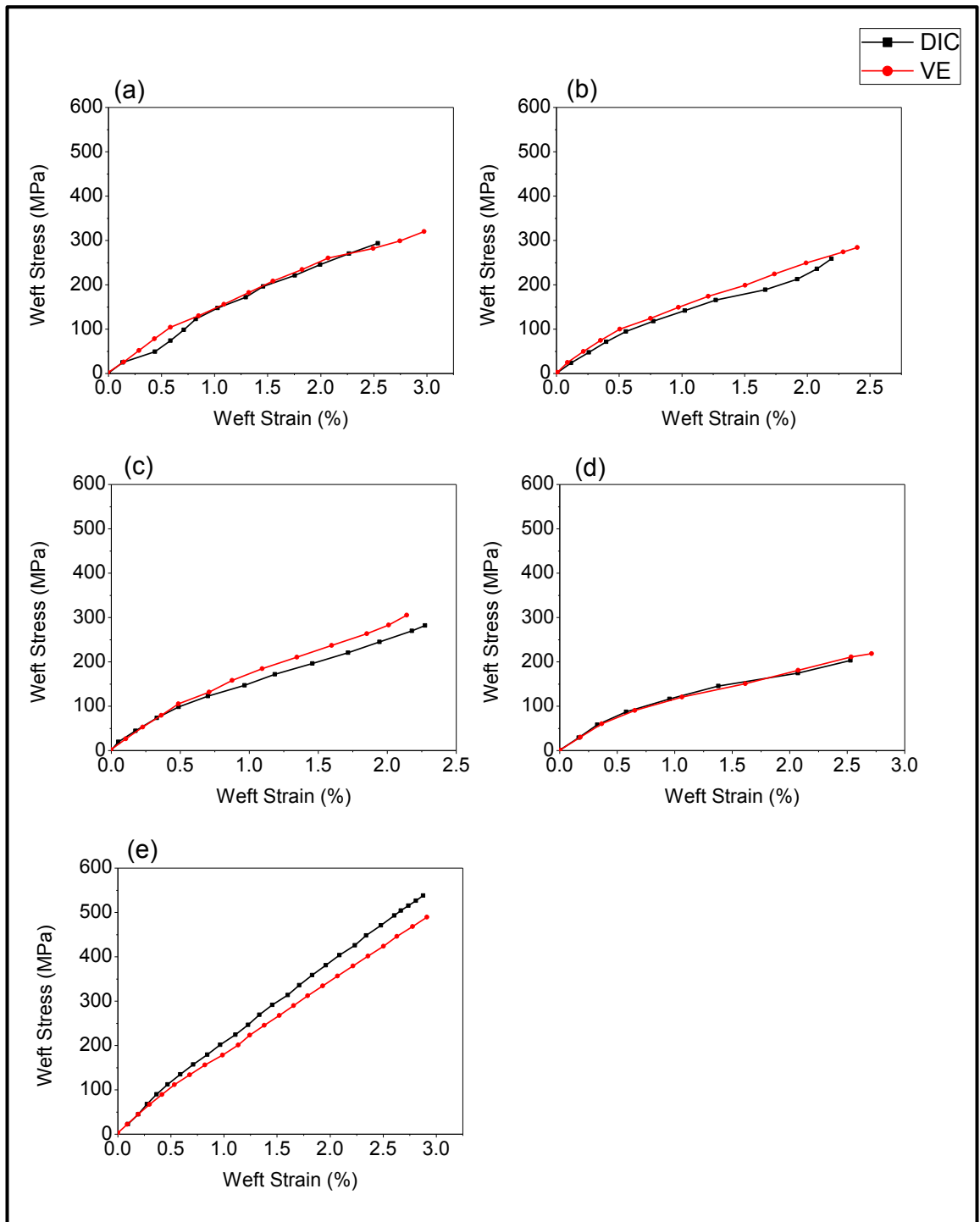
Figure 4.20 Comparison of average strain values from DIC and video extensometer in the weft direction (a) Layer-to-layer (b) Angle interlock (c) Twill angle interlock (d) Modified angle interlock (e) UD Cross-ply

4.4 Summary

Tensile strength, modulus, strain-to-failure and local strain behaviour of four different 3D woven composites: layer-to-layer, angle interlock, twill angle interlock and modified angle interlock, were evaluated in the both warp and weft directions to study the influence of weft binder on in-plane properties. A comparative analysis of 3D woven composites with a UD cross-ply laminate was also performed in this study.

The results showed that the ultimate strength and modulus of UD cross-ply composites are higher than those of the 3D woven composites because of the presence of straight yarns in both directions (warp and weft). The difference in ultimate strength is more significant for AI structures in the warp direction and MAI in the weft direction. In those directions the combined effect of crimp, stress concentration at the binder yarn points, and number of binder yarns per unit area contributed to lower the tensile strength of AI and MAI structures. However the modulus of the 3D woven composites was less affected by the presence of binder yarn, and even the modulus of TAI was even slightly higher than the UD laminate in the weft direction. Among the 3D woven structures, the modified angle interlock exhibited the highest tensile strength in the warp direction but the lowest strength and stiffness in the weft direction, which was a consequence of high crimp % and more binder yarns along the loading direction. LTL and TAI had almost the same strength in both warp and weft directions, however the long binder floats of TAI reduced the binder crimp and increased the amount of aligned tows in the loading direction, resulting superior modulus in both the warp and weft directions. It was observed for the 3D woven composites that the binder crimp, shearing of the binder yarn at the cross over point and the presence of resin-rich areas around the binder are the reasons for the strength reduction in both the warp and weft directions.

Strain concentration at binder interlacement points was also observed in the surface strain maps of 3D woven composites. The strain maps revealed that the average strain within the 3D woven composites was quite heterogeneous and that the levels of localized strain were mainly higher than the strain to failure. The strain maps represent weave behavior under tensile load. Further analysis of local strain profiles showed that in 3D woven composites maximum strain occurs at the binder interlacement point in both the warp and weft directions. The splitting of warp yarns and specimen rupture at the interlacement point in the warp and weft directions, respectively, verifies the localized strain concentration due to binder yarn interlacement. The average strain values obtained from both the video extensometer and DIC were fairly similar.

The results showed the dependency of the tensile properties of 3D woven composites upon weave structure, crimp percentage and fibre volume fraction in each direction. By altering the binder path, strength and stiffness properties in the required direction can be improved. The strength and stiffness properties of composite materials are affected by notches. The effect of these notches on the tensile properties of weft bound 3D woven composites will be discussed in the next chapter.

5 Open hole tension behaviour of weft interlaced 3D woven composites

5.1 Introduction

The effect of the presence of notches on the strength of composite materials is one of the main concerns for designers because it causes a large decrease in strength compared with an unnotched laminate. It also exaggerates the complex damage and failure mechanisms of laminate during the loading cycle and causing a wide range of effects, which are not present in unnotched component. Most research has been performed to understand the fracture behaviour and strength reduction of unidirectional (UD) tape and 2D woven composite laminates containing holes or cracks [66, 130-139]. It was observed that due to the yarn interlacement, the failure mechanism of woven fabric composites appear different from the UD tape composites. The notch sensitivity of woven fabric laminates under tension is generally the same as a tape laminate of similar configuration. The fabric laminates tend to be more resistant to splitting and delamination than unidirectional tape laminates, while the undulating nature of the fabric inhibits these damage mechanisms preventing crack propagation in the matrix. This increased resistance to fracture tends to result in a higher notched strength for woven laminates [134, 140, 141]. The notched strength and fracture toughness of composites for specific applications can further be improved by using 3D fibre architecture. Research has shown that 3D woven composites offer higher damage tolerance and fracture and notch insensitivity than 2D laminates [10, 12, 115, 142, 143]. However the prediction of the mechanical properties of 3D composites is a challenging task, as their deformation and failure mechanisms are very complex. Early studies showed that 3D woven composites had higher fracture and lower notch sensitivity in

tension, compression and fatigue. The reduced notch sensitivity of 3D woven composites was partly attributed to the presence of geometrical flaws that were broadly distributed, both spatially and in strength; and partly to the coarseness of the reinforcing yarns, leading to extensive debonding and reduced stress intensification around sites of failure [10, 115].

While the notched behaviour of 3D woven composites has been studied in the past, no work has been reported on the notched strength of weft-bound 3D woven composites under tensile loading. In this chapter, the tensile behaviour of four different 3D woven glass/epoxy laminates and a UD cross-ply laminate, all containing a single hole is investigated. The effect of the weave structure on notch sensitivity is investigated experimentally in both warp and weft directions and DIC is used to analyse the damage propagation at different load levels.

5.2 Experimental procedure and specimen geometry

An open-hole tension test was performed on the four different 3D woven composites LTL, AI, TAI, MAI and the UD cross-ply laminate in both the warp and weft direction.

Test specimens were cut from the laminates in accordance with ASTM test standard D5766, to be tested in both the warp and weft directions. A diamond saw with water cooling/lubricant was used to cut 36 mm wide and 200mm long, straight sided specimen coupons from the panels. Then according to the test standard a hole with a diameter (a) to width (W) ratio, $a/W = 1/6$, was drilled at the centre of each specimen as per the standard. The drilling was carried out with a steel-tipped drill. A metal clamp was used to hold the specimen in place.

Open hole tensile testing was carried out according to ASTM standard D5766 [144]. Tests were performed in both the warp and weft directions. The experimental values of

notched strength, σ_n, are based on the gross cross-section area. A video extensometer and DIC were used for strain measurement, both being non-contact strain measuring devices. An Instron 5982 R2680 testing machine was used to perform the tests.

5.2.1 Strain measurement with the video extensometer

The notched specimens were marked in the longitudinal direction in the active gauge length using a stencil at a distance of 25mm from the hole to measure axial strain. After marking, the specimens were tested in both the warp and weft directions at a constant speed of 2 mm/min as shown in Figure 5.1a. Five specimens were tested for each sample type and the average notched strength was calculated.

5.2.2 Surface strain measurement using DIC

DIC was performed on one specimen from each structure (3D woven and UD cross-ply) to analyze local strain as depicted in Figure 5.1b. Specimen preparation and image capturing criteria have already been described in Chapter 4. The strain maps at different load levels were obtained to analyze damage progression in each direction.
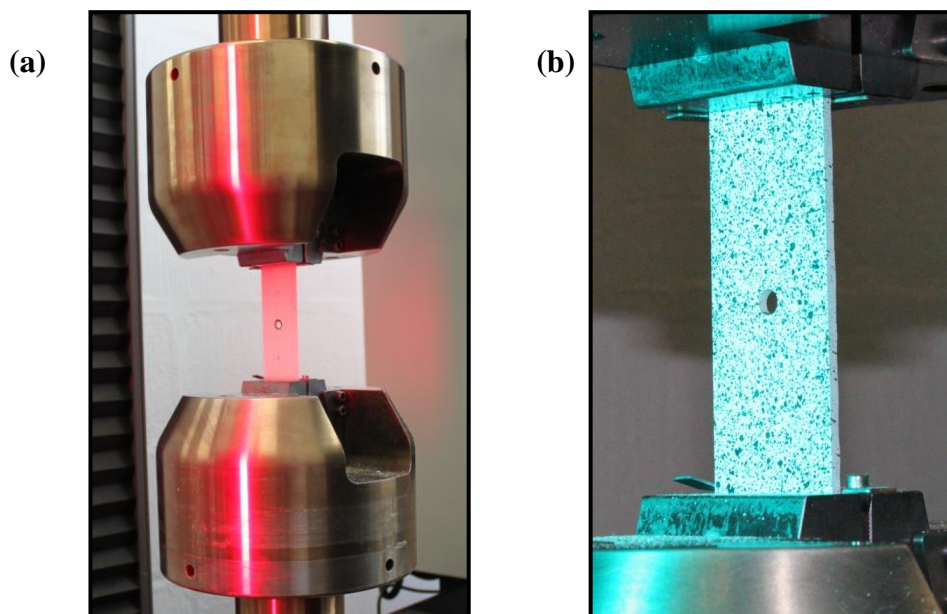
Figure 5.1 Open hole tensile test of specimen by using (a) Video extensometer (b) DIC

5.3 Results and discussion

Load-extension and stress-strain graphs for S2glass/epoxy UD cross-ply and 3D woven laminates are shown in Figure 5.2 and Figure 5.3. The notched and un-notched strength values in both the warp and weft direction are listed in Table 5.1 and Table 5.2.
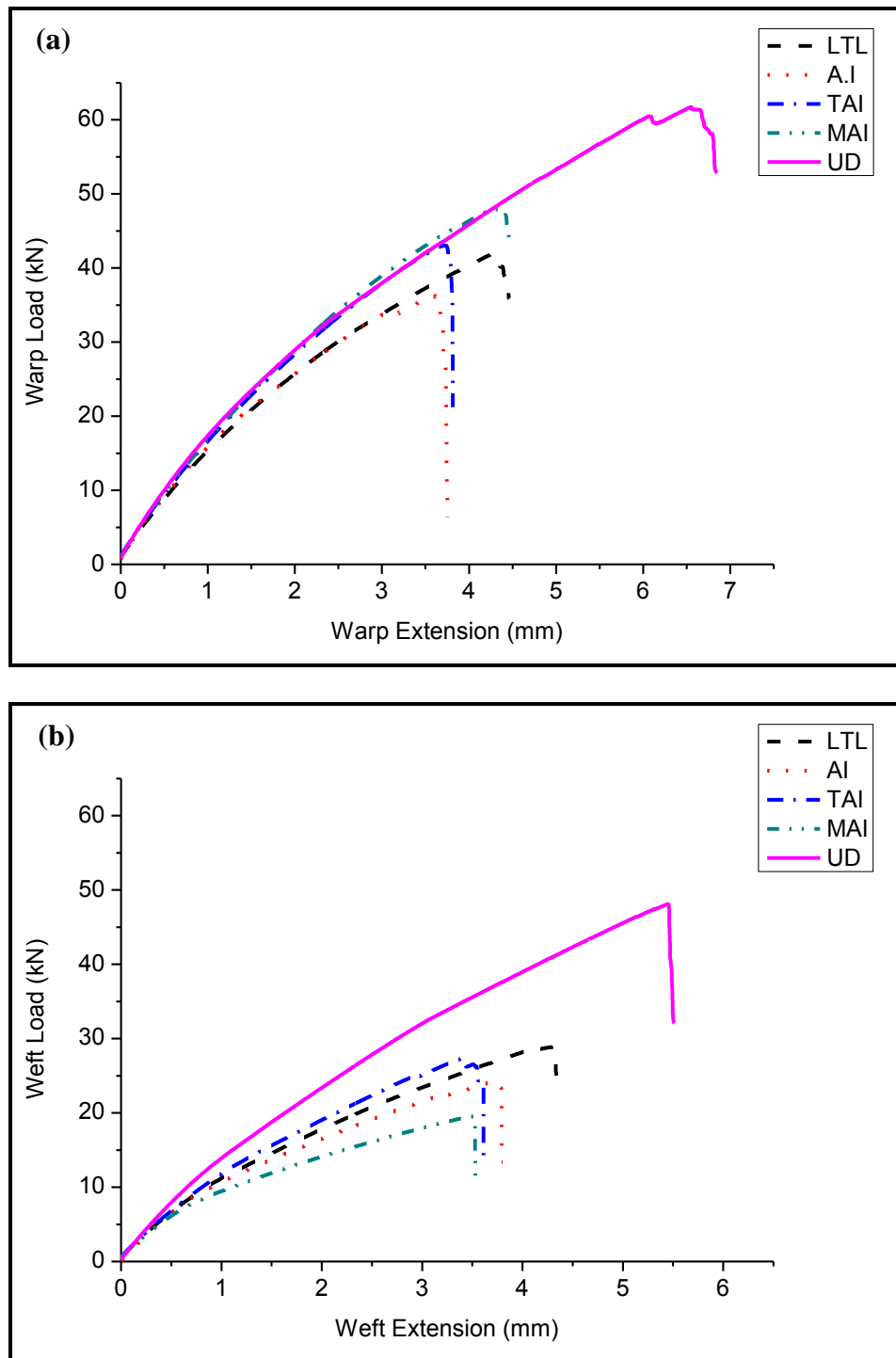
Figure 5.2 Load-extension curves (a) Warp direction (b) Weft direction

The highest notch strength in the warp direction was found for UD cross-ply followed by MAI, LTL), TAI, and AI. Whereas in the weft direction, UD cross-ply had the highest strength, and for 3D woven structures the notch strength decreased in the following sequence: LTL, TAI, AI then MAI.
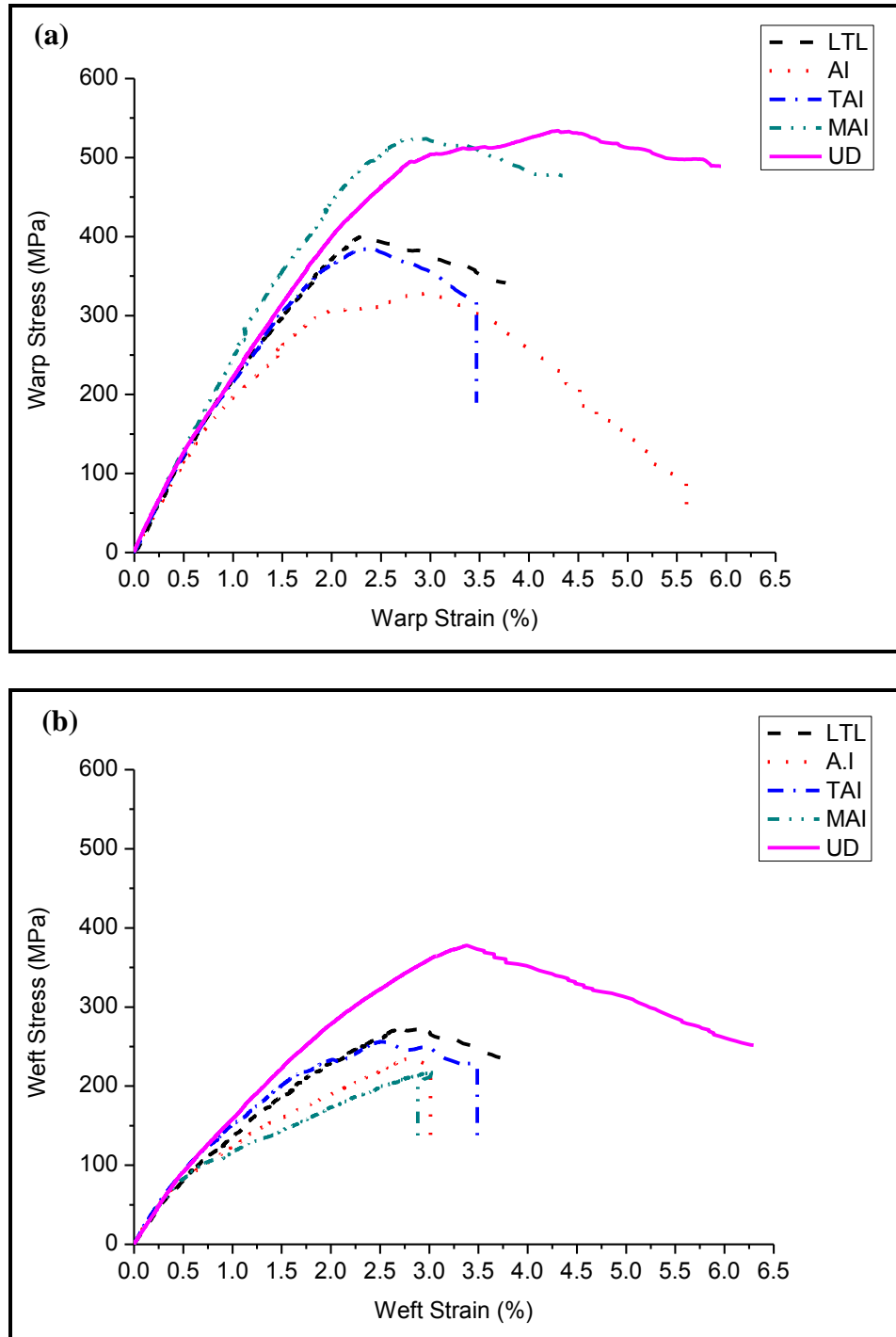
Figure 5.3 Stress-strain curves (a) Warp direction (b) Weft direction

The stress-strain curves exhibited non-linear behaviour with the degree of non-linearity dependent on the alignment of the yarns in the loading direction, as well as the fabric structure. This non-linear behaviour is more pronounced in the weft direction of 3D woven structures due to a lower number of straight yarns along the loading direction. Several discontinuities on the stress-strain curves indicate the gradual failure of the notched laminates, in both warp and weft directions.

The elastic modulus of the notched specimens was measured within a strain range of 0.1% - 0.3% in both the warp and weft directions, as shown in Figure 5.4 and Figure 5.5 respectively. However, the effect of the notch on laminate stiffness is not that significant, and this data falls in the same range as the moduli of the unnotched specimens.
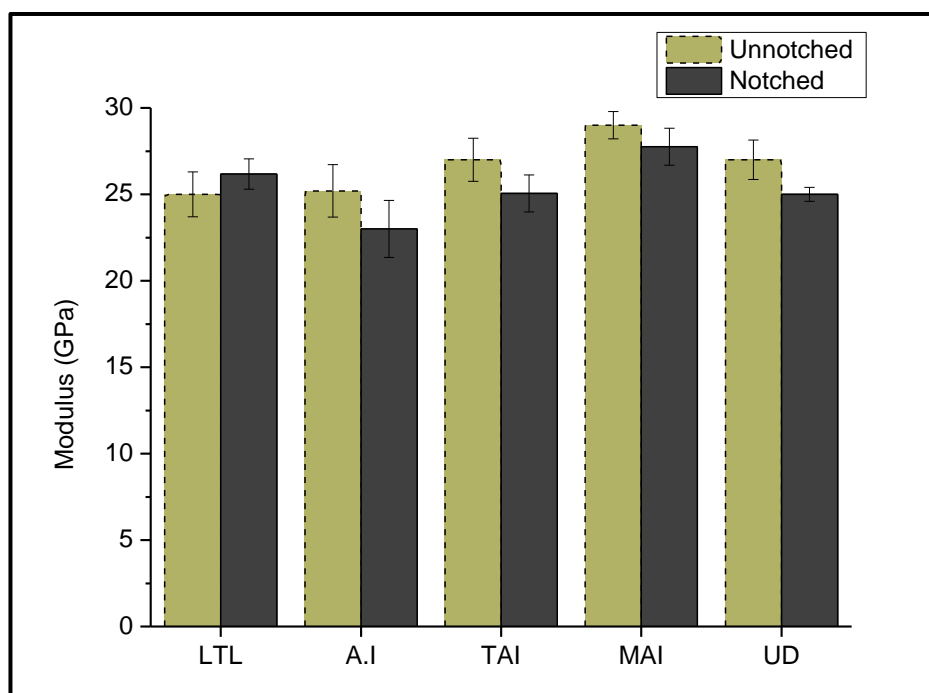
Figure 5.4 A comparison of notched and unnotched modulus in the warp direction

Normalised strength (σ_n/σ_{un}) values for 3D woven and UD laminates are shown in Table 5.1 and Table 5.2 for the warp and weft direction, respectively. The strength was normalized by dividing notched strength by the unnotched strength of specimens

presented in Chapter 4. Figure 5.6 and Figure 5.7 display the notch behaviour of 3D woven and UD laminates in comparison to notch sensitive (ideally brittle) and notch insensitive (ideally ductile) materials. The equation of line for the notch sensitive and notch insensitive materials [145] are calculated as following:

Notch Sensitive (Brittle materials):

$$\sigma_n / \sigma_{un} = (1-D/W)/ K_T \qquad\qquad (1)$$

$$K_T = 2+ (1-D/W)^3$$

Notch Insensitive (Ductile materials)

$$\sigma_n / \sigma_{un} = (1-D/W) \qquad\qquad (2)$$

Where, σ_n = Notched stress, σ_{un} = Unnotched stress, D= Hole diameter,

W=Specimen width and K_T = Stress concentration factor
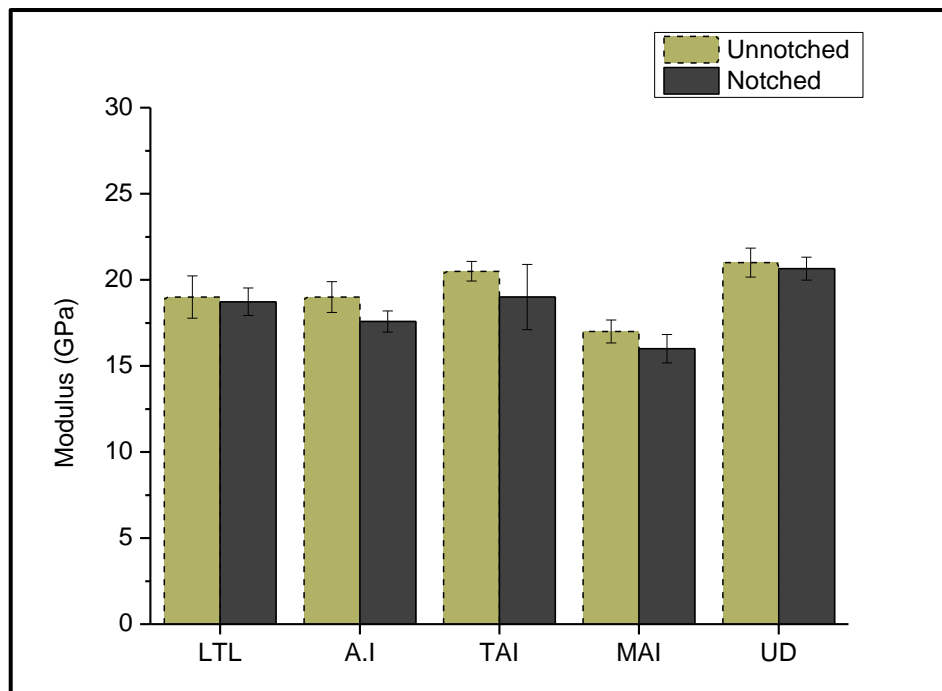
Figure 5.5 A comparison of notched and unnotched modulus in the weft direction
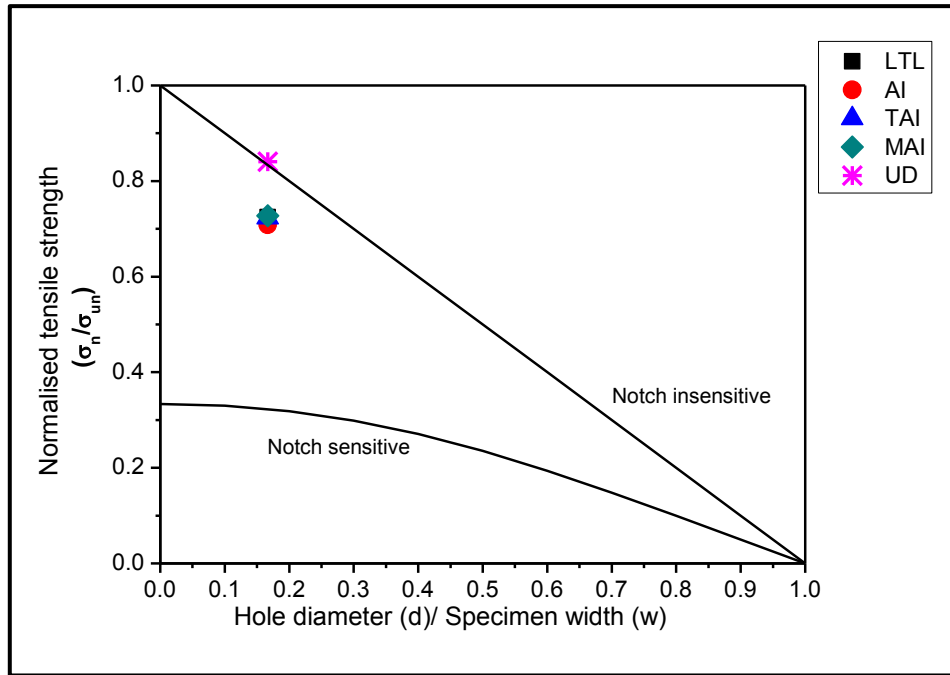
Figure 5.6 Notch sensitivity/normalised strength in the warp direction

(Notch sensitive = σ_n / σ_{un} = (1-D/W)/ K_T, Notch insensitive = σ_n / σ_{un} = (1-D/W))

Table 5.1: Notch-sensitivity parameters in the warp direction

Structure	Warp Stress (MPa)		(σ_n / σ_{un})
	Unnotched failure Stress (σ_{un})	Experimental Notched Stress (σ_{un})	
Layer-to- Layer	563 ± 19.71	408 ± 15.59	0.72
Angle Interlock	476 ± 24.12	337 ± 10.73	0.71
Twill Angle Interlock	520 ± 23.78	376 ± 12.92	0.72
Modified Angle Interlock	704 ± 31.81	512 ± 10.71	0.73
UD Cross-Ply	614 ± 30.69	516 ± 15.60	0.84

The normalized strength is a measure of the notch sensitivity of each structure and a higher value means the material is less notch sensitive. The normalized strengths show that 3D woven and UD cross-ply laminates are notch insensitive in both the warp and

weft directions. In the warp direction, UD cross-ply laminate attains high normalised strength, suggesting that the laminate is less notch sensitive. The higher failure stress of notched UD laminate is due to increased delamination which allows more shear cracking, whereas in the 3D woven composites delamination and yarn splitting are constrained due to binder yarn which inhibits these stress relieving and energy-absorbing mechanisms at the notch tip. In the weft direction, however the undulation of the binder yarns makes it easier to yield to damage, so the 3D woven composites achieved a higher normalized strength and failed in a more ductile manner, especially the LTL, MAI and TAI structures. As mentioned by Cox [10] and Tsai [142], any geometrical irregularities such as yarn crimp enhance the notch insensitivity of a material through load redistribution.
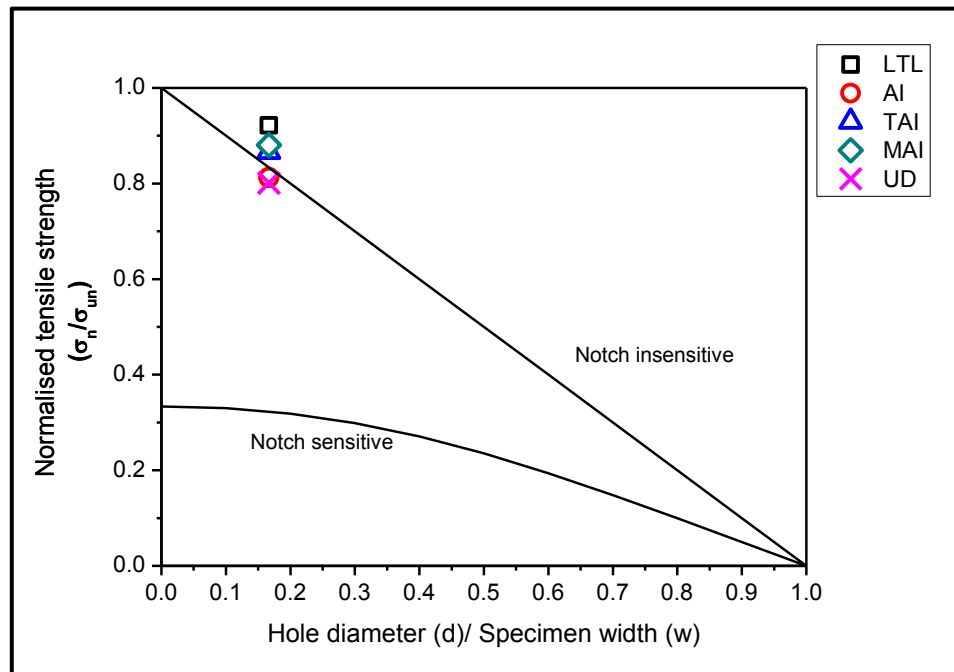
Figure 5.7 Notch sensitivity/normalised strength in the weft direction

(Notch sensitive = σ_n / σ_{un} = (1-D/W)/ K_T, Notch insensitive = σ_n / σ_{un} = (1-D/W))

Table 5.2: Notch-sensitivity parameters in the weft direction

Structure	Weft Stress (MPa)		(σ_n / σ_{un})
	Unnotched Stress (σ_{un})	Experimental Notched Stress (σ_{un})	
Layer-to Layer	293 ± 17.80	270 ± 2.50	0.92
Angle Interlock	272 ± 19.21	221 ± 8.84	0.81
Twill Angle Interlock	291± 18.34	252 ± 15.08	0.87
Modified Angle Interlock	218 ± 3.58	192 ± 16.14	0.88
UD Cross-Ply	495 ± 24.75	397 ± 15.06	0.80

DIC analysis of the 3D woven composites shows that when the 3D woven specimens were loaded in the warp direction, cracks initiated at 90^0 to the loading direction, and then propagated along the warp direction where resistance is lower due to longer floats of warp yarns in the loading direction. Whereas in the weft direction, specimen cracks propagate at 90 degree to the loading direction, beyond 75% of failure load damage propagates in both the longitudinal and transverse directions. Crack propagation leads to delamination, yarn splitting and the failure of the laminate. The failed specimens verify the phenomenon of crack propagation observed by DIC. In the UD cross-ply laminates, there are no interlacements between the yarn layers, so that after the crack initiation damage propagates along the loading direction for both warp and weft specimens.

The damaged area is a combination of matrix cracking, delamination, fibre breakage and fibre pull-out etc. After testing, specimen photographs (Figure 5.8 and Figure 5.9) show that in the 3D woven structures the damaged area is more concentrated around the hole in the weft direction, whereas in the warp direction the damaged zone is more than half of the gauge length and spread along the loading direction. However, for the UD

cross-ply laminates delamination occurs along the entire gauge length, in both warp and weft directions.
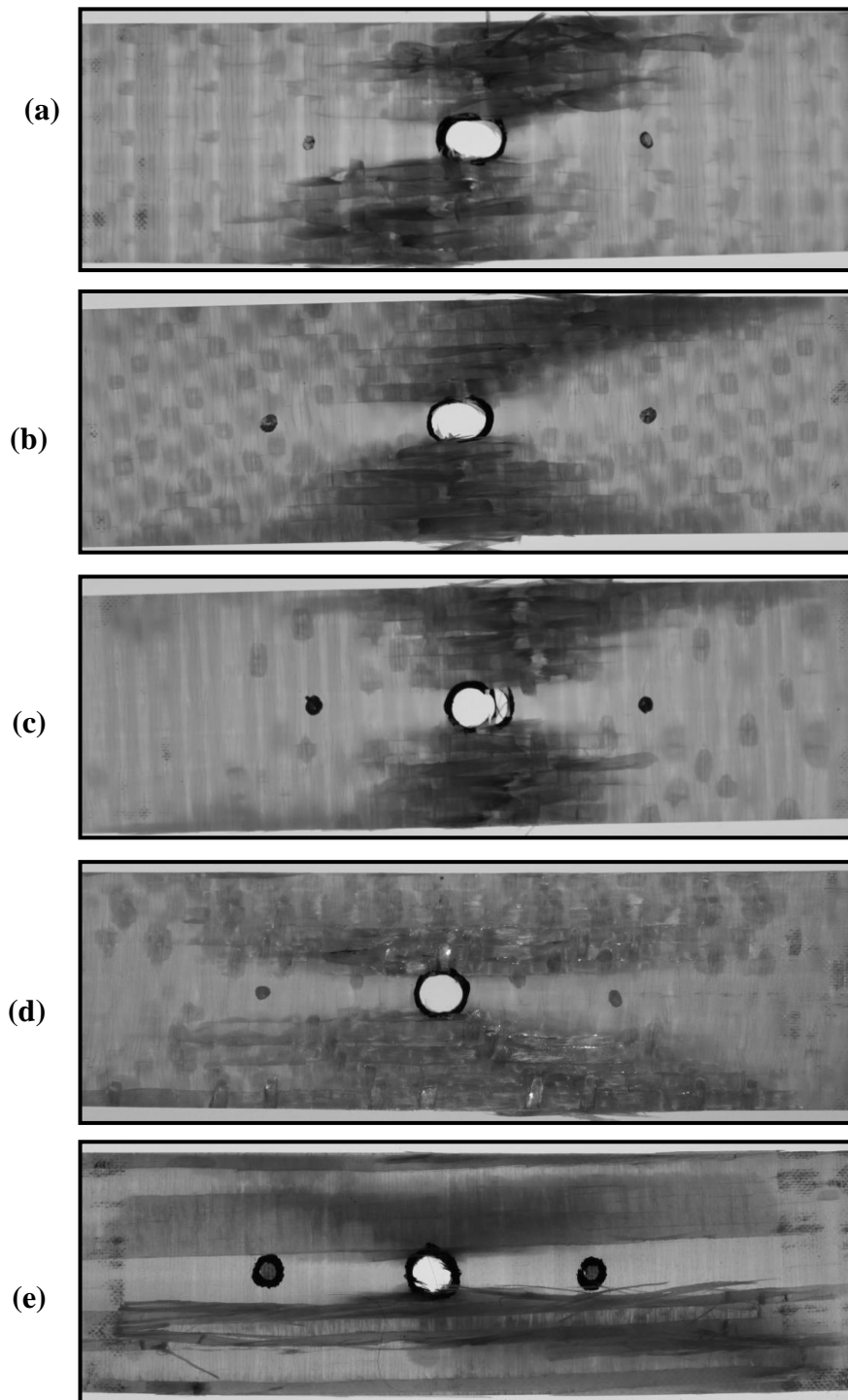
Figure 5.8 Tested specimen in warp direction (a) Layer-to-Layer (b) Angle Interlock (c) Twill Angle Interlock (d) Modified Angle Interlock (e) UD Cross-Ply

(Images taken on a light table and damage shown as dark areas)
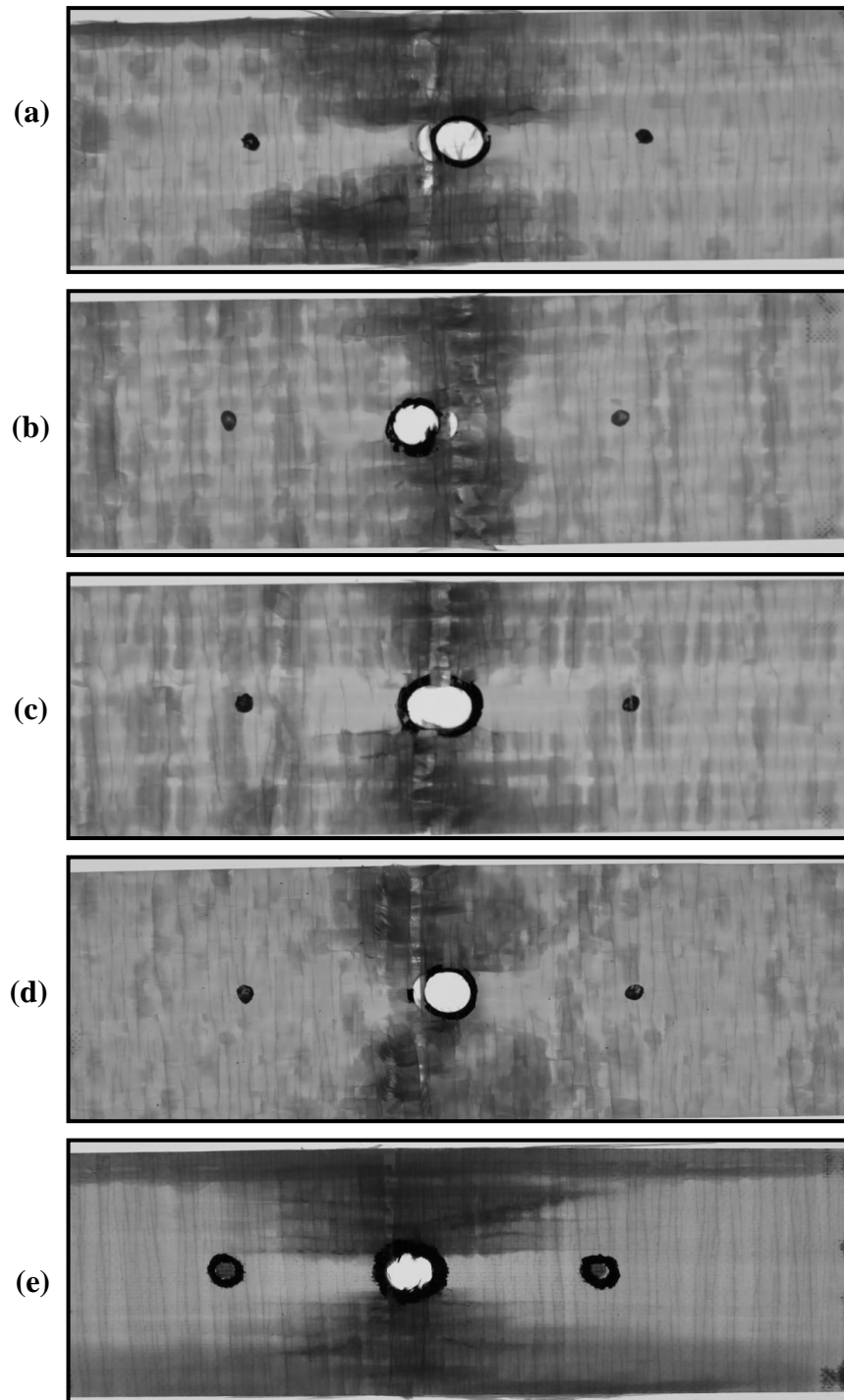
Figure 5.9 Tested specimen in weft direction (a) Layer-to-Layer (b) Angle Interlock (c) Twill Angle Interlock (d) Modified Angle Interlock (e) UD Cross-Ply

(Images taken on a light table and damage shown as dark areas)

5.4 Damage mechanism

The progression of damage in 3D woven and UD cross-ply laminates at 50%, 75%, and

95% of the failure load is shown in Figure 5.10 to Figure 5.14. Visual observation and

DIC images show that axial splitting in the 3D woven structures is limited compared to that which occurs in the UD cross-ply laminate. As in the 3D woven structures, warp (0 °) and weft (90 °) yarns are interlaced through the binder yarns in the thickness direction. When the notched specimens of 3D woven composites were loaded in tension, cracks were initiated at 90 ° to the loading direction and then propagated in both the longitudinal and transverse direction until they ran into a binder yarn. When the cracks reached the point of interlacement, the binder yarn hindered the crack path with the crack following the direction where the resistance is lowest. As the load increases, the damage zone increases in the form of delamination and yarn splitting. In the warp loaded specimen, the stress relieving and energy absorption mechanism is inhibited by the binder yarns, as they restrict crack propagation and delay the splitting of yarns along the loading direction. Whereas in a weft loaded specimen, the binder yarns are along the loading direction and the straightening of the binder yarns lets the damage grow more easily, with the stress being relieved in the form of extensive matrix cracking, delamination and transverse splitting. This behaviour is similar to the observation made by Tsai [142] for the fatigue behaviour of notched 3Dl multilayer angle interlock woven composite plates.

The visual observations made during loading and DIC images of 3D woven composites at 50% and 75% load, respectively, shows that in the warp direction the damage propagates along the loading direction in the form of matrix cracking and delamination, however, no splitting of warp yarns was observed at these load levels. In LTL, TAI and MAI the damage is mainly concentrated around the hole edges, whereas in the AI structure high stress concentration at binder interlacement points leads to distributed and a higher level of damage at 75% loading. As the load increases the size of the damage zone increases also, with yarn splitting occurring in between 90-95% of the failure load.

However, the splitting of warp yarns in the 3D woven structures was less extensive compared to the UD laminate, with the failed specimen photographs verifying this behaviour. As yarn splitting occurred near the failure load, a lower ultimate tensile strength of notched specimens was achieved in the warp direction, consequently affecting the notch sensitivity of the material. Irrespective of the weave architectures, all the 3D woven composites have almost the same normalized strength or notch sensitivity in the warp direction.

In the weft direction the damage mechanism is the same as in the warp direction and no yarn splitting was observed at 75% load. However the undulation of the binder yarn allows the damage to form more easily along the binder yarn, reducing the stress concentration by extensive matrix cracking and delamination. Therefore a high notched strength as well as notch insensitivity was achieved in the weft direction compared to the warp direction. The LTL has the highest notch strength followed by MAI, TAI and AI. The notched strength of the LTL structure is 4% higher than the TAI and MAI, however the difference is not that significant. This small difference can be attributed to weave architecture. As in the LTL structure, the binder yarn penetrates half the thickness of the structure, and then returns back so the damage can propagate more easily into the layers which are not bound by the binder yarns. In the interlock structures all the layers are bound by the binder yarn as the binder yarn is moving from the top to the bottom of the structure and so the damage cannot propagate easily. Specifically in the AI structure, crimp and the sharp curve of the binder yarn at the binder interlacement points affect the load carrying capability of the binder yarns, consequently reducing the ultimate notched strength. A comparison of the DIC images also shows more damage in the form of matrix cracking and delamination at similar load levels (50%, 75%, 95%) occurred in the weft direction specimens. Photographs of failed

specimens (Figure 5.9) show that failure occurred due to the straightening of binder yarn at the cross-over point, when the two halves of specimens slightly slid over each other.

The UD laminate exhibits almost the same normalized strength in both the warp and weft direction. The higher failure stress of UD laminate in the warp direction is due to increased delamination and more shear cracking of $0°$ fibres. In UD cross ply laminate, damage was propagated along the loading direction for both warp and weft specimens. The DIC images show that axial splits at each side of the hole in the zero direction plies occurred at between 50% to 75% of failure load with axial splits accompanied by transverse splits, following a load of 75%, in the weft direction. Photographs of failed specimens (Figure 5.8e and Figure 5.9e) also show the same behaviour.
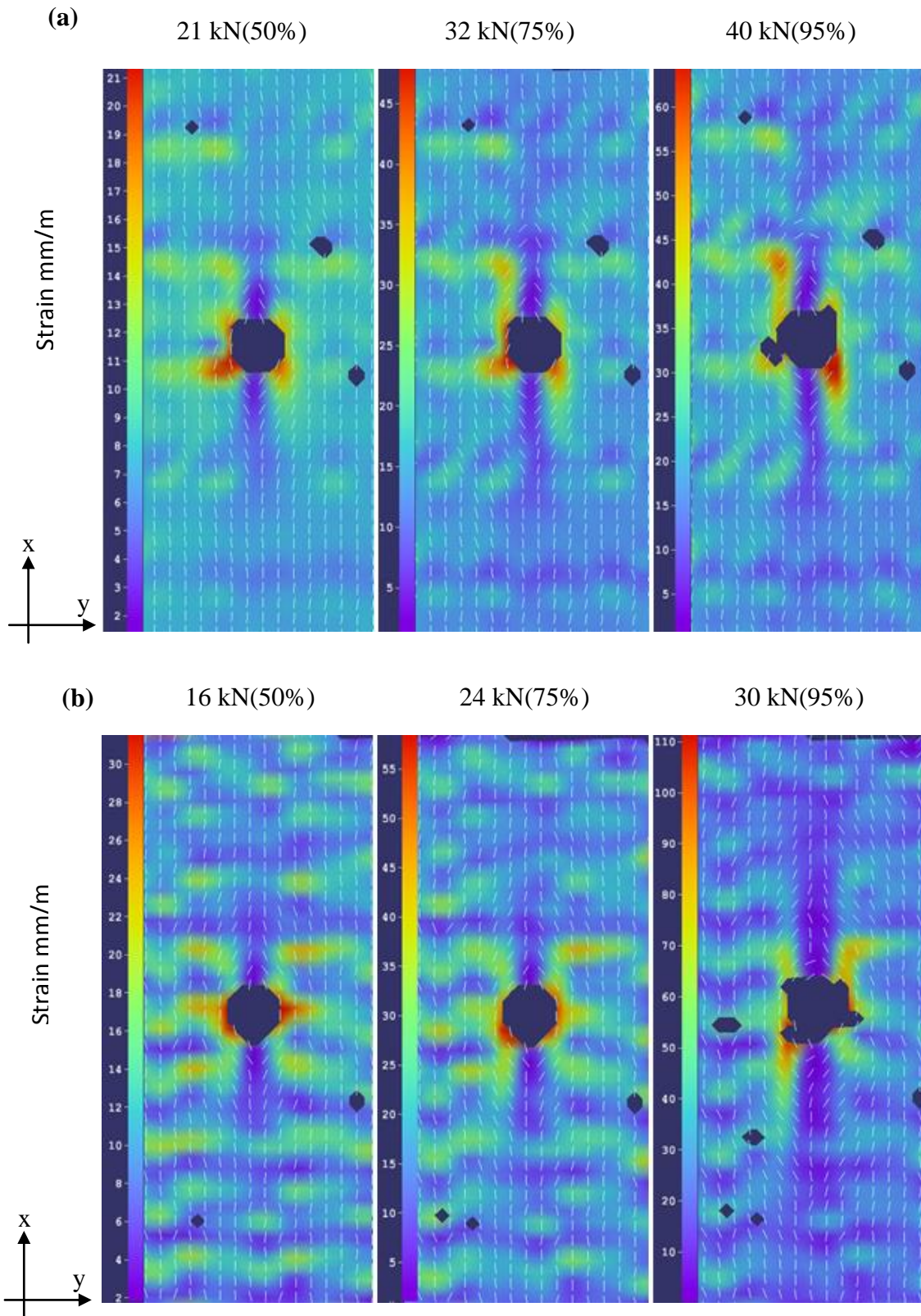
Figure 5.10 DIC strain images of damage progression in layer to layer structure at different
load levels (a) Warp direction (b) Weft direction
(x is the loading direction , hole diameter =6 mm , specimen width=36 mm)
(Purple and orange colours represent the lowest and the highest strain values, respectively
where the maximum strain value increases with the load)
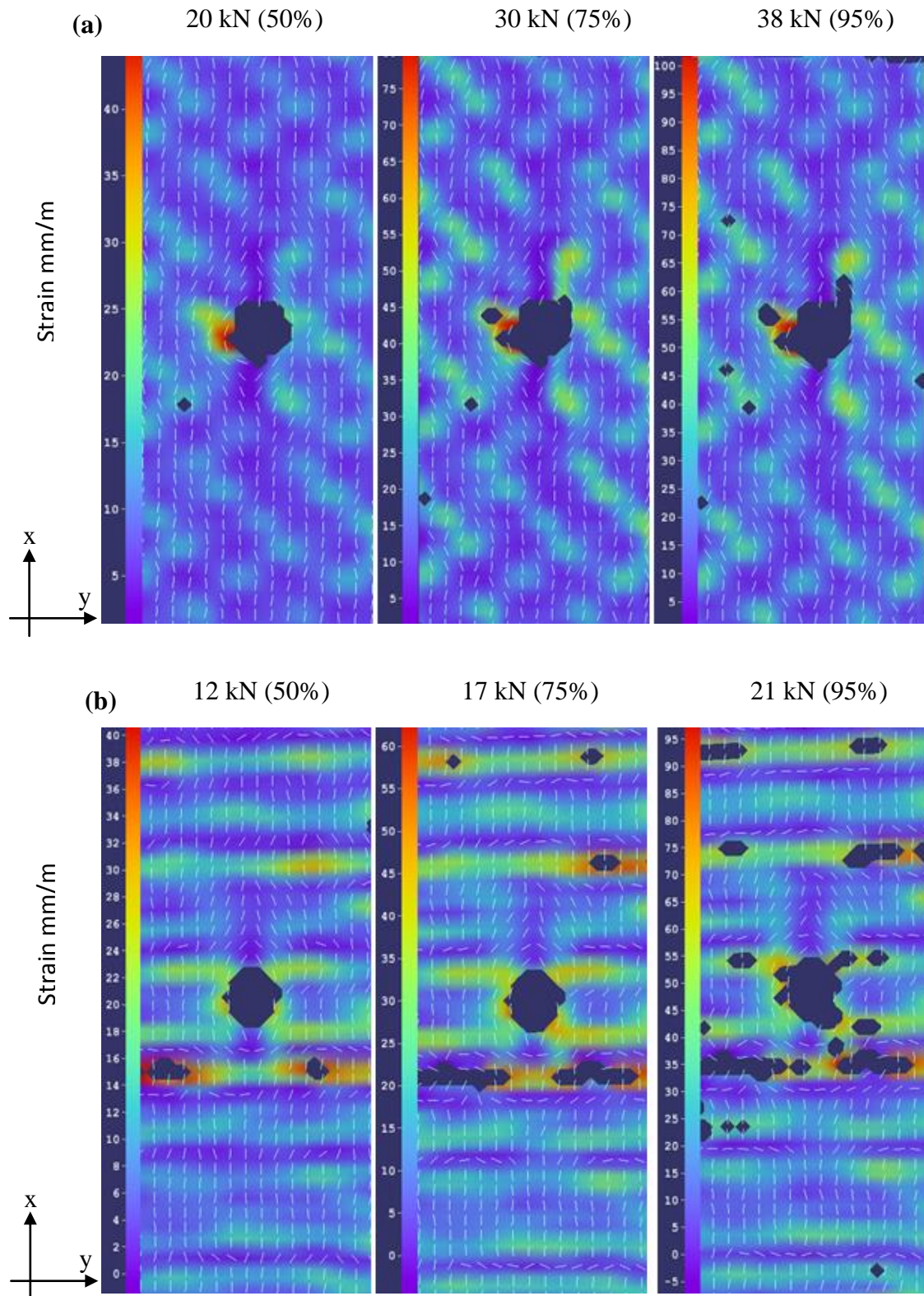
Figure 5.11 DIC strain images of damage progression in angle interlock structure at different load levels (a) Warp direction (b) Weft direction
(x is the loading direction , hole diameter =6 mm , specimen width=36 mm)
(Purple and orange colours represent the lowest and the highest strain values, respectively where the maximum strain value increases with the load)
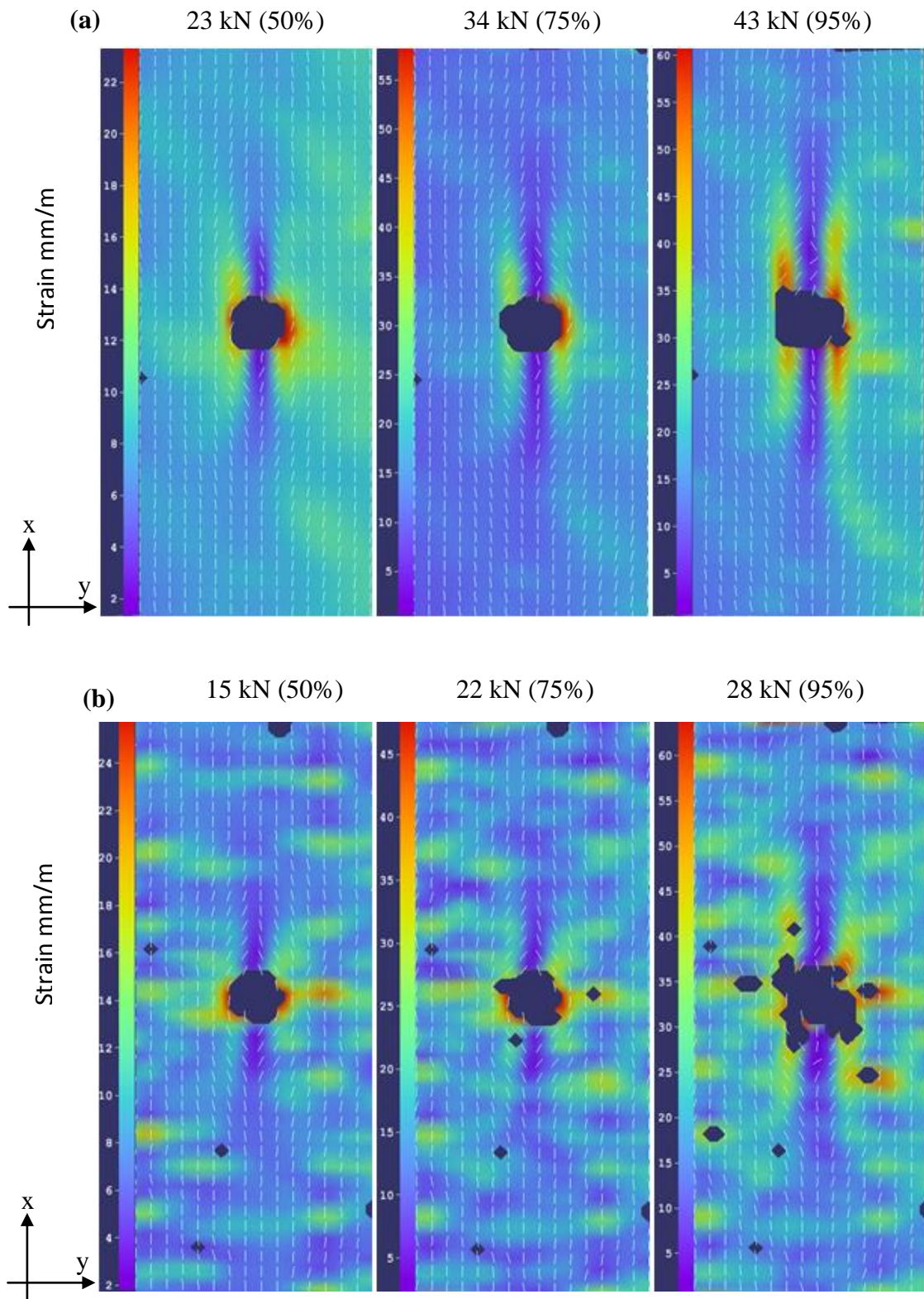
Figure 5.12 DIC strain images of damage progression in twill angle interlock structure at different load levels (a) Warp direction (b) Weft direction
(x is the loading direction , hole diameter =6 mm , specimen width=36 mm)
(Purple and orange colours represent the lowest and the highest strain values, respectively where the maximum strain value increases with the load)
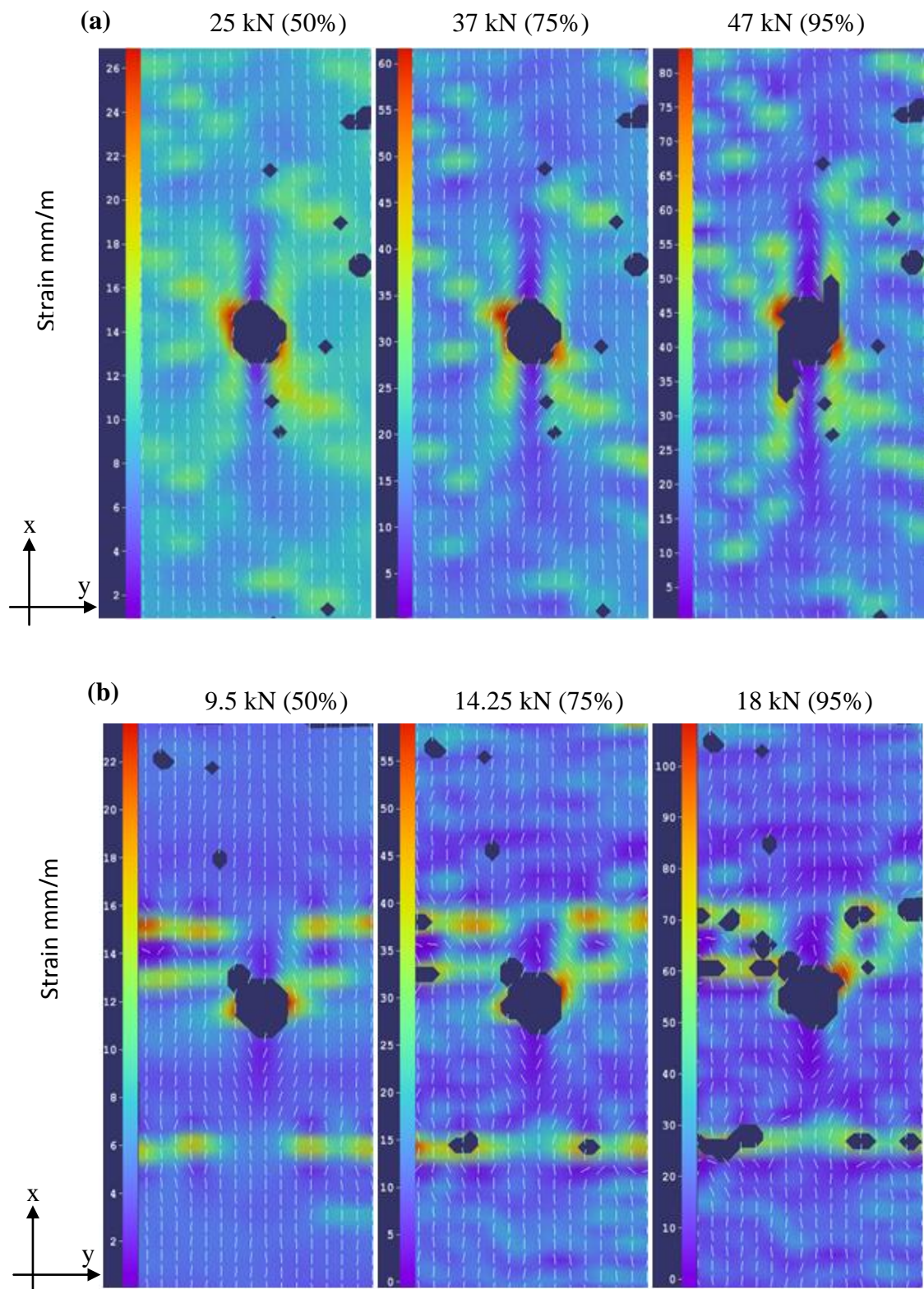
Figure 5.13 DIC strain images of damage progression in modified angle interlock structure at different load levels (a) Warp direction (b) Weft direction
(x is the loading direction , hole diameter =6 mm , specimen width=36 mm)
(Purple and orange colours represent the lowest and the highest strain values, respectively where the maximum strain value increases with the load)
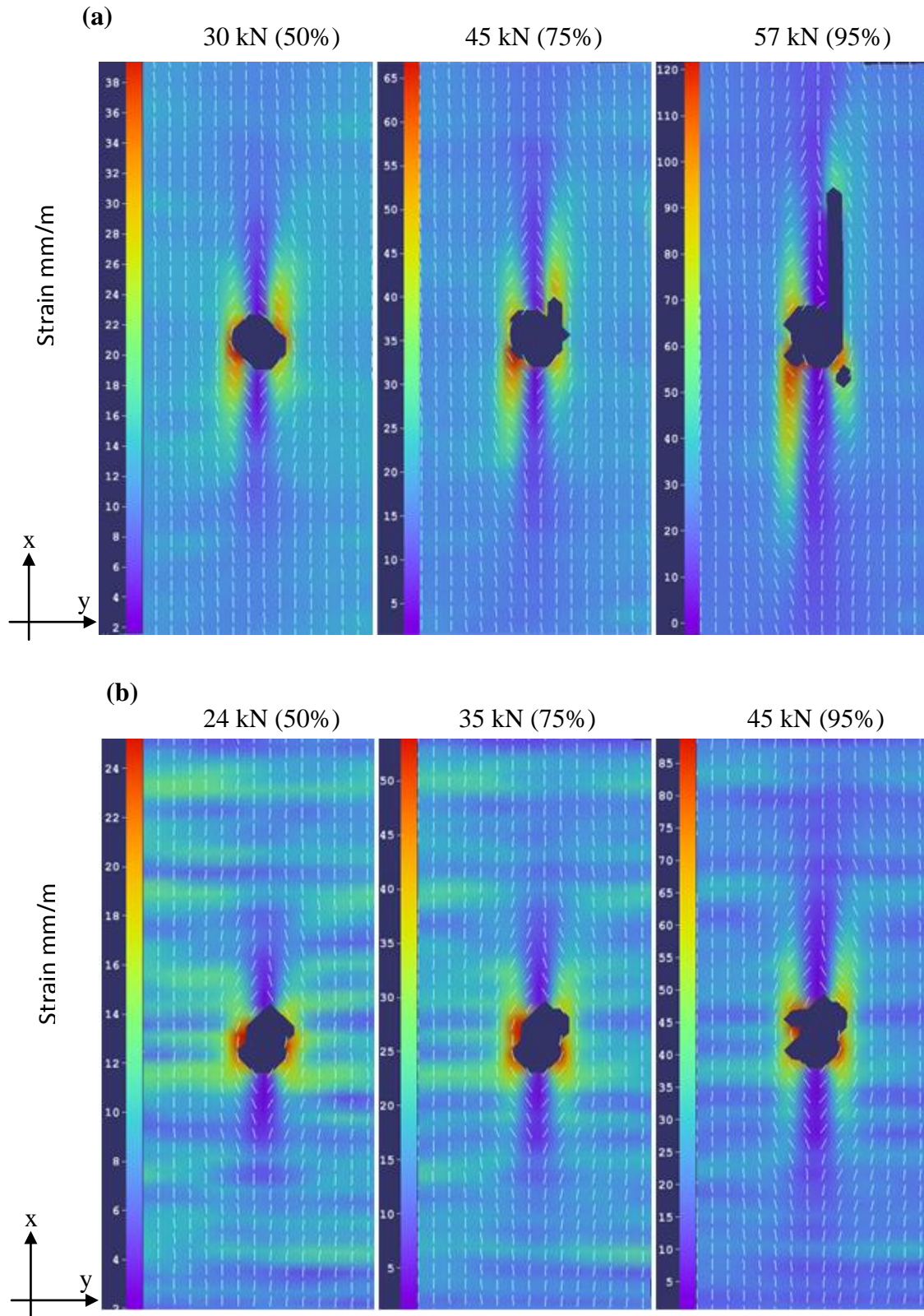
Figure 5.14 DIC strain images of damage progression in UD cross-ply at different load
levels (a) Warp direction (b) Weft direction
(x is the loading direction , hole diameter =6 mm , specimen width=36 mm)
(Purple and orange colours represent the lowest and the highest strain values, respectively
where the maximum strain value increases with the load)

5.5   Summary

An open hole tension test was performed on four different 3D woven composites and UD cross-ply laminate in both the warp and weft directions. It was observed that 3D woven and UD cross-ply laminate are notch insensitive in both the warp and weft directions. The UD cross-ply laminate had almost the same normalized strength and damage behaviour in both of these directions. However, in the warp direction specimens the increased delamination and yarn splitting of the UD laminate led to higher ultimate notched strength as well as notch insensitivity.

Within the 3D woven composites, the notch sensitivity in the warp direction turned out to be almost the same for all the weave architectures. The constraint of delamination and yarn splitting due to the binder yarn inhibit these stress relieving and energy-absorbing mechanisms, causing a lower ultimate notched strength. In the weft direction, however the binder yarns are along the loading direction so the straightening of binder yarns makes it easier for damage to grow; stress is relieved in the form of extensive matrix cracking, delamination and transverse splitting. Therefore the 3D woven composites achieved a higher normalized strength and failed in a more ductile manner, especially the LTL, MAI and TAI structures. TAI and MAI have the same normalized strength, with LTL and AI exhibiting the highest and lowest normalized strengths, respectively. High delamination damage in the LTL structure reduces the stress concentration, resulting in a higher notch strength. Whereas in the AI structure, the crimp and sharp curve of the binder yarn at the binder cross-over point affects the load carrying capability of the binder yarns, consequently reducing the ultimate notched strength.

It can be concluded that the notch sensitivity of a 3D woven material in a required direction under tensile loads can be improved by manipulating the weave architecture. The next chapter will explain the effect of weave architectures on the impact resistance and damage tolerance of 3D woven composites under compressive loads.

6   Impact resistance and damage tolerance of 3D woven composites with different fibre architecture

6.1   Introduction

Three-dimensional textile structural composites are an emerging group of materials that are being used in aircraft, marine and civil infrastructure application. These 3D woven composites are prime examples of advanced materials with potential uses in all these areas [9].

3D woven composites provide sufficiently high in-plane mechanical properties and at the same time improve fracture toughness, impact damage resistance and post impact mechanical properties by suppressing delamination damage [146]. A detailed literature review on the impact and post-impact compression properties of 3D woven composites was presented in Chapter 1.

The impact behaviour of 3D woven glass/epoxy composites, in comparison to unidirectional cross-ply laminate, is discussed in this chapter. Low velocity impact tests at various energy levels (5 J, 10 J, 15 J, 20 J, 25 J, 30 J) were performed on the laminates and energy absorption calculated for these impact energies. Afterwards, a CAI (Compression After Impact) test, ultrasonic scan and electron microscopy are used to evaluate the damage resistance and damage tolerance of these materials. Furthermore, the effect of open hole and impact damage on the normalized compressive strength of composites will also be discussed.

6.2   Impact testing

The impact damage resistance of a composite is typically measured by a drop weight impact test. The energy impacted in these tests may be carried out by either varying

the drop height or by varying the striker/impact mass while maintaining constant velocity. Variation in drop height changes both the impact energy and the impact velocity.

In this study, the incident energy and velocity of the impactor were varied by altering the height of the impactor above the specimen. The theoretical impact energy was calculated using the following equation:

$$E = mgh \qquad (1)$$

with the theoretical velocity at impact at:

$$v = \sqrt{2E/m} \qquad (2)$$

where, E = Impact energy, m = Impactor mass, h = Impact height ,

v = Impact velocity

However, some energy and velocity was lost due to friction in the system.

A CAI testing method introduced by Hogg and Prichard [147] was followed to carry out the test. This procedure uses a reduced specimen size, when compared to ASTM D7136, as materials were limited. The test procedure and specifications for specimens will be described in the following section.

6.2.1   Miniature (QMW) impact test specifications

Impact damage resistance evaluation was carried out on the four different 3D woven composites LTL, AI, TAI, MAI and the UD cross-ply laminate, in both the warp and weft directions. The specimen geometry was nominally 55 mm wide by 89 mm long. Specimens were cut and impacted at both the warp and weft direction specimens. For warp-impacted specimens the length of the specimen was cut along the warp yarn and for weft-impacted specimens the length of the specimen was cut along the weft yarn. The test was performed using an instrumented falling weight impact machine (Instron ceast 3950) and a Queen Mary and Westfield (QWM) designed support

fixture [147]. The support fixture and striker dimension are shown in Figure 6.1, while the total mass of the impactor was 5.80 kg. The specimens were clamped between two rectangular metal plates, each with a circular opening of 40 mm in diameter and struck by a 20 mm diameter hemi-spherical indenter. A rebound brake was activated in the test system to avoid multiple impacts on the specimens. The impact test history curves, including impact force, time, displacement and energy of the specimens were obtained using the instrumented tip.

Seven different energy levels (0, 5, 10, 15, 20, 25, 30 J) were applied using non-penetrating blows. Due to material limitation, four specimens per energy level were tested in both warp and weft directions for the 3D woven and the UD cross-ply laminate. The respective maximum impact energy was sufficient to cause delamination damage saturation.
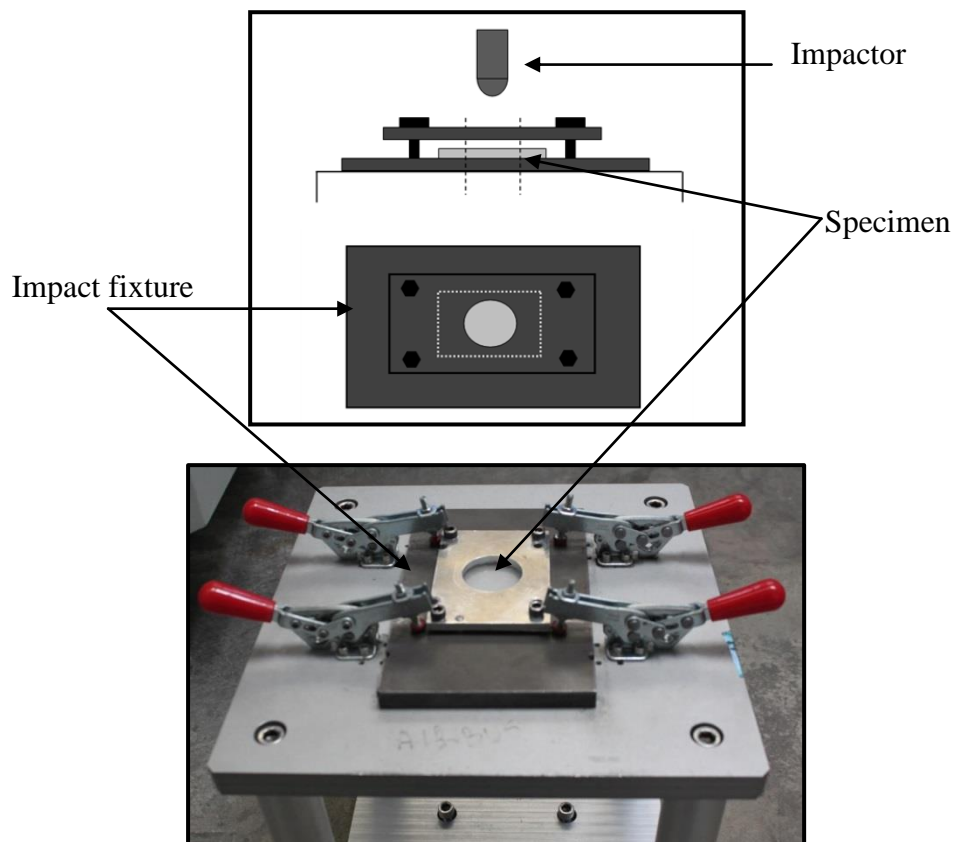
Figure 6.1 Schematic representation and photograph of the miniature (QMW) impact fixture

6.2.2 Damage determination

The damage caused by delamination and fracture was determined both non-destructive and destructively. A C-scan ultrasonic technique was used to determine the damage area of the impacted specimens. Then the damage area and width was calculated from the C-scan images using Image J software. Scanning electron microscopy (SEM) involved sectioning the specimens to show the detailed nature of cracking that a non-destructive technique is unable to identify.

6.3 Compression after impact

Low velocity impact can cause delamination damage within composite panels, which significantly reduces their residual compressive strength and strain-to-failure. To assess the compressive strength degradation after impact damage and the resistance of the composites to delamination, an in-plane compression was performed on the impacted specimens; the testing procedure is called a compression after Impact (CAI) test.

For the present study a CAI testing method introduced by Prichard and Hogg [147] was followed to carry out the test. The test and specimen specifications will be described in the following section.

6.3.1 Miniature (QMW) CAI test procedure

Resistance to impact induced damage in compression using the miniature [147] (QMW) specimens was conducted on an Instron 5980 at a constant cross-head speed of 0.5 mm/min. The specimen boundary conditions were simply supported laterally and fully built in at both the top and the bottom. These supporting conditions combined with a clearance gap between the frame and the loading top support plate allows the specimen to fail in compression by minimizing the out-of-plane

deformation of the specimen. Compression tests were conducted on both undamaged as well as damaged samples, using the fixture shown in Figure 6.2.
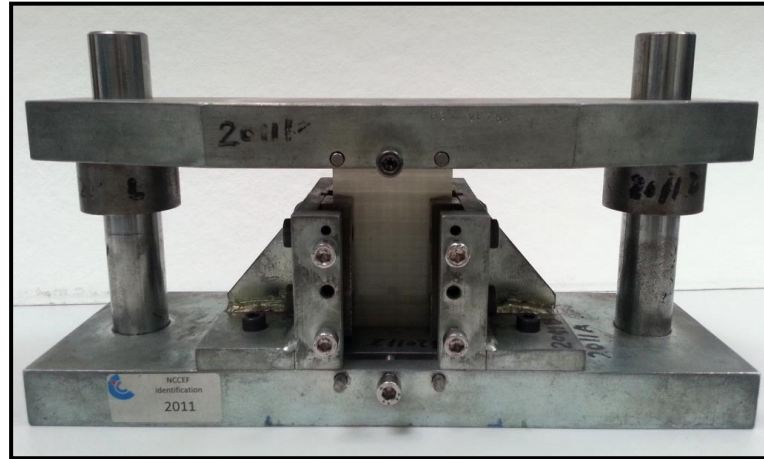
Figure 6.2 Test fixture for CAI test

6.4 Open hole compression

An open hole compression test was also carried out using the Boeing jig shown in Figure 6.3, with a hole to width: ratio of 6:1. Specimens measuring 305 x 38 mm were cut and then a circular hole of 6.35 mm in diameter was drilled at the centre of the specimens. The holes were introduced with a steel-tipped drill. A metal clamp was used to hold the specimen in place. The compression test was carried out according to ASTM standard D6484. For each material, four specimens were tested: three with a hole and one without in order to compare the notched and unnotched strength of the material. The compression tests were performed in both the warp and weft directions. The experimental values of notched strength ,σ_n , is based on the gross cross-sectional area of the specimen.

Figure 6.3 Test fixtures for open hole compression test

6.5 Results and discussion

6.5.1 Impact test

A comparison was carried out looking at the four different 3D woven and UD cross-ply laminates at different levels of impact energy, ranging from 5 J to 30 J, using an instrumented drop weight impact tower. In each direction (warp & weft) four specimens were tested for each impact energy. The variation of impact parameters such as force, impact energy, absorbed energy and elastic energy versus time or deflection will be examined to understand the response of 3D woven composites under impact loading.

The force-time curves for 3D woven and UD cross-ply laminate are presented in Figure 6.4 and Figure 6.7, whereas force-deformation curves are depicted in Figure 6.5 and Figure 6.8 for 10 J, 20 J and 30 J impact energies. Figure 6.6 provides the comparison of contact force with different impact energies.

(a)
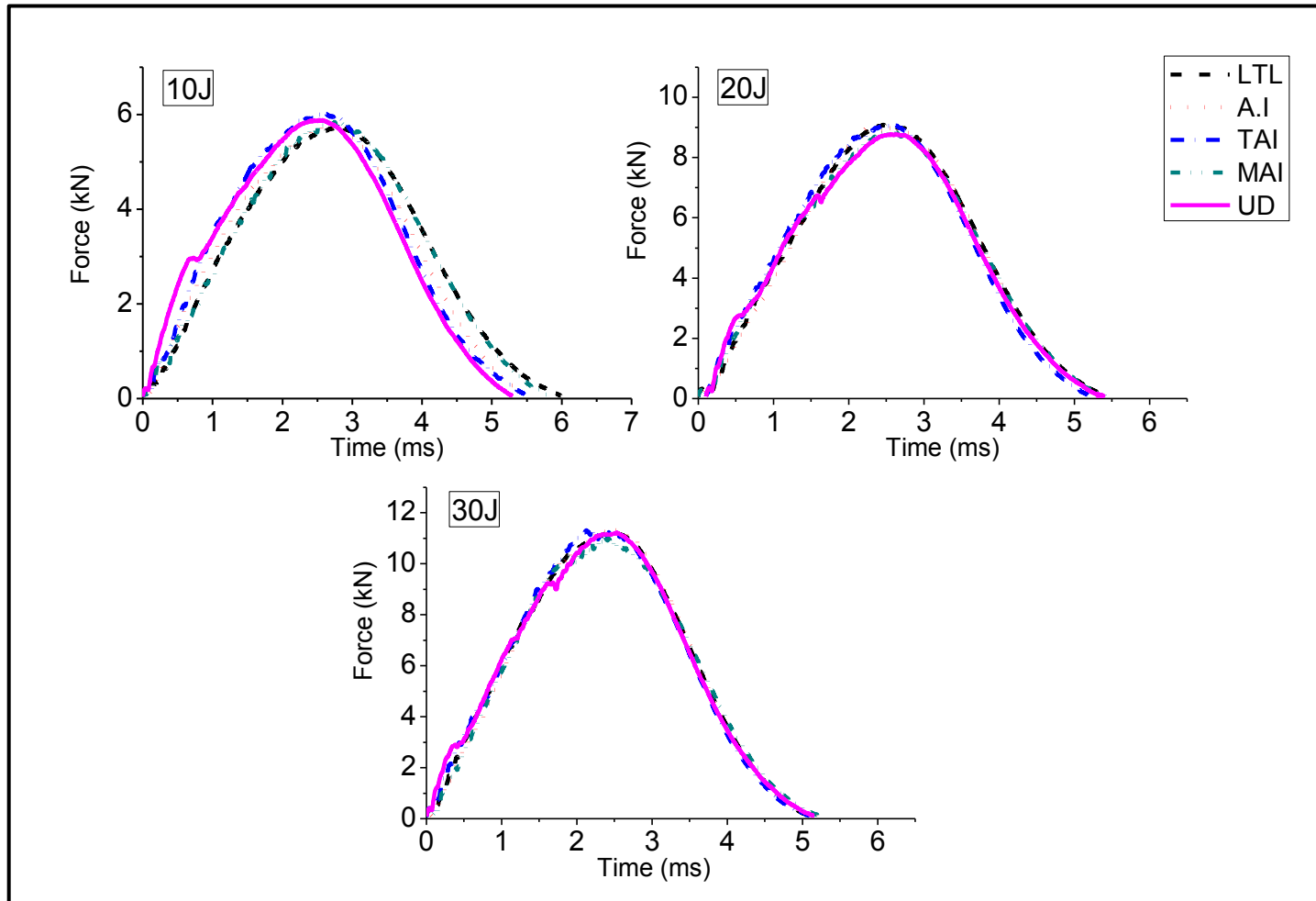
Figure 6.4 Force-time curves of materials at different impact energies in the warp direction
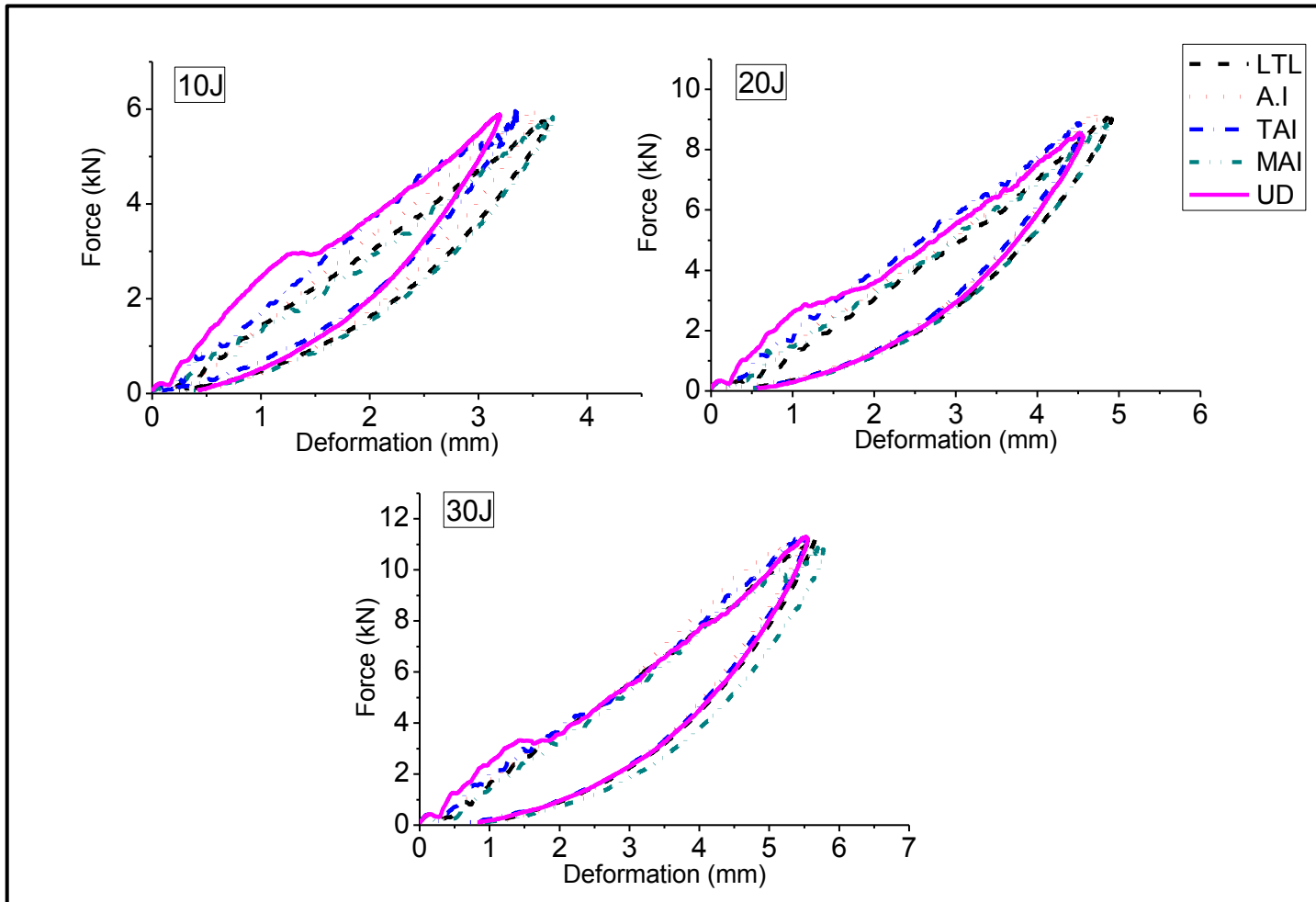
Figure 6.5 Force-deformation curves of materials at different impact energies in the warp direction

All the force-time curves (Figure 6.4 and Figure 6.7a) are bell-shaped for the 3D woven and UD laminates, dropping off at almost the same point. In the warp direction, the 3D woven and UD cross-ply laminate exhibit the same maximum force with the different impact energies, which increases with the increase of impact energy. A similar behaviour was also observed for permanent deformation while the slightly higher, maximum deformation/deflection of 3D woven composites may indicate that these composites are more flexible. As the energy increases the stiffness of UD laminate decreases due to the increase in damage area. After an impact energy of 10 J, the force-deformation and force-time curves of TAI and UD exhibit the same bending stiffness, while beyond 15 J impact energy this difference of stiffness becomes negligible for the other 3D woven composites as well. The C-scan images of damage area for the 3D woven and the UD laminates at different impact energies are represented in Figure 6.18 and Figure 6.19.

Figure 6.7 and Figure 6.8 show that in the weft direction the maximum force and deformation response of all the laminates is similar to warp impacted specimens up to 15 J impact energy. After 20J, however MAI exhibit the highest deformation and the lowest force as well as bending stiffness. Similarly, TAI shows the highest force and minimum deformation for the 20-30 J impact energies; differences in force, permanent deformation and bending stiffness are negligible for LTL, AI, TAI and UD laminates. The lower stiffness of MAI in the weft direction leads to a higher permanent deformation as well as deflection of the specimens during an impact event, which is more prominent in the weft direction. Because the ratio of the weft stuffer and binder yarn is 50:50 and the binder yarns do not fully contribute towards the stiffness of the structure (as they are not straight and pass through the thickness direction to bind the structure together). The structure is less stiff and more

deformable in the weft direction, as compared to the warp direction. This effect becomes more evident with an increase in energy. Another factor contributing to higher deformation may be the lower thickness of the MAI laminate compared to other 3D woven composites.
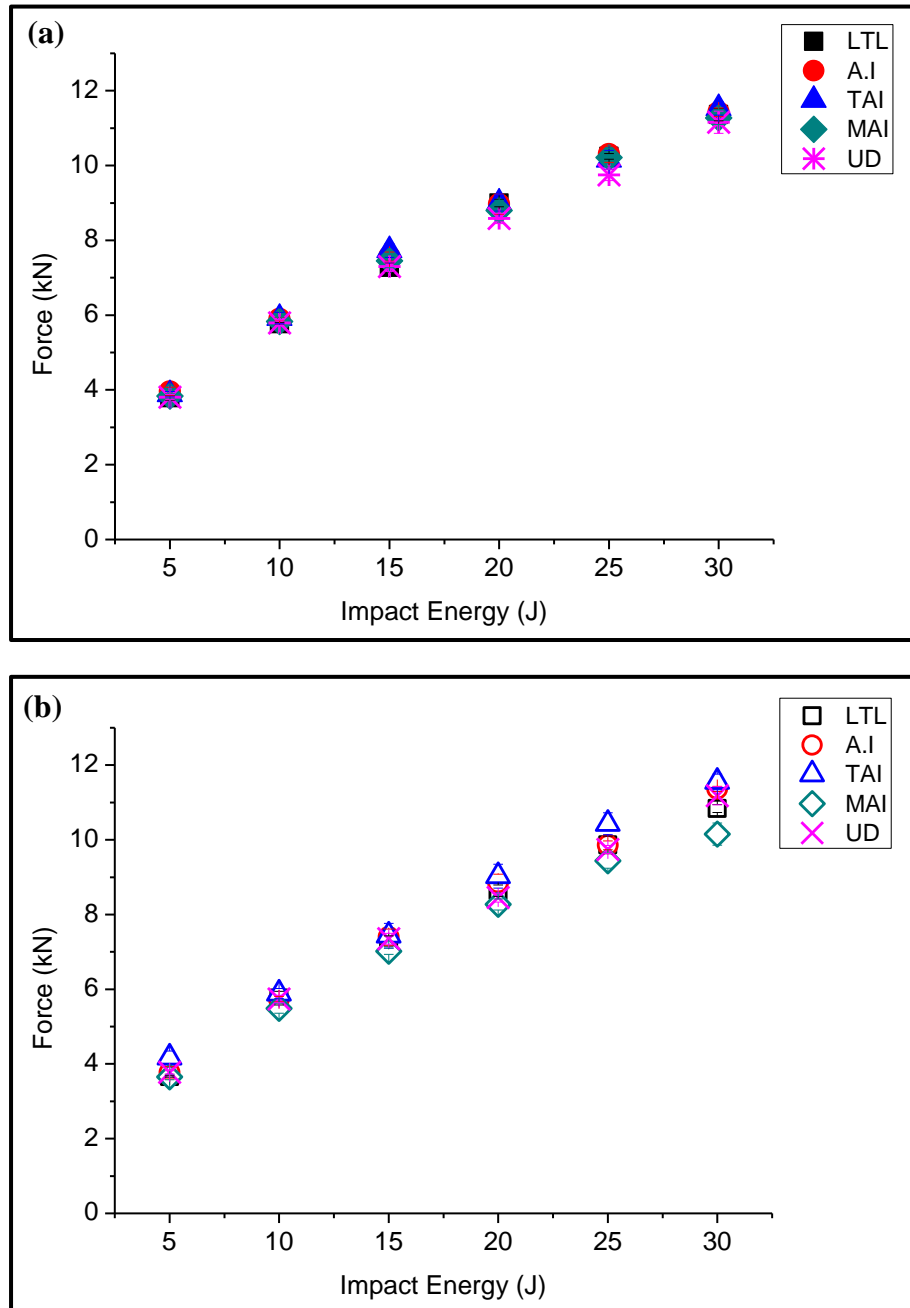
Figure 6.6 Comparison of force at different impact energies (a) Warp direction (b) Weft direction

(Data points are so close that all the error bars are emerged with each other and no clear error bars can be seen on the graphs.)
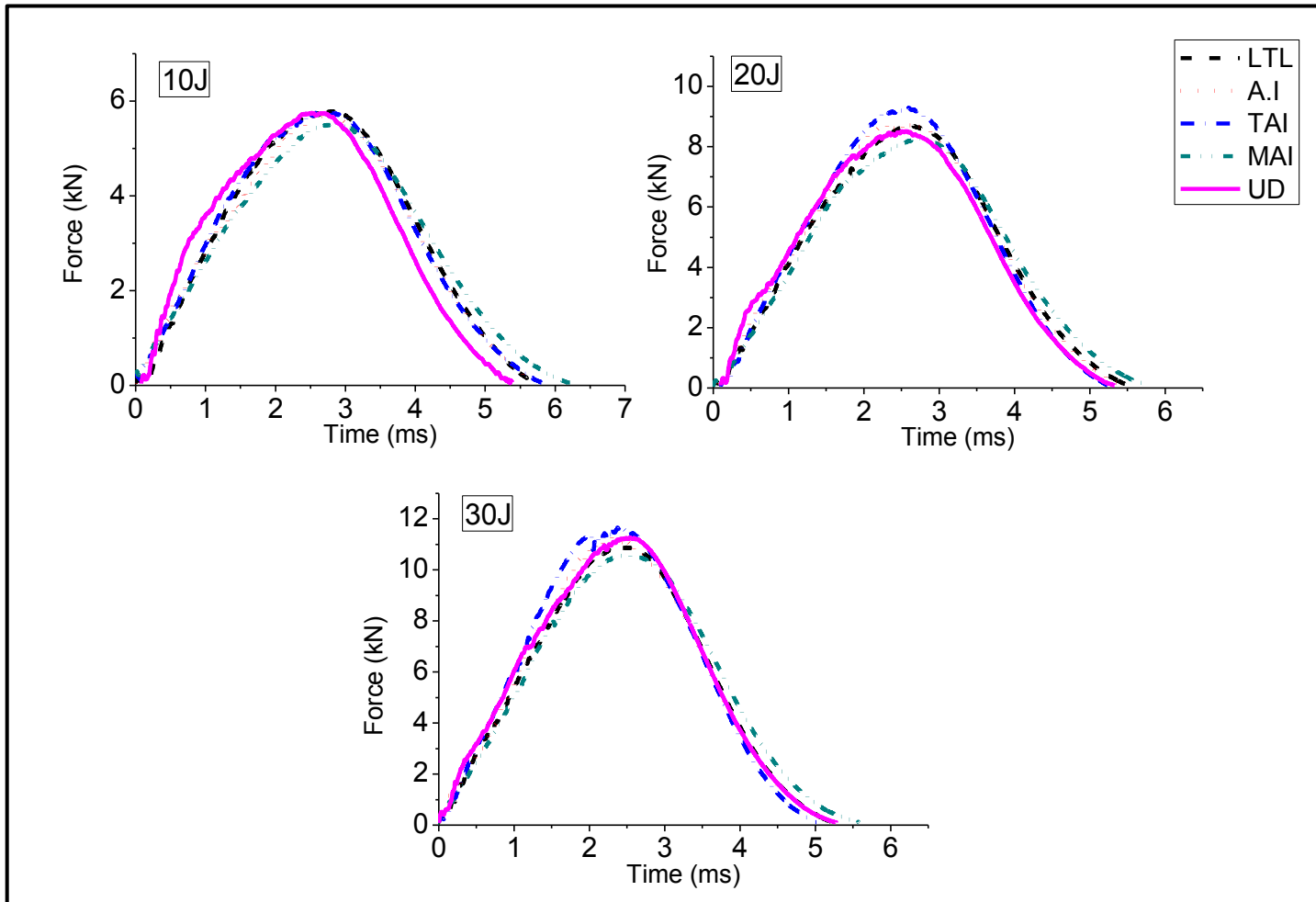
Figure 6.7 Force-time curves of the materials at different impact energies in the weft direction
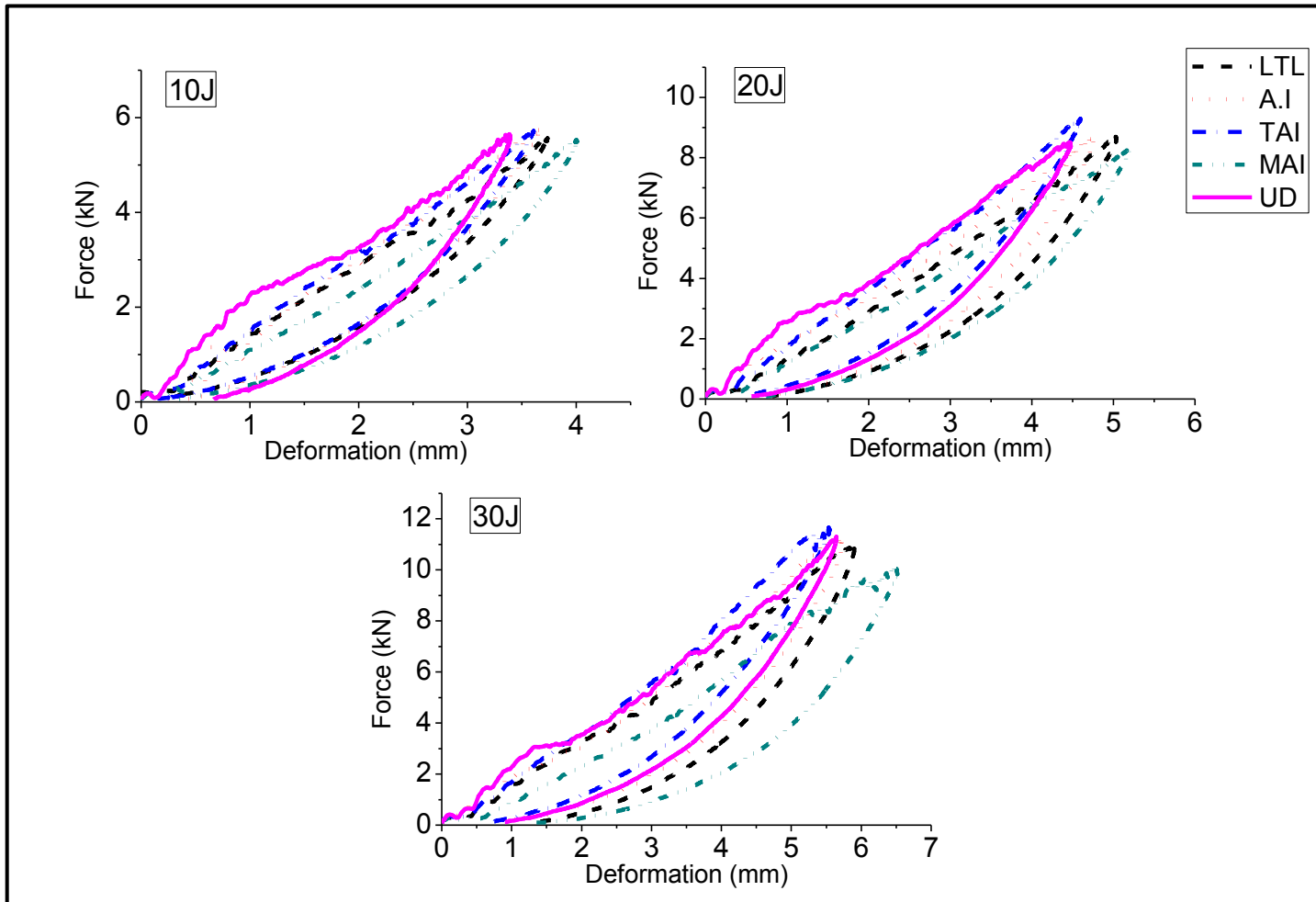
Figure 6.8 Force-deformation curves of the materials at different impact energies in the weft direction

The force and deformation in all the specimens increases with the increase of impact energy. In contrast to the 3D woven composites, a load drop for the UD cross-ply laminate can be observed at 3 kN, and is called the incipient damage point or damage initiation point. The distinct load drop followed by the change of stiffness is only observable in the UD cross-ply laminate, no such load drop is observed for any of the 3D woven structures. This load drop indicates damage initiation such as internal delamination or fibre/matrix failure which usually takes place close to the back surface of the impacted specimens. Whereas in some 3D woven structures the oscillations in the force-displacement curve just before the maximum deformation indicate delamination/fibre breakage on the non-impacted side of the specimen for the 20-30 J impact energies such as the weft- impacted MAI specimens.

For the 3D woven and the UD cross-ply laminate the increase in absorbed and elastic energy, with respect to impact energy is compared in Figure 6.10. Both absorbed and elastic energy were calculated from the energy-time curve as shown in Figure 6.9.
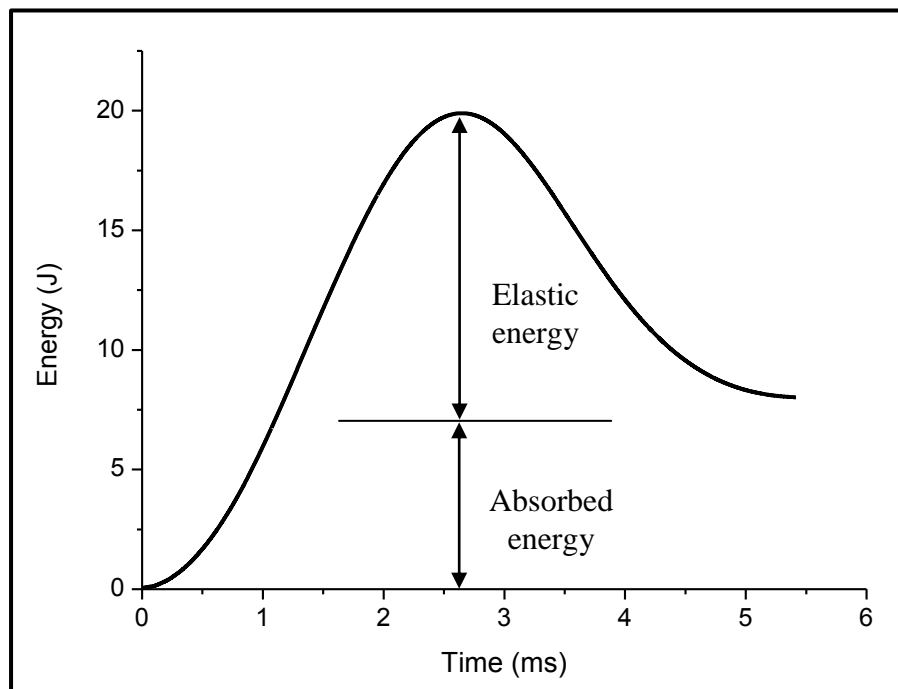
Figure 6.9 Calculating elastic and absorbed energy from energy-time curve

The absorbed energy increased with the incident impact energy, whilst the elastic energy decreased with an increase in impact energy. The elastic energy of the 3D woven composites and the UD laminate decreases in the same sequence as the absorbed energy increases in both directions. It was found (Figure 6.10a and c) that the amount of absorbed energy is almost the same in both the warp and weft directions; however, the order is different for high impact energies. A comparison of the absorbed energy and the damaged area in both the warp and the weft directions is represented in Figure 6.10, Figure 6.11 and Figure 6.12.

In the warp direction for 5-15 J energy the UD cross-ply laminate absorbs more energy and exhibits a larger damaged area, whereas for 20J and 30J impact energies, the TAI and MAI structures absorb the same amount of energy with an area of damage which is approximately half the damaged area of the UD laminate. Similarly, in the weft direction for 25 J and 30 J impact energies the MAI structure absorbs more energy, followed by the LTL structure, when compared to the UD laminate. MAI composites absorb more energy in the form of fibre breakage at the non-impacted face of the specimens. TAI structure exhibit the lowest energy absorption along the weft direction. The comparison of absorbed energy and damaged area with respect to impact energy showed that the amount of damaged area in the UD laminate is double for the same amount of absorbed energy, when compared to the 3D woven composites. For the 3D woven structures, both the C-scan images (Figure 6.18 and Figure 6.19), and the comparison of the damaged area show that the amount of damaged area in the weft direction specimens is less than for the warp direction specimens, especially for high impact energies.
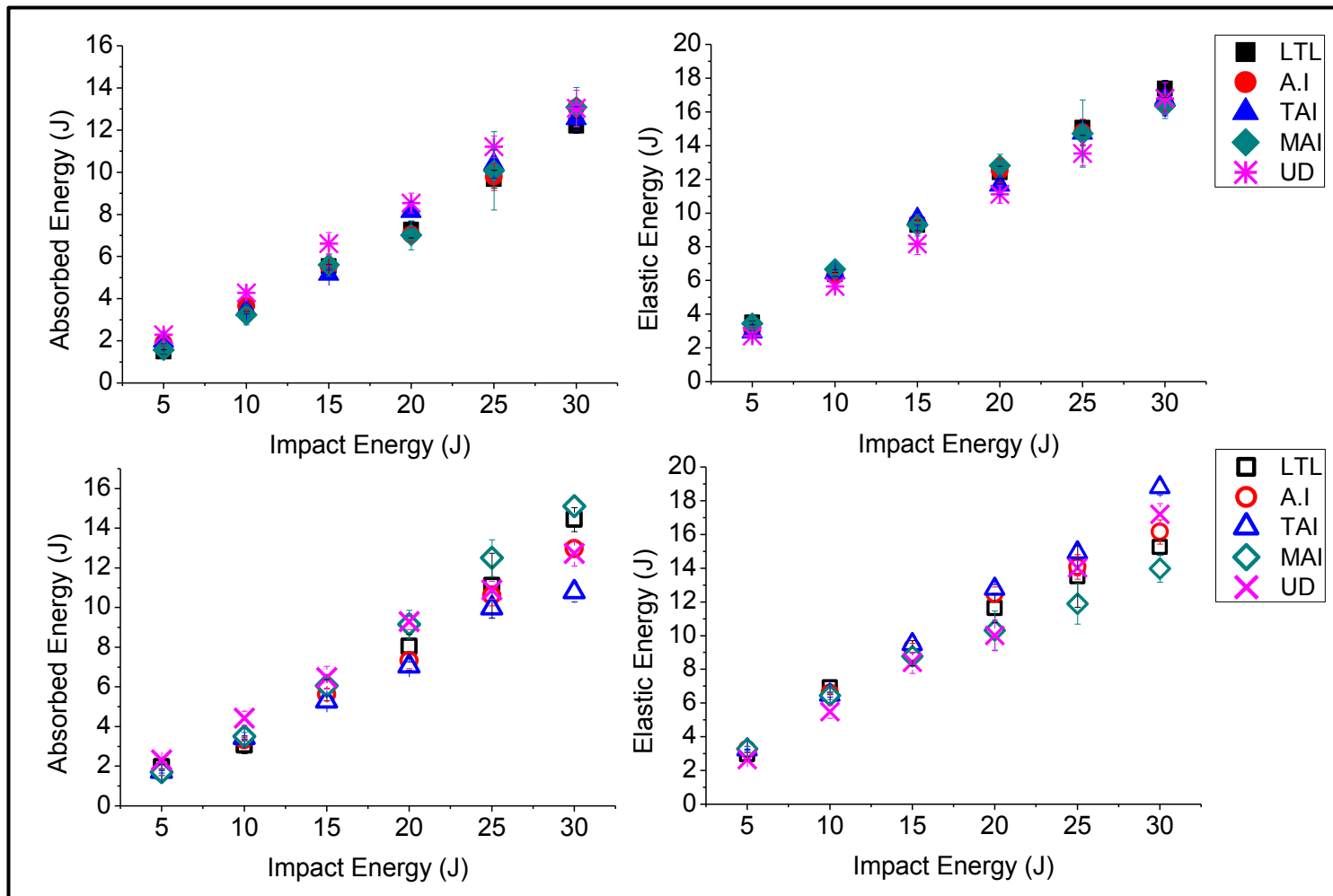
Figure 6.10 Absorbed and stored elastic energy of the composites at different impact energies; (a &b) Warp direction, (c &d) Weft direction
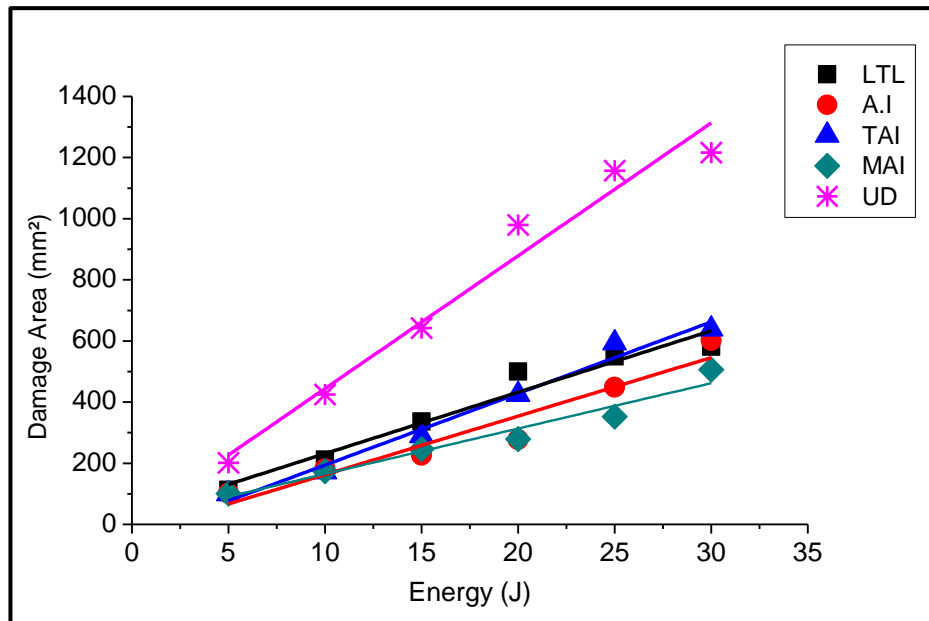
Figure 6.11 Damage area in the warp direction at different impact energies

In the warp-impacted specimens, the damage propagates more in the longitudinal direction or along the warp (0 º) direction, and the shape of damage is elliptical; whereas in the weft-impacted specimens, the damaged shape is more or less like a diamond, while the damage propagation is a little bit more in the transverse direction, with the difference not as prominent as in the warp direction.
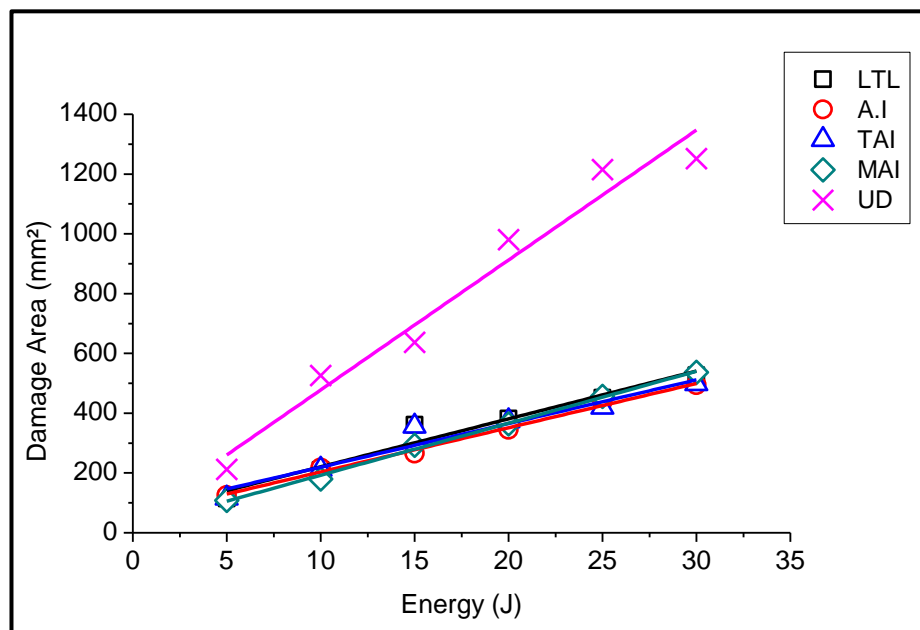
Figure 6.12 Damage area in the weft direction at different impact energies

146

In both directions, the effect of the damaged shape is more prominent for 15 J to 30 J impact energies. However, in both the longitudinal and transverse directions, the width-wise extent of impact-induced delamination damage lies within the support fixture boundary. In contrast, the UD cross-ply laminate has the greatest extent of impact induced damage for a given incident energy; after the 20 J impact the damage width extended a little beyond the fixture boundary in both the warp and weft directions.

6.5.1.1 Damage assessment

Visual inspection of the physical damage apparent in the material showed that the damage increases with an increase in impact energy. The rear face of the specimens exhibit more evidence of damage, and splitting of surface tow with delamination was observed for the UD cross-ply laminate. For the 3D woven structures, damage was more concentrated at the point of impact, while less delamination could be seen at various impact energies when compared to UD laminate

Internal inspection by c-scan also shows that there is an increase in the damaged area with an increase in the impact energy. As mentioned earlier, different damage shapes, elliptical and diamond, were observed for the 3D woven composites in warp- and weft-impacted specimens, respectively. During an impact event, the damage propagates in both a longitudinal and transverse direction until they run into a binder yarn. The binder yarns act as a crack arrestor, suppressing delamination by reducing the crack driving force. Therefore the damage width and propagation depends on the distance between two binder yarns as well as the position and number of the binder yarns per unit area under and around the impactor. More binders situated around the impacted area means a restriction of damage propagation in both the longitudinal and transverse directions. In warp-impacted specimens, the damage propagates more in the warp direction due to the

longer floats of warp yarn, and the damage shape becomes elliptical with an increase in impact energy. A similar phenomenon was observed by King [92] for 3D woven orthogonal composites; whereas in the weft-impacted specimens, the damage area is roughly diamond-shaped because binder yarns are placed along the length direction, impeding the spread of delamination damage in that direction. However, the damage propagates a little bit more in the transverse direction because the warp floats are at 90º to the length direction (or the distance between the two binder yarns in the transverse direction is more than in the longitudinal direction). However, the difference in longitudinal and transverse damage propagation is not as prominent as for warp-impacted specimens. Similarly, diamond-shaped damage was observed by Tan et al [148] for high binder densities. Micrographs of 3D woven structures subjected to 20 J impact energy are depicted in Figure 6.14 to Figure 6.17. These figures demonstrate that the binder yarn suppress delamination through crack bridging and crack arresting even in the case of fibre damage of the binder tow. During an impact event, binder yarn interlacement creates more hindrance to crack propagation and delamination damage. So the matrix crack/delamination damage is arrested at the point of each binder intersection and causes less interfacial damage. It was also observed that the damaged area of the non-impacted surface was greater than that of the impacted surface confirming that damage spreads in a through-thickness direction, causing a cone effect.

In the UD cross-ply laminate, damage propagation follows the direction of yarns lying in the outer layers for the 5-15 J impact energies. However, after experiencing a 15 J impact energy, the damage propagates equally in the both warp and weft directions with the damage shape becoming almost circular.

6.5.1.2   Damage resistance and impact tolerance

Naik et al define damage resistance as the energy required to cause a unit area of damage (J/cm^2) [149]. Damage/impact resistance is the ability of a material to absorb impact energy with minimal damage.

The damage resistance for 3D woven and UD cross-ply laminates is calculated as the inverse of the gradient of the lines presented in Figure 6.11 and Figure 6.12. The damage resistance appears to be lowest for the UD cross-ply, and significantly higher for the 3D weaves in both the warp and weft direction as depicted in Figure 6.13.
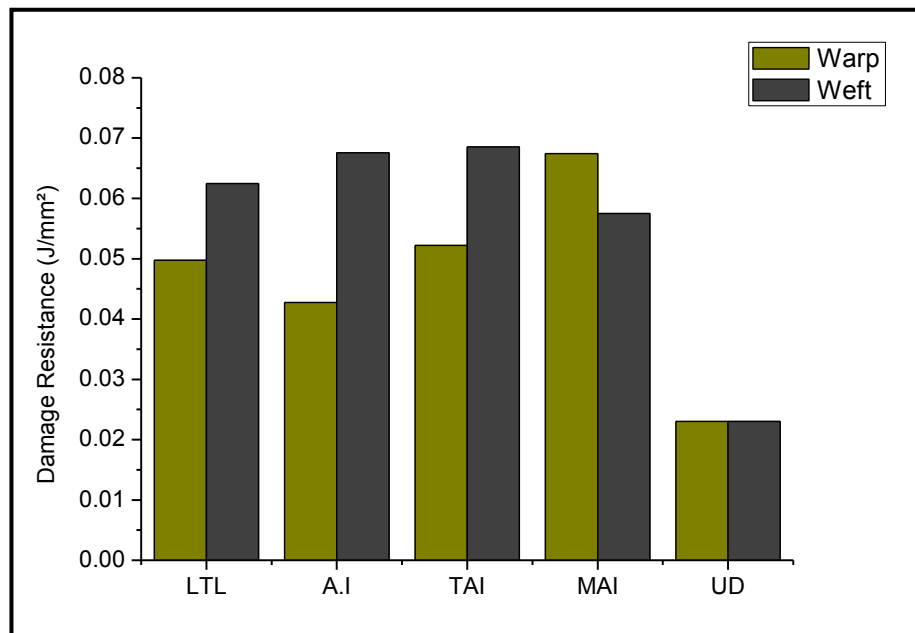
Figure 6.13 Damage resistance in warp and weft direction

Within the 3D woven composites, overall the damage resistance of the MAI structure is better than other 3D woven structures, followed by TAI, LTL and AI. 3D woven composites have a high damage resistance in the weft direction compared to the warp direction, except for MAI. For various levels of impact energy, the lower stiffness of the weft-impacted MAI structure specimens cause more damage; as a consequence, the structures depict low damage resistance in the weft direction. For the UD laminate, the

yarn orientation has no effect on damage resistance, while less energy is required to cause unit area damage.

During impact, energy is absorbed in the form of matrix cracks, delamination initiation, propagation and fibre fracture. The energy absorption for 3D woven composites and UD laminate is nearly the same for the different impact energies. However, the damaged area produced by 3D woven composites is half that of the UD cross-ply laminate at the same impact energy. The through-thickness/binder yarn minimizes the development of delamination damage and subsequent propagation by enhancing interlaminar fracture toughness. For a given impact energy, 3D woven composites have high damage resistance and impact tolerance, when compared to UD cross-ply laminate.

Impact direction
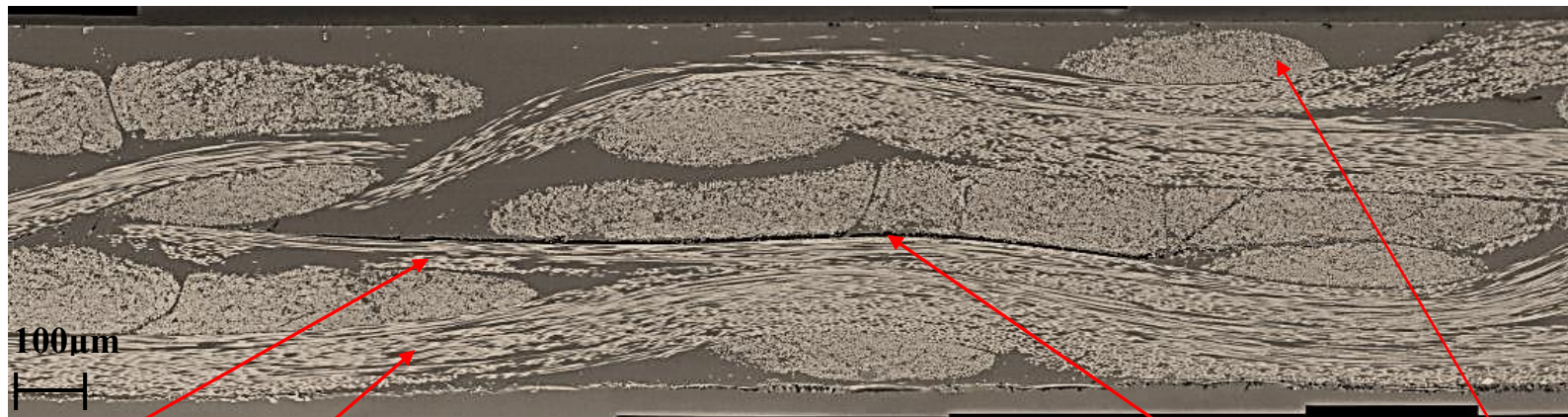
(a)

| Weft stuffer | Warp yarns | Bridging effect of weft binder | Delamination between warp and weft yarn | Weft binder |
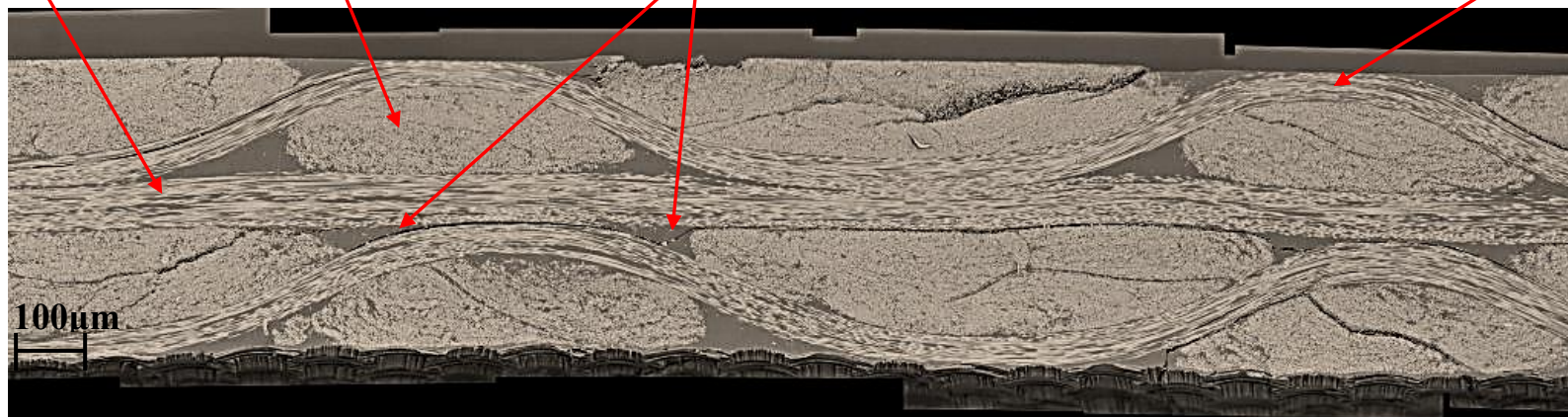
(b)

Figure 6.14 Micrographs of layer-to-layer structure showing impact induced features (a) Delamination between warp and weft interface and (b) bridging effect of binder yarn to crack propagation

Impact direction

(a)

100μm
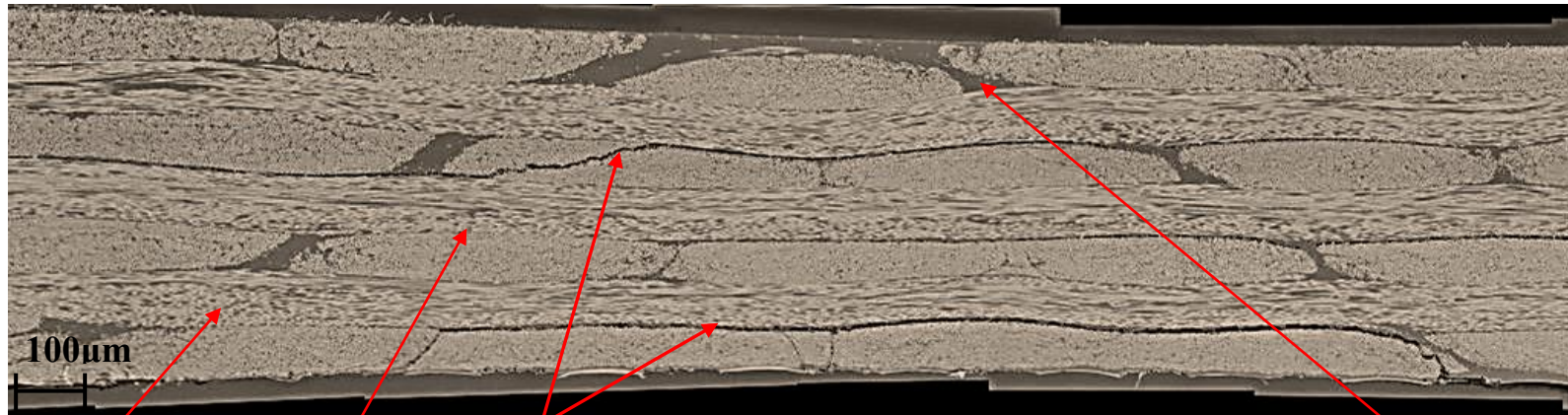
Weft stuffer | Warp yarns | Delamination within warp yarns and between warp and weft yarn interface | Bridging effect of weft binder | Weft binder

(b)

100μm
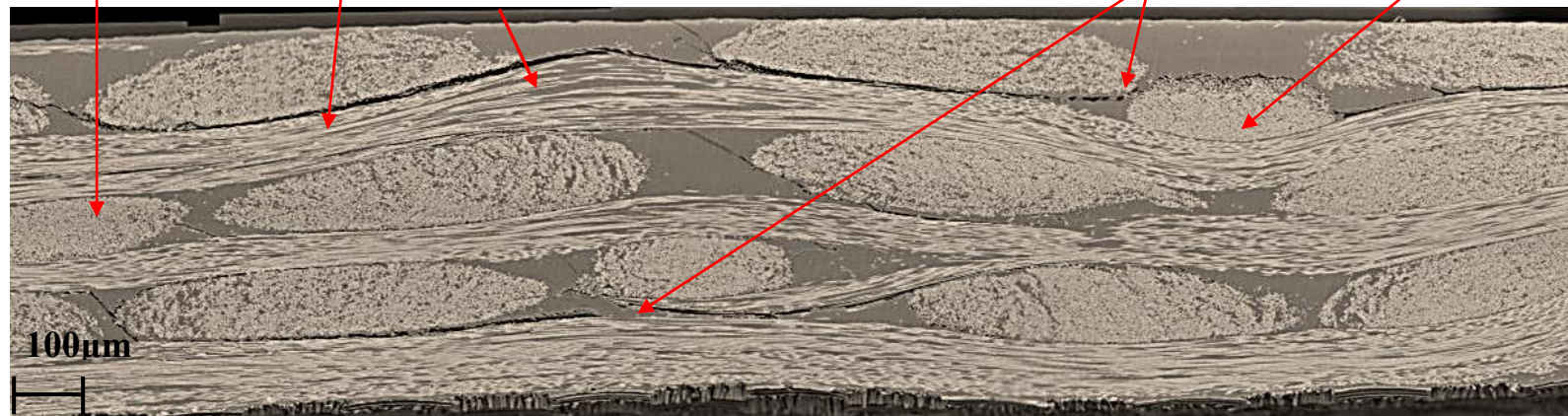
Figure 6.15 Micrographs of angle interlock structure showing impact induced features (a) Delamination between warp and weft interface and (b) bridging effect of binder yarn to crack propagation

Impact direction

| Weft stuffers | Warp yarns | Delamination between warp and weft yarn interface | Bridging effect of weft binder | Weft binder |

(a)

(b)
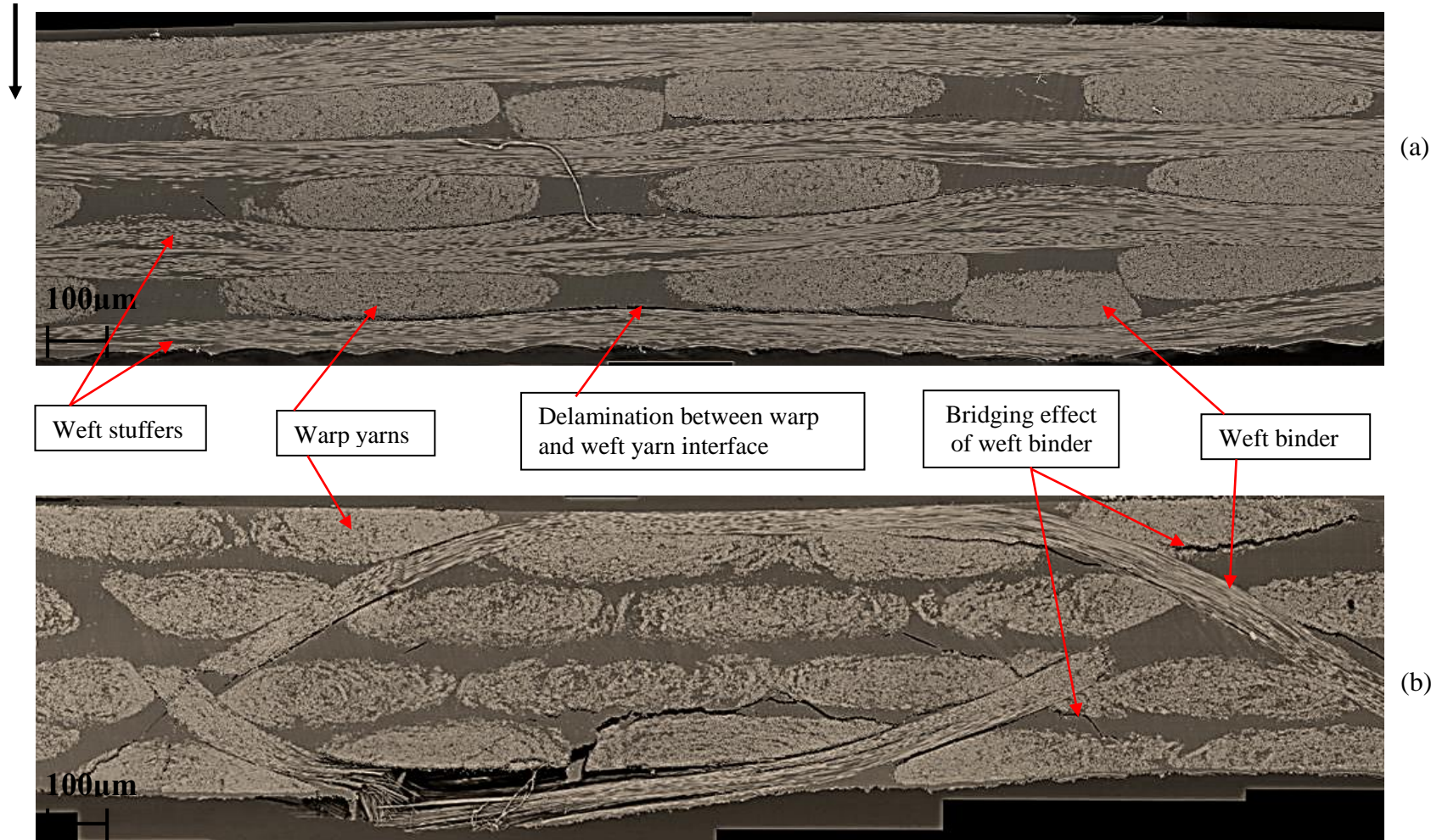
Figure 6.16 Micrographs of twill angle interlock structure showing impact induced features (a) Delamination between warp and weft interface and (b) bridging effect of binder yarn to crack propagation

Impact direction

100μm

(a)

| Weft stuffers | Warp yarns | Delamination between warp and weft yarn interface | Bridging effect of weft binder | Weft binder |

(b)
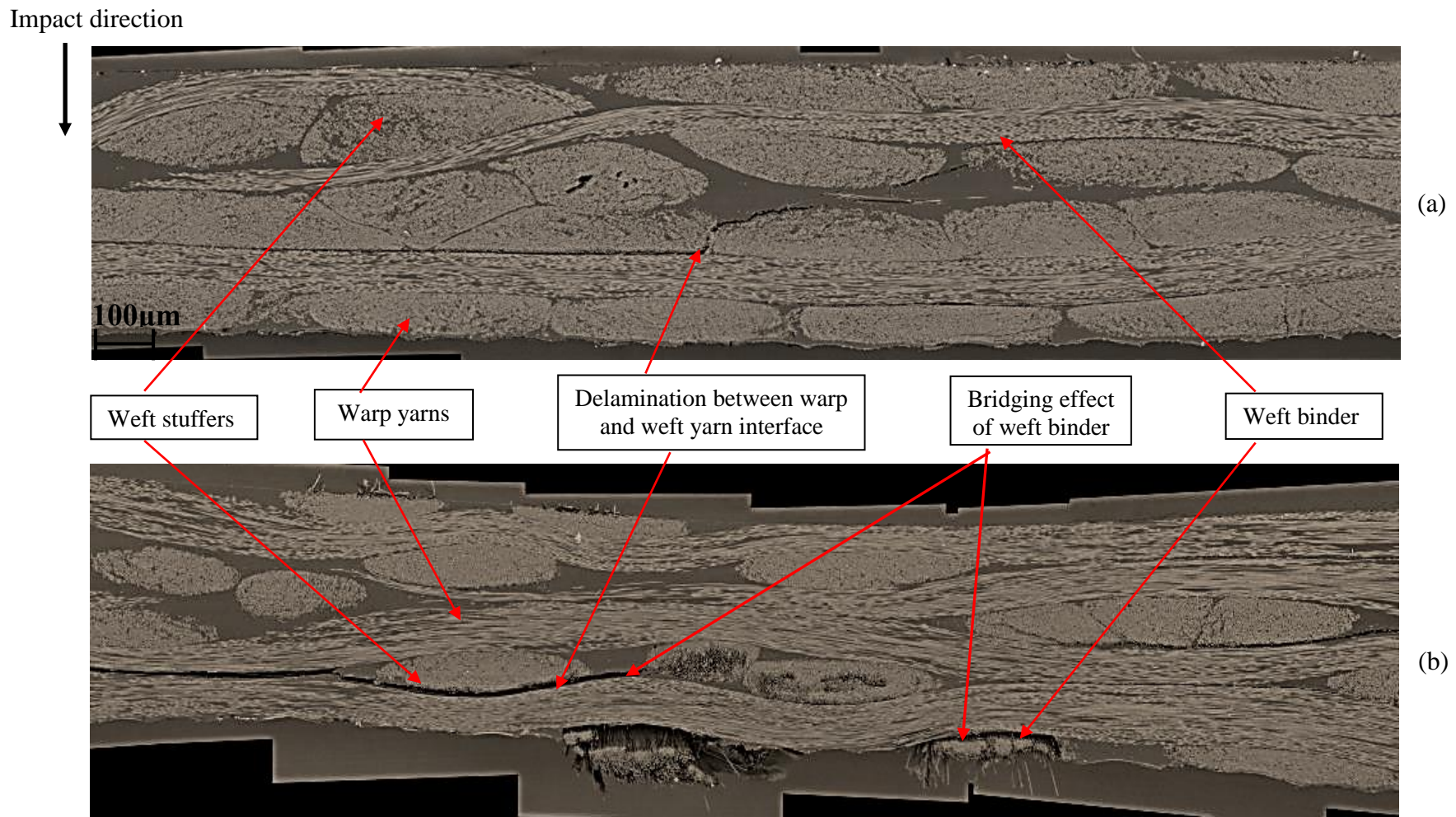
Figure 6.17 Micrographs of modified angle interlock structure showing impact induced features (a) Delamination between warp and weft interface and (b) bridging effect of binder yarn to crack propagation

154

	5J	10J	15J	20J	25J	30J	
							Layer-to-layer
							Angle interlock
							Twill angle interlock

155

5J	10J	15J	20J	25J	30J

Modified angle interlock

UD cross-ply
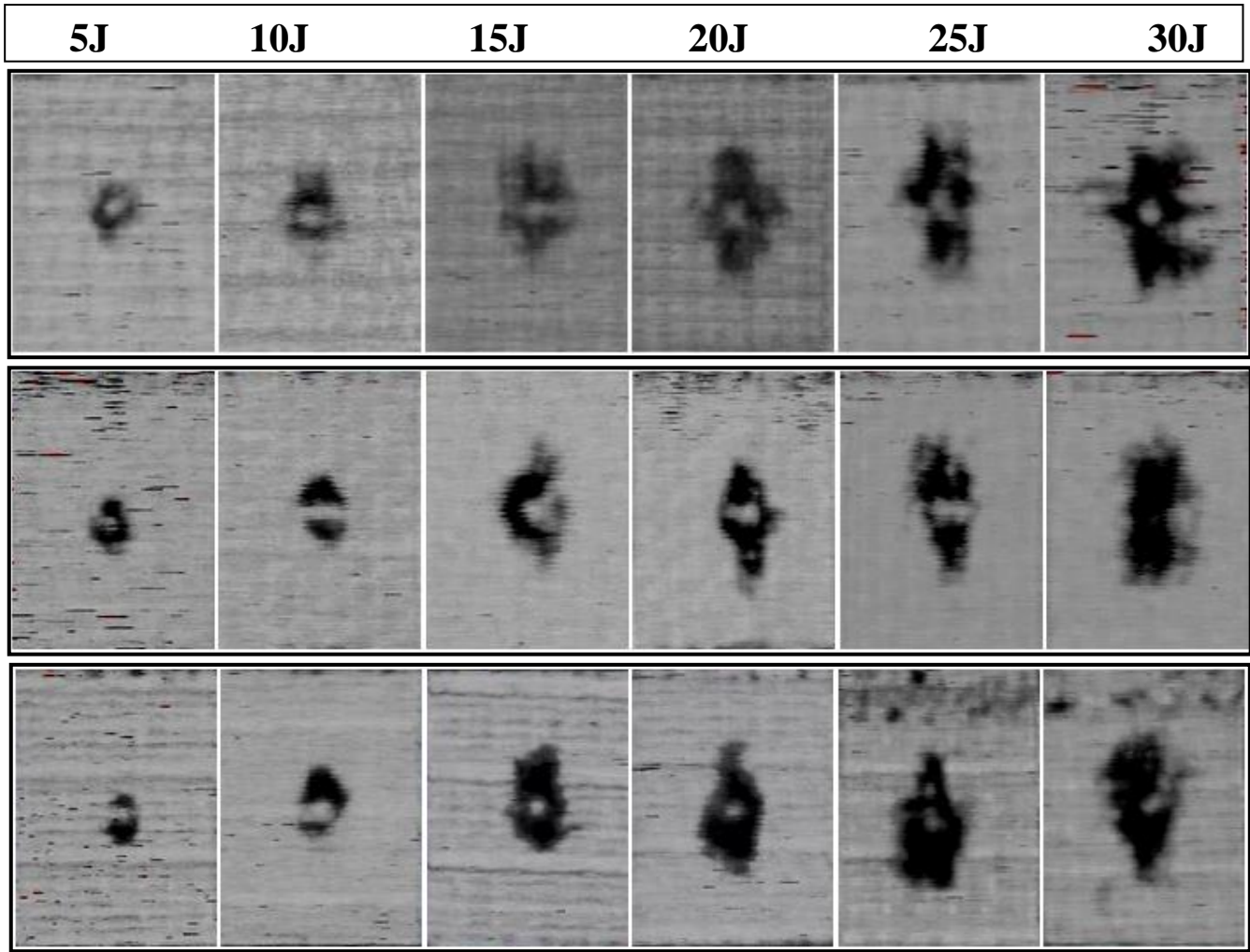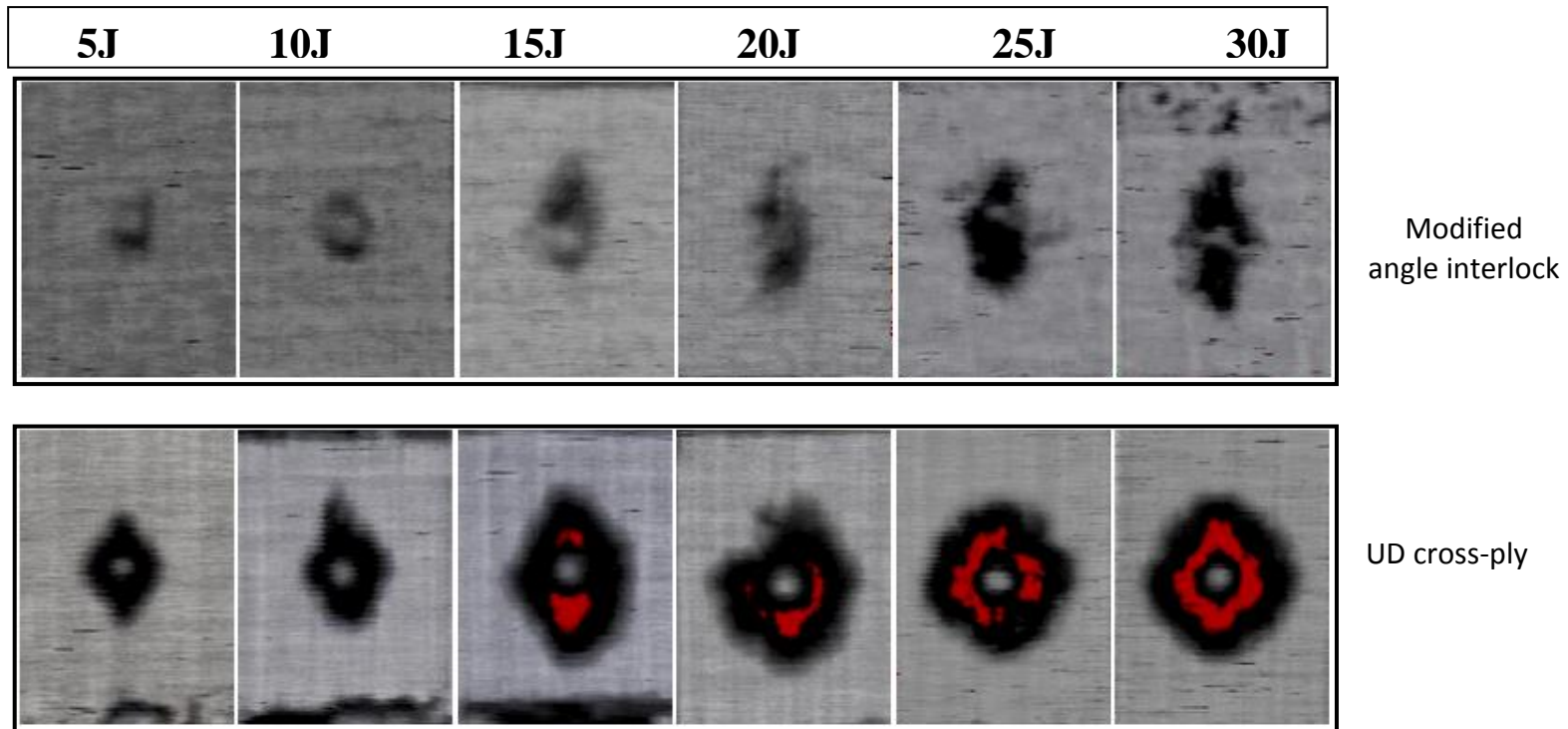
Figure 6.18 C-scan images of damaged area in the warp direction at different impact energies

	5J	10J	15J	20J	25J	30J	

Layer-to-layer

Angle interlock

Twill angle interlock

Continued

5J	10J	15J	20J	25J	30J	
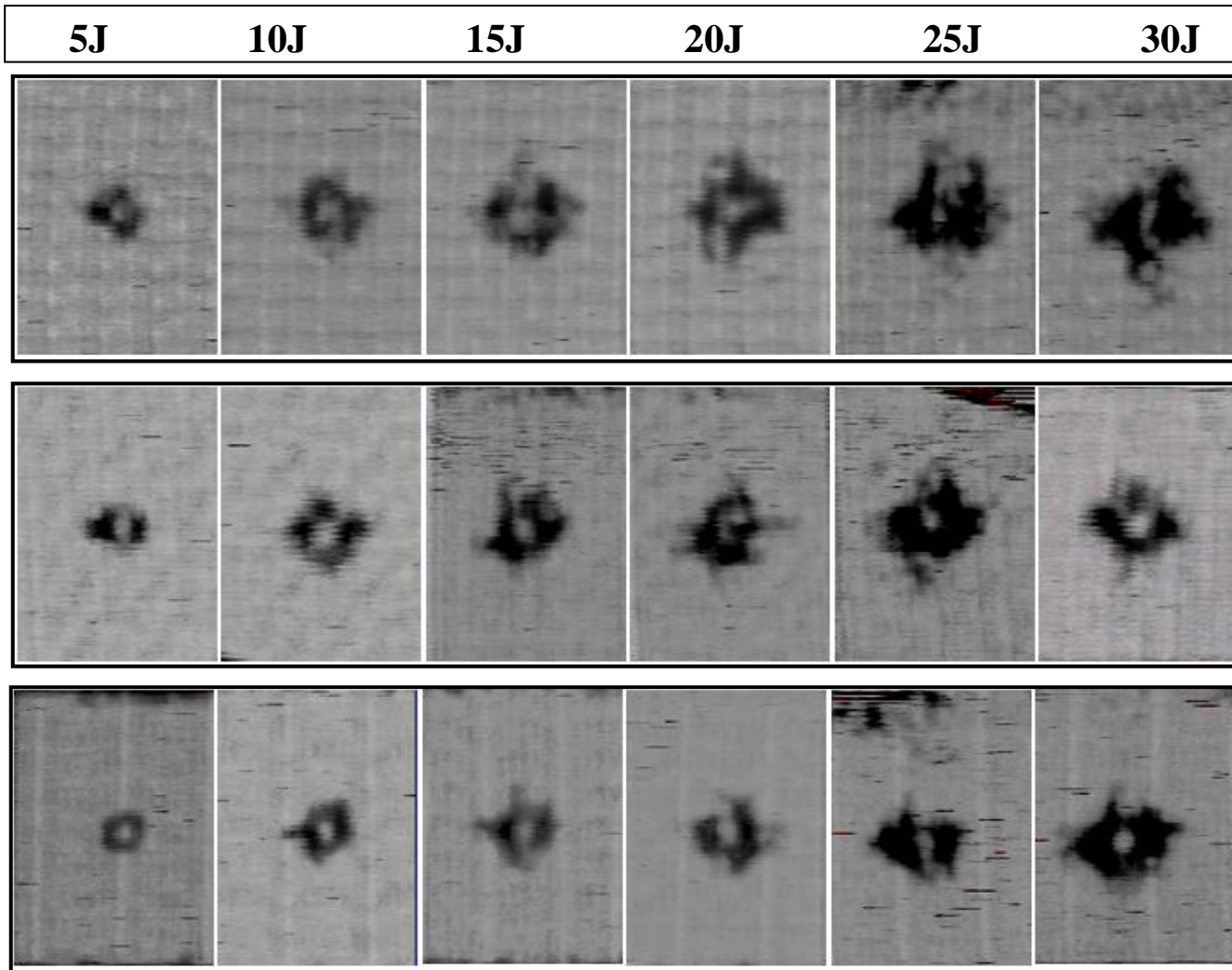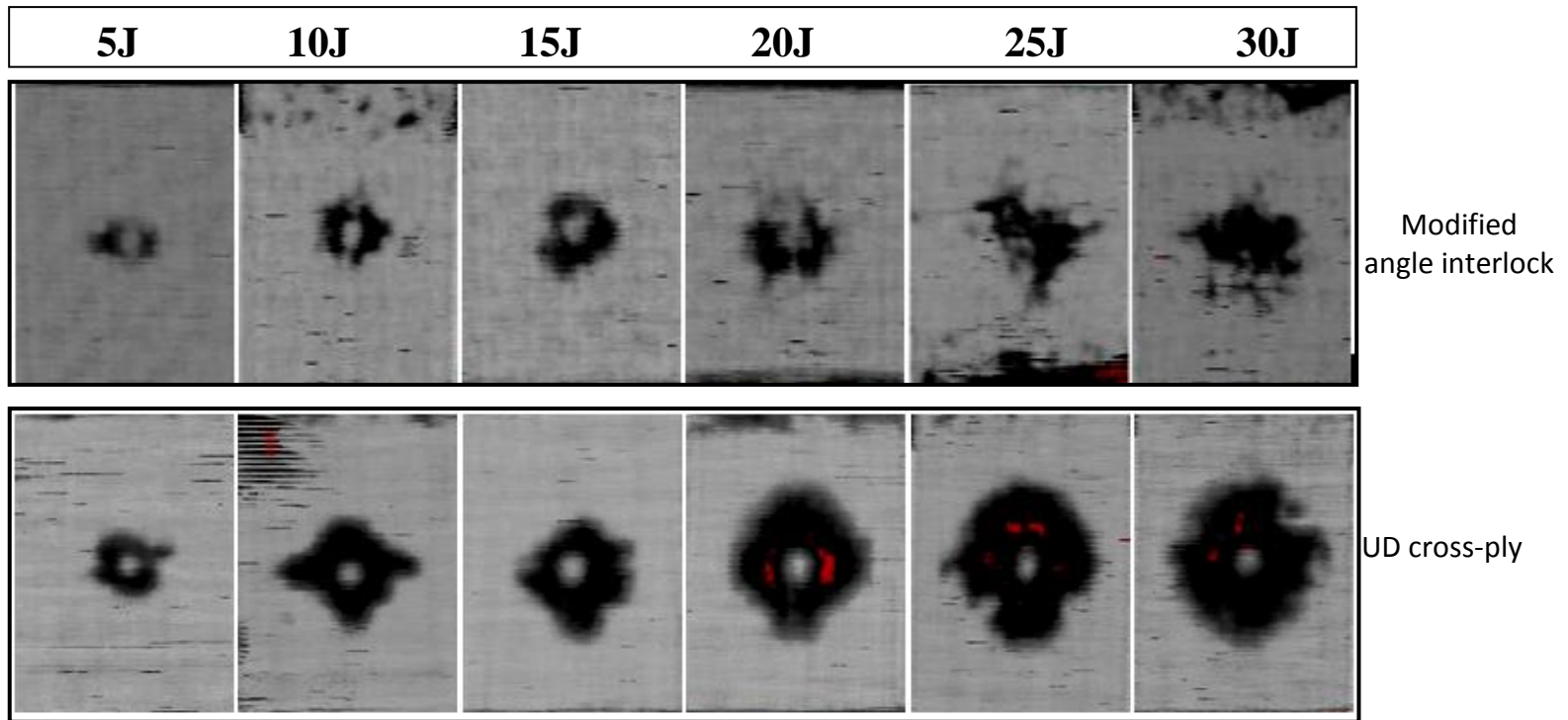
Figure 6.19 C-scan images of damaged area in the weft direction at different impact energies

6.5.2 Residual strength evaluation

Data for compression after impact strength and normalized strength of the 3D woven and the UD cross-ply laminates is shown in Figure 6.20 and Figure 6.27 respectively. The compressive strength is normalized according to the following equation:

$$\sigma_{nor} = \sigma_n / \sigma_{un} \qquad (1)$$

Where, σ_n = Notched compressive strength and σ_{un} = Unnotched compressive strength

The CAI and normalized strength is presented as a function of impact energy. There is a gradual reduction in the strength with respect to the impact energy.

Figure 6.28 and Figure 6.29 represents normalized compression strength as a function of damage width for the CAI and open hole compression test. For open hole compression specimens, the hole diameter is used as the characteristic damage width. This figure indicates strength reduction with the increase of impact energy, as well as the comparison of notch sensitivity of the material for holes and low velocity impact.

6.5.2.1 CAI as function of impact energy

The UD cross-ply laminate has the highest undamaged strength, as well as superior strength retention, with an increase in impact energy, when compared with 3D woven composites in both the warp and weft direction on the basis of impact energy (Figure 6.20). In both the warp and weft direction, strength dropped sharply at low energy levels especially up to 15 J impact energy and the strength retention in the warp direction appeared higher than in the weft direction. Similarly for 3D woven composites, the residual compressive strength in the warp direction is higher than in

159

the weft direction due to the high volume fraction of warp yarns. The trend line shows that in the warp direction, MAI, TAI and AI have better residual strength than LTL, while in the weft direction TAI shows the highest residual strength, followed by LTL, AI and MAI.
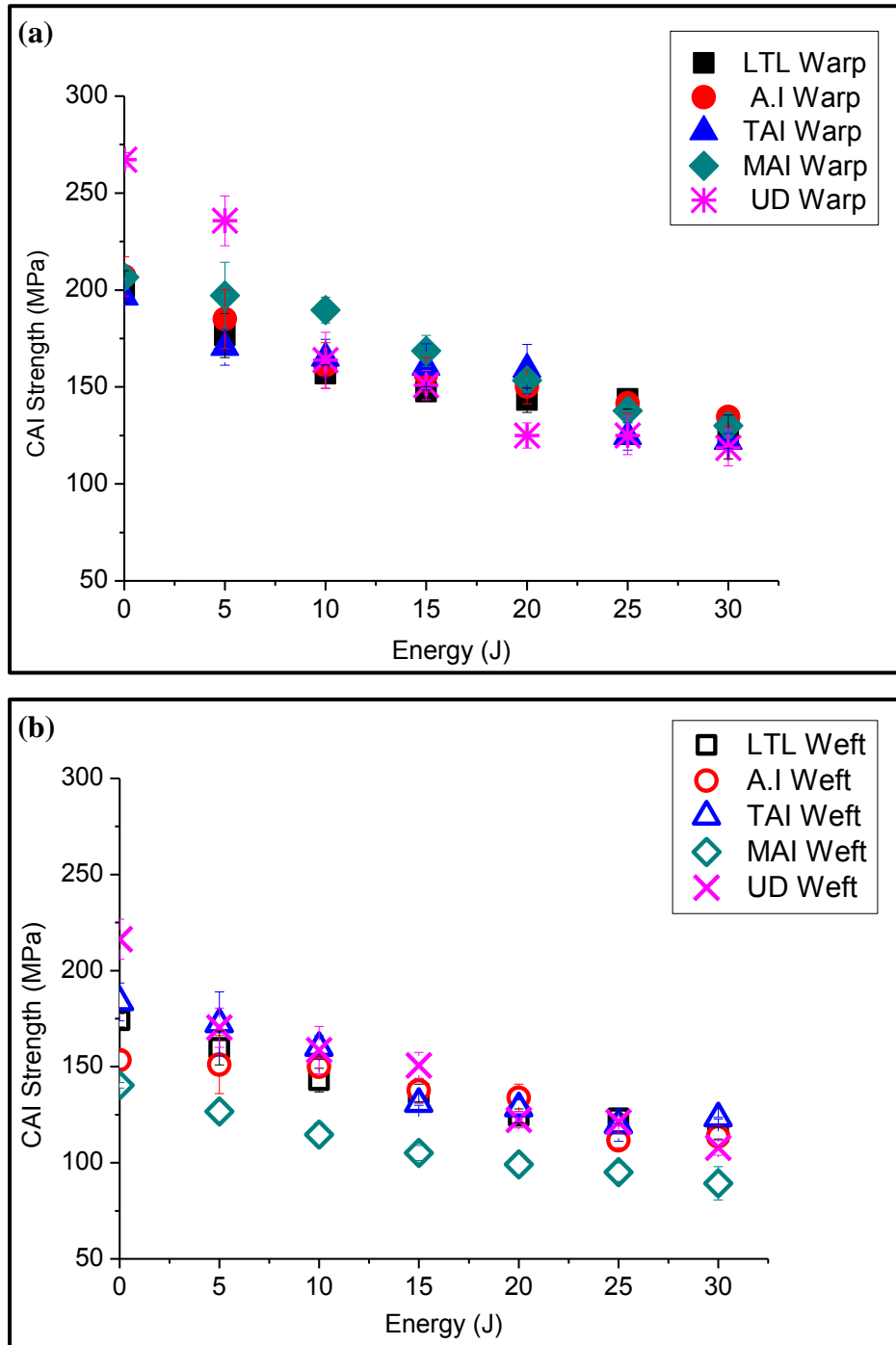
Figure 6.20 Compression after impact strength (CAI) vs impact energy (a) Warp direction
(b) Weft direction

The residual strength values and rate of change of compression strength with respect to impact energy is similar for the 3D woven structures in both directions. However, the MAI shows the lowest strength values in the weft direction and there may be two reasons for this: first, the damaged area and damage width of the weft impacted specimens were higher than for the other 3D woven structures; secondly, this structure has fewer straight yarns (weft stuffer) and more binder yarns along the loading direction. Therefore, when the specimens were loaded along the weft direction, they showed less strength as compared to the other woven structures in the same direction. In TAI, the binder passes over the two warp yarns and causes less disturbance to these as well as to the long binder floats, which also contribute to the strength generated under compressive load. This could be the reason for the better performance of the TAI structure, in both the warp and weft directions. Due to the weave pattern, the LTL and AI have more straight (or less wavy) yarns in the weft and warp directions respectively. This weave behaviour consequently affects the strength properties in the representative direction. This is because the compression after impact strength of a composite laminate is a primary function of undamaged compression strength. The undamaged compression strength is controlled by fibre architecture, fibre volume fraction and geometrical flaw defects such as crimp, damage to the fibres, manufacturing defects etc [10, 103].

In the CAI test, impacted specimens started to break from the impacted region and the damage extended to the edge, leading to the final failure. The specimens failed in a shear mode with local kinking. The shear failure occurred at an angle of 35-60 degree to the loading direction, and after the failure specimens were still in one piece. For 3D woven specimens, the warp yarn and weft stuffers buckled outwards under the compression load, although the warp yarns were constrained at those

points where the weft binder interlaced with them. As a result of local pressure exerted by the binder yarns the failure occurred in the warp yarns as well as in the weft stuffer; the warp yarns failed with a local kink band, while delamination failure occurred within the weft stuffer when the specimens were loaded along the warp direction. Similarly the weft stuffers and weft binder failed due to kinking when the loading direction was parallel to the weft yarns. Figure 6.21 depict the photographs of failed specimens, following the CAI test and open hole compression test show a similar failure pattern. The micrographs, presented in Figure 6.22 to Figure 6.25 show the compressive failure of 3D woven structures in both warp and weft direction during the open hole compression testing.

LTL	A.I	TAI	MAI	UD

(a)

(b)
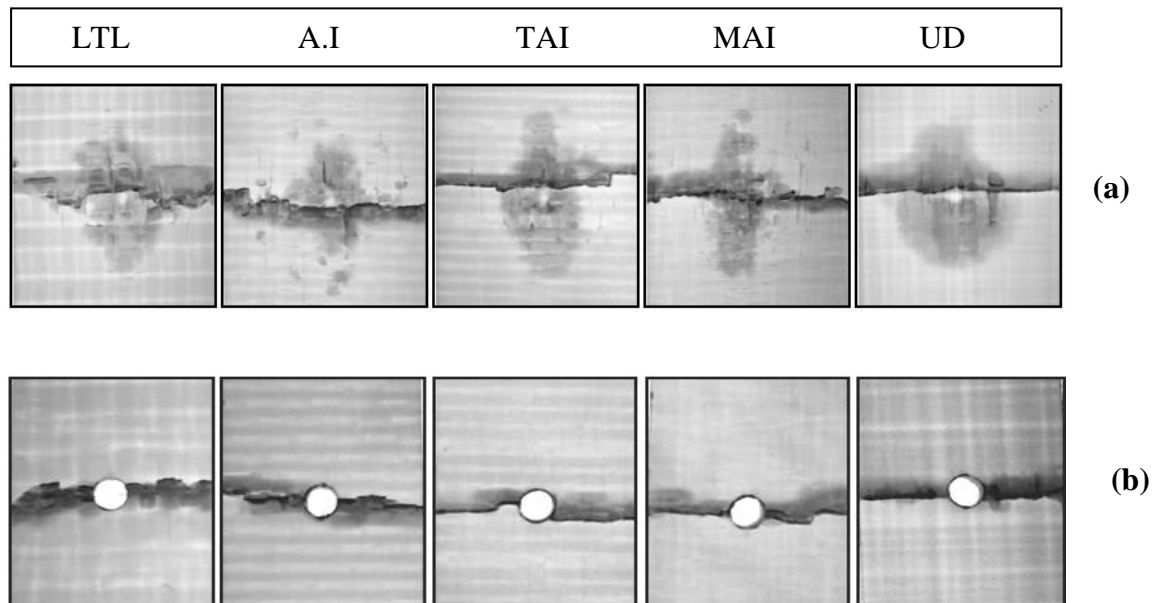
Figure 6.21 Photographs of failed specimens show similar damage propagation across the specimen width in both warp and weft direction after (a) CAI test at 30J impact energy (b) Open hole compression test

Loading direction

(a)

100μm

Delamination within weft stuffer yarn

Kinking in warp yarn

Delamination within warp yarn

Kinking in weft binder

(b)

100μm
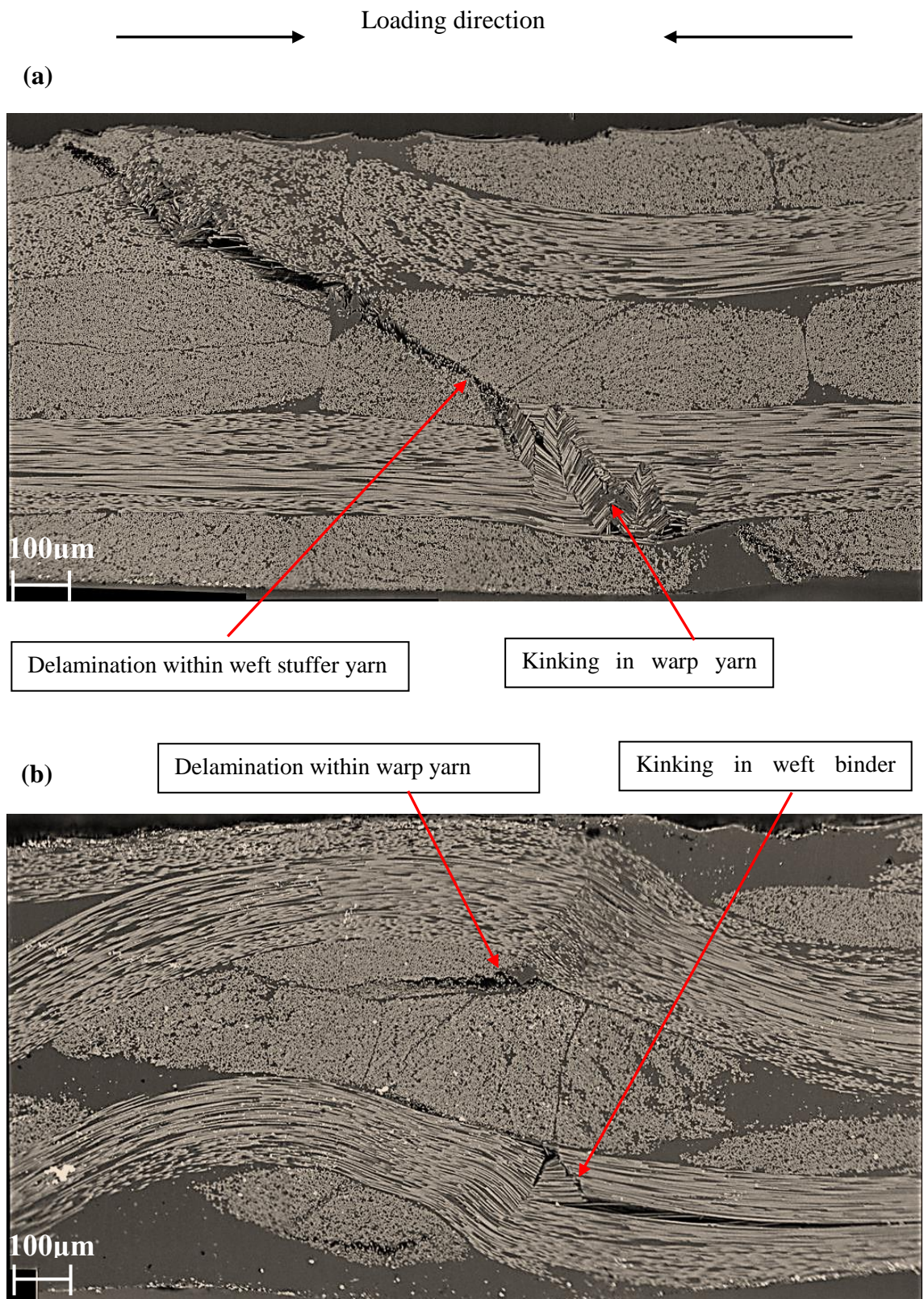
Figure 6.22Fracture of layer-to-layer structure in compression (a) Along the warp yarns (b) Along the weft yarns

(a)

100μm

Delamination within warp yarn and weft stuffer

Kinking in warp yarns

Delamination within warp yarn

Kinking in weft stuffer

(b)

100μm
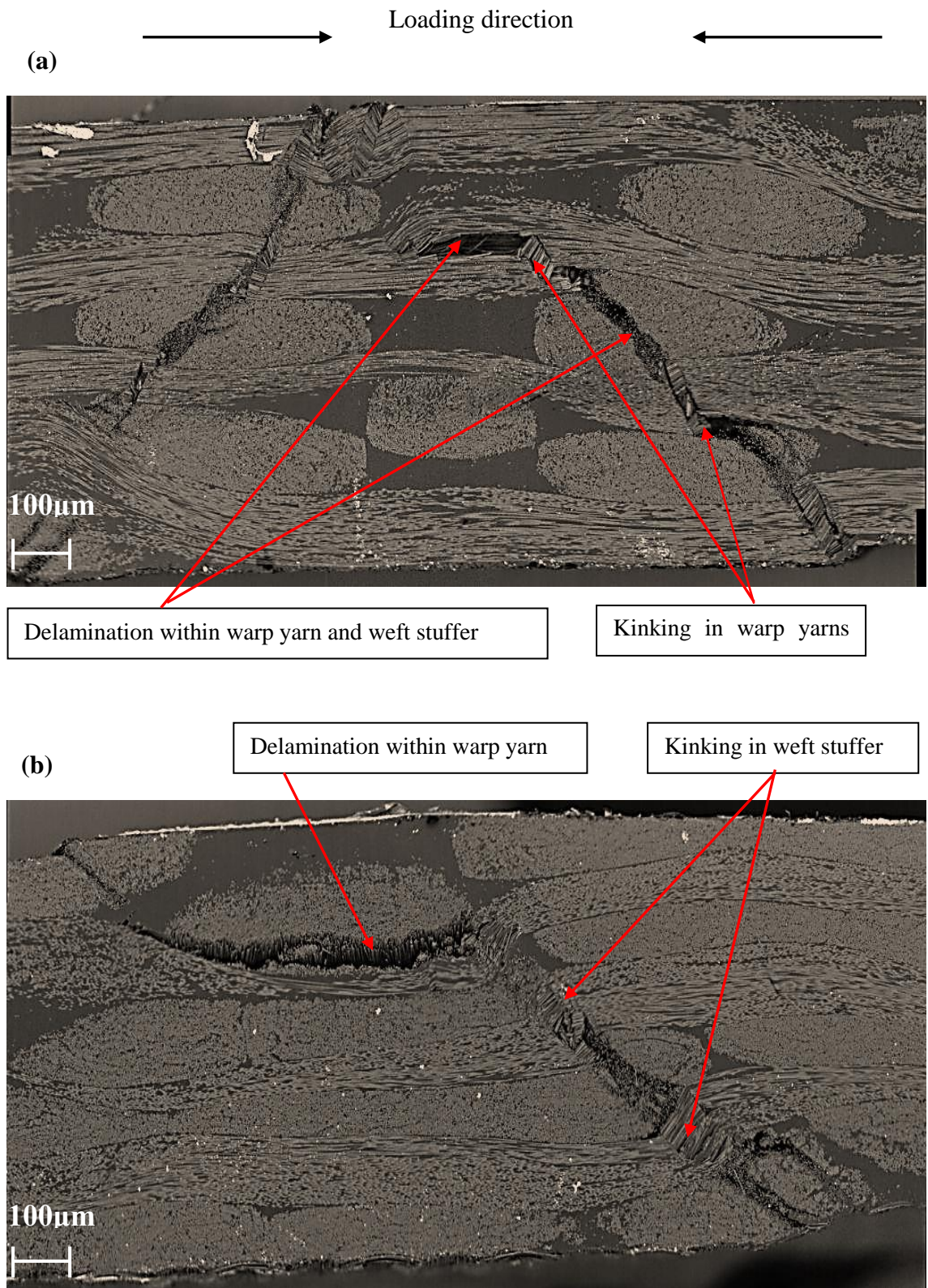
Figure 6.23 Fracture of angle interlock structure in compression (a) Along the warp yarns (b) Along the weft yarns

(a)

Kinking in warp yarns   Delamination within weft stuffer

Kink band in weft binder   Delamination within warp yarn   Kinking in weft stuffer

(b)
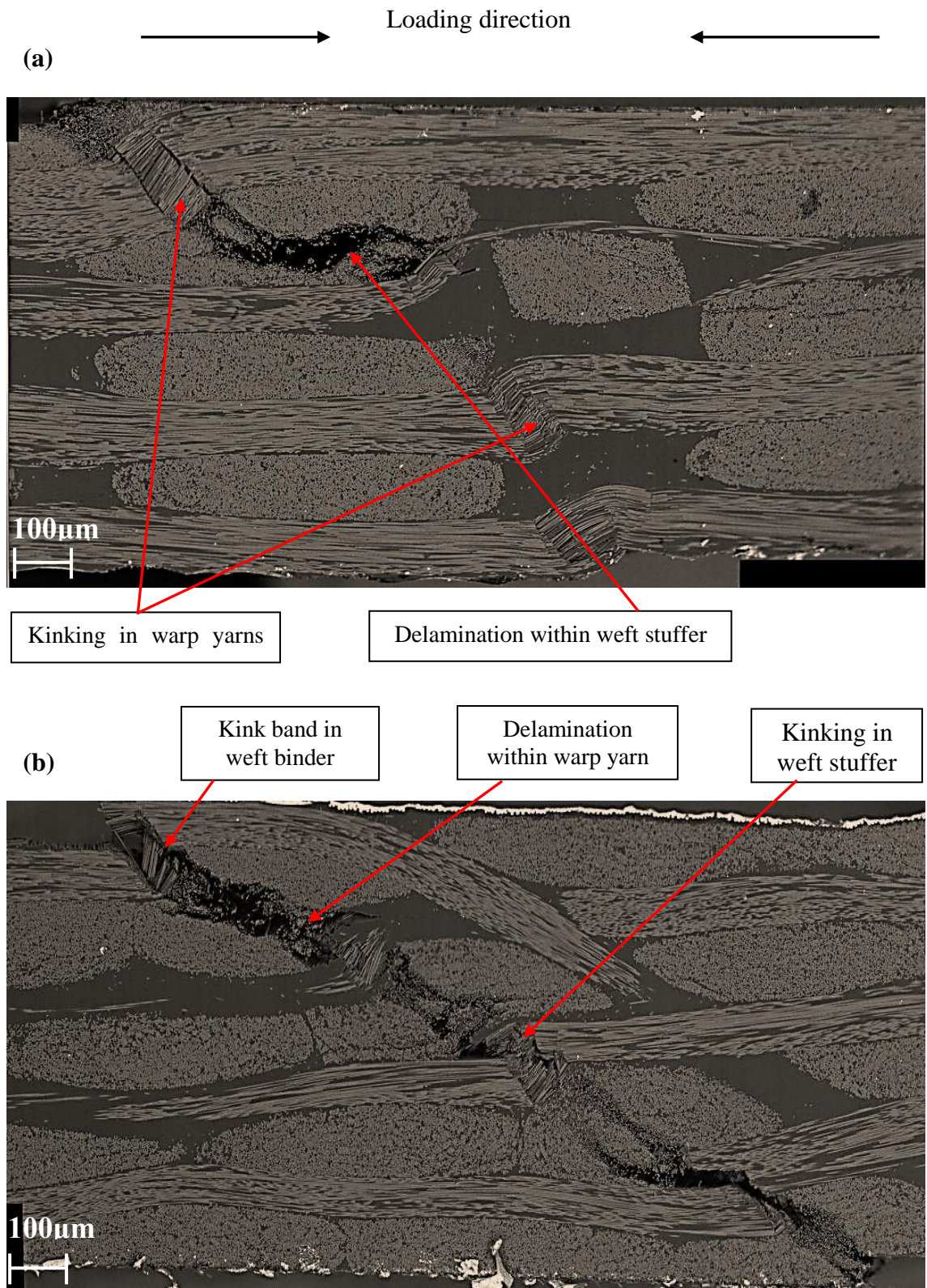
Figure 6.24 Fracture of twill angle interlock structure in compression (a) Along the warp yarns (b) Along the weft yarns

(a)

100μm

Delamination within weft stuffer

Kinking in warp yarns

Delamination within warp yarn

Kinking in weft binder

(b)

100μm
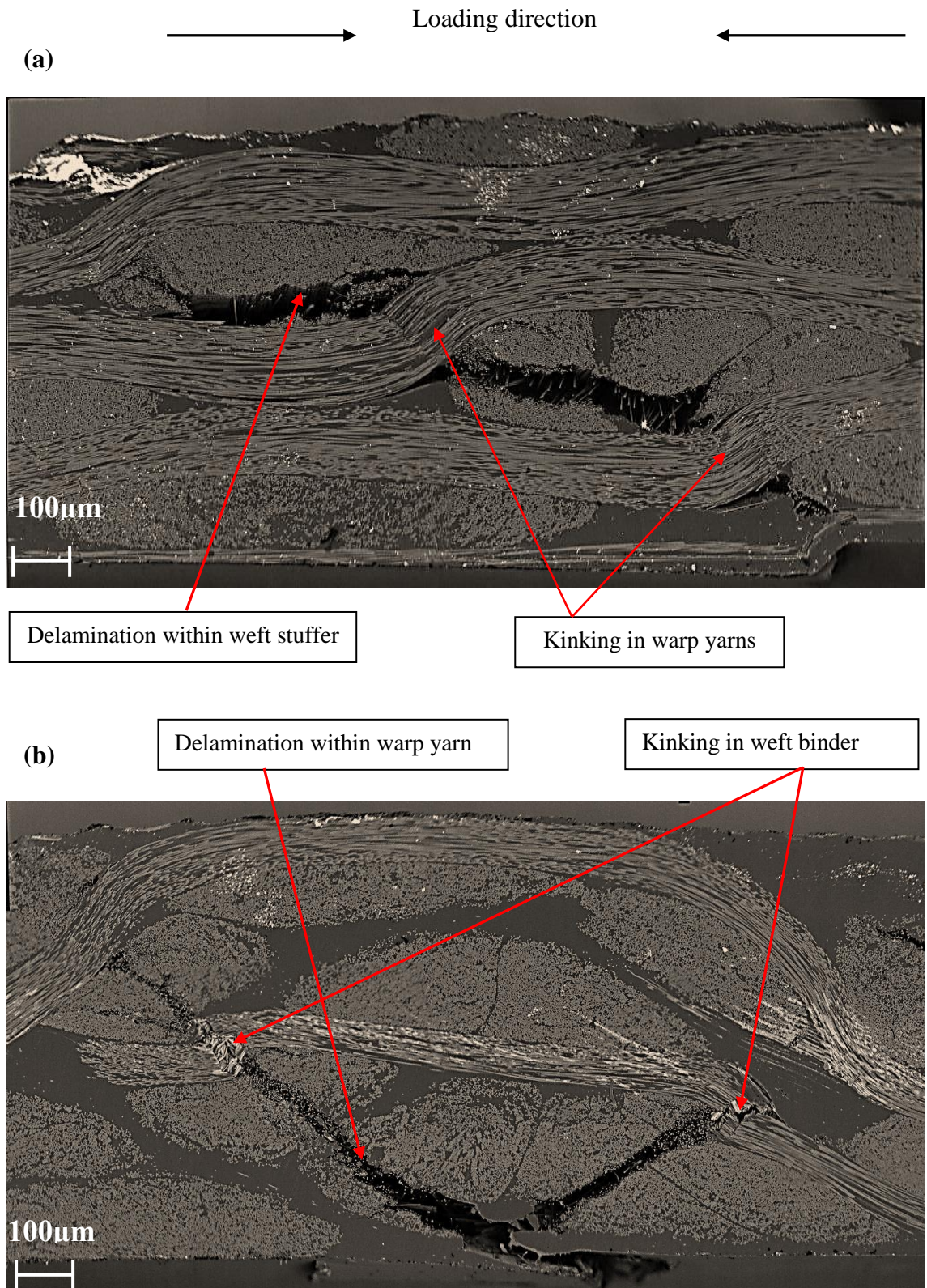
Figure 6.25 Fracture of modified angle interlock structure in compression (a) Along the warp yarns (b) Along the weft yarns
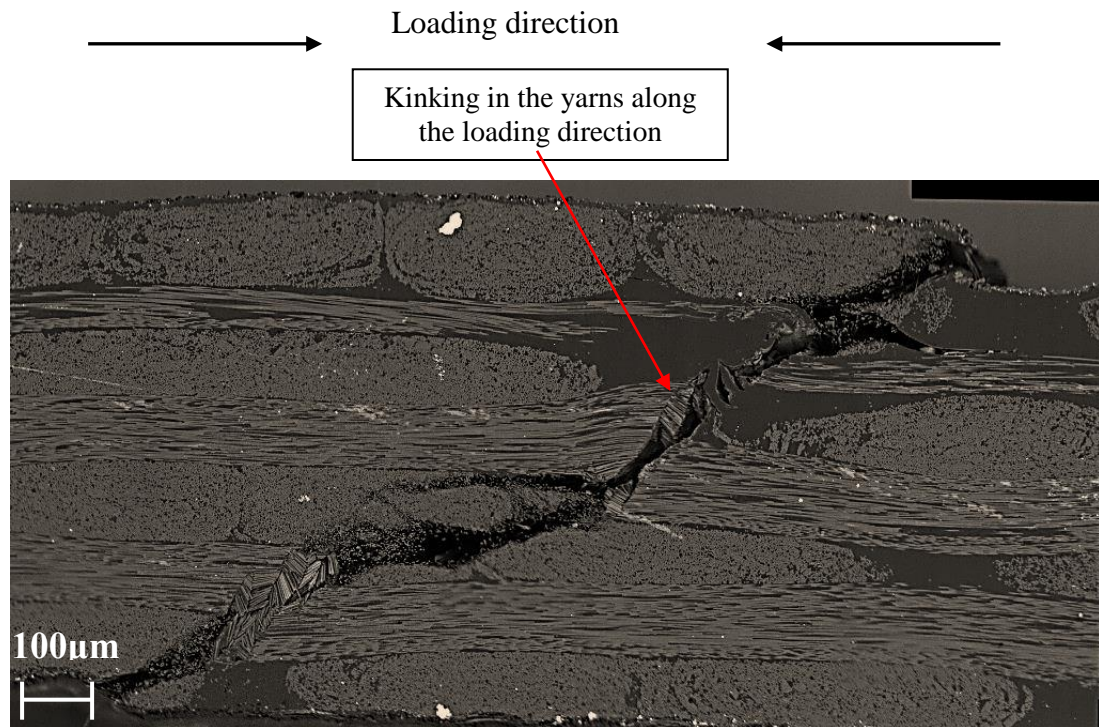
Figure 6.26 Fracture of UD cross-ply under compression

6.5.2.2 **Normalised compressive strength as a function of impact energy**

Normalized compressive strength as a function of impact energy is represented in Figure 6.27. The plot shows that the 3D woven composites are more damage tolerant than the UD cross-ply laminate, in both the warp and weft directions. Strength decreases with an increase in impact, and the strength reduction is higher for the UD laminate. However, a gradual decrease in normalized compressive strength can be observed for 3D woven composites. Within the 3D woven composites, the normalized strength (or notch insensitivity) of MAI is higher up to an impact energy of 15 J, and beyond that all the structures exhibit the same normalized strength in the warp direction. In the weft direction, however the AI shows the highest normalized compressive strength or notch insensitivity. It can be assumed that the high stress concentration at the binder interlacement point precedes the delamination crack growth at lower load levels, increasing the ultimate compressive strength of the

impacted specimens by load redistribution; LTL, TAI and MAI experienced a similar

strength reduction along the weft direction.
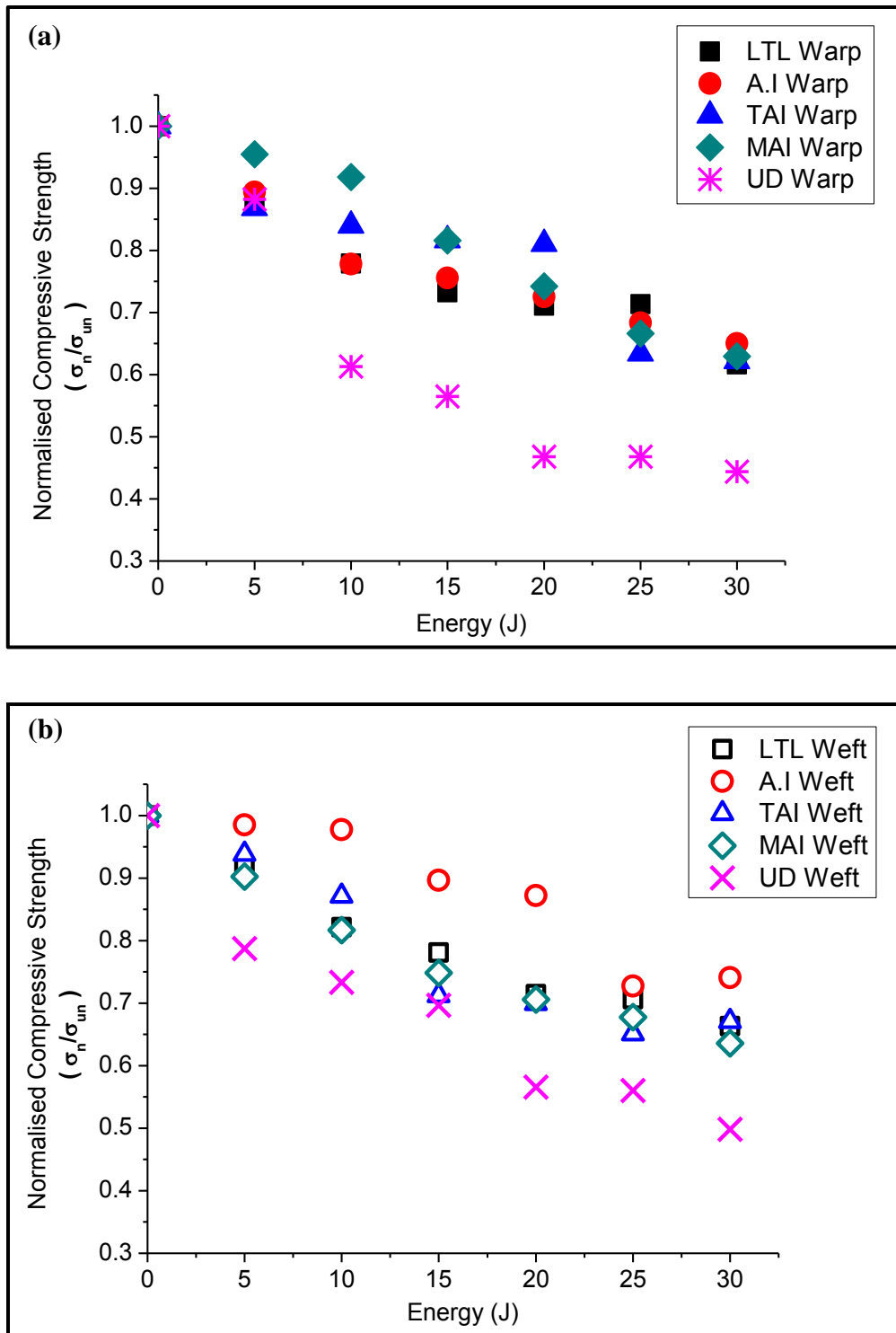
Figure 6.27 Normalised strength vs impact energy (a) Warp direction (b) Weft direction

6.5.2.3 Normalised compressive strength as a function of damage width

The damage tolerance/notch sensitivity under compression of 3D woven and UD laminate for open hole and impact damage is compared in Figure 6.28 and Figure 6.29. The normalized compressive strength is plotted as a function of damage width. The plot displays that for low velocity impacts the strength decreases with an increase in energy level or damage width. At the highest energy level (30J) the 3D woven and UD laminate retains almost 62% and 44% of their undamaged compressive strength, respectively (Figure 6.27). The 3D woven and UD laminate composites retain most of their undamaged strength up to a damage width of 15 mm and these values are: 87% (LTL), 89% (AI), 86% (TAI), 95% (MAI) and 88% (UD) in the warp direction, and 91% (LTL), 98% (AI), 93% (TAI), 90% (MAI and, 78% (UD) in the weft direction. Beyond a damage width of 15 mm the strength of the UD laminate reduces steeply, especially in the warp direction. Whereas a gradual decrease in normalized compressive strength with the damage extent can be observed for 3D woven composites. Likewise, evaluating the normalized compressive strength ($\sigma_n/\sigma_{un)}$ of the open hole (OHC) as a function of damage width also indicates that 3D woven composites are less notch sensitive than UD cross-ply laminate. Furthermore, the normalized strength of 3D woven structures for small holes is almost the same in both directions, following the same trend as normalized strength at 5J impact energy. That is, except for the AI structure whose normalized OHC strength is lower than the normalized strength measured at 5J impact energy. This difference can an effect of the specimens, because due to material availability only one specimen was tested to measure the unnotched strength for open hole compression.
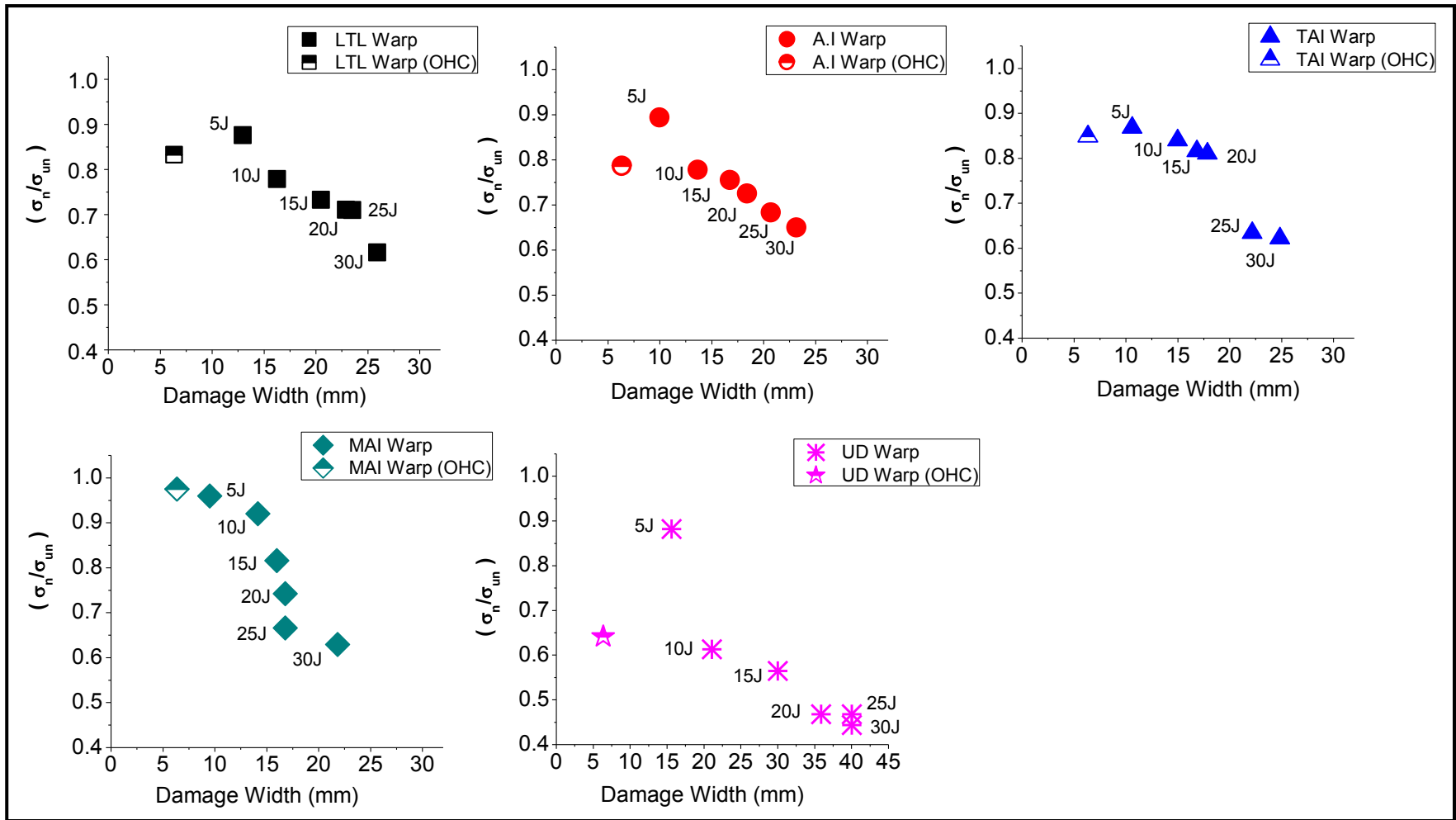
Figure 6.28 Normalized compression strength vs damage width in the warp direction
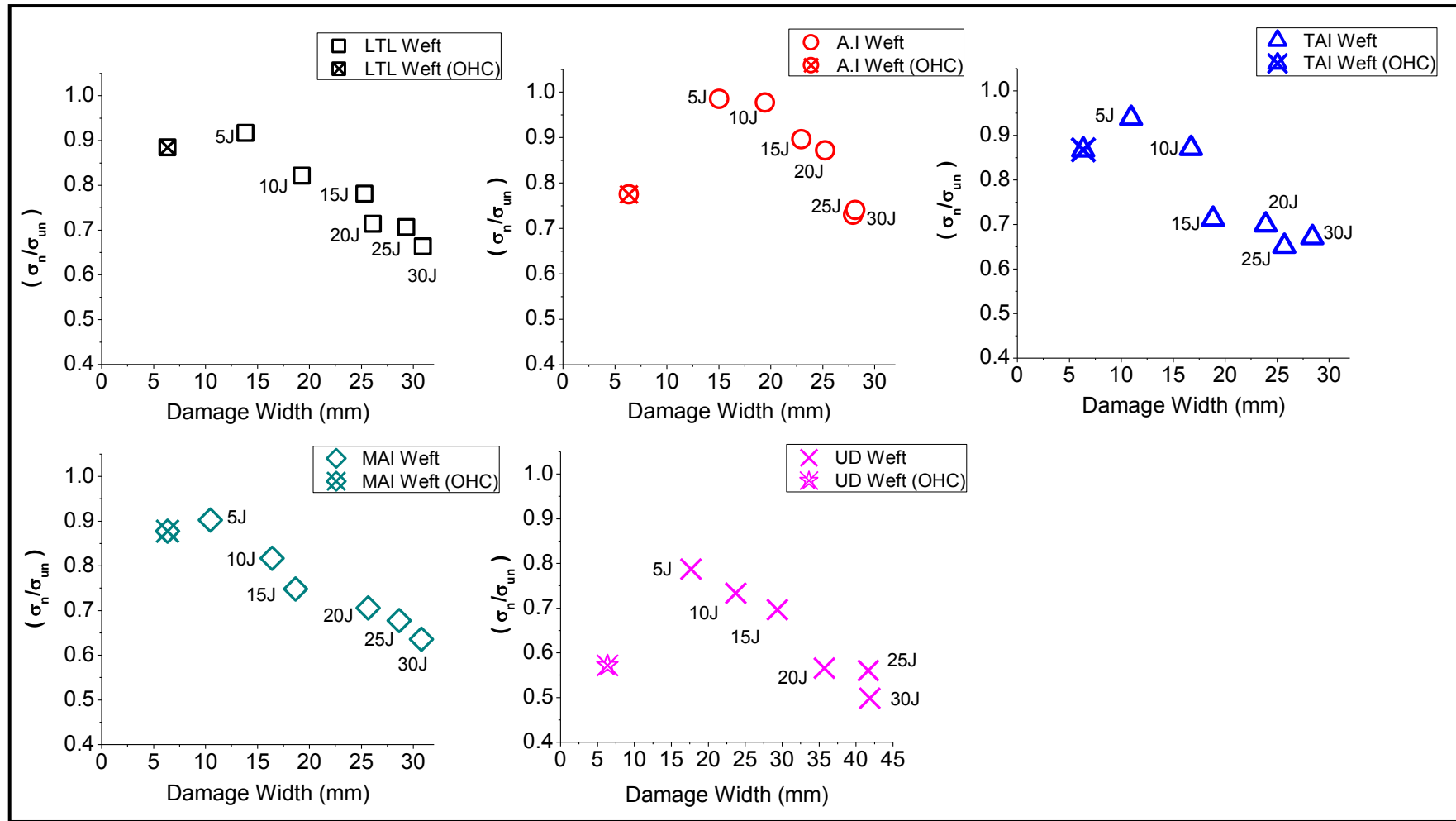
Figure 6.29 Normalized compression strength vs damage width in the weft direction

Beyond the 15 mm damage width, the strength of the UD laminate reduces steeply. The comparison of residual compressive properties for an open hole and low velocity impacts indicates that the presence of the hole is more severe than an impact damage, even if the area of the damage is almost doubled. The UD cross-ply laminate is more sensitive to notches than are the 3D woven composites. The binder yarn in the 3D woven improved the damage tolerance of the panels by suppressing delamination and further development of the fracture under compression failure.

6.6 Summary

This part of the research showed that fibre architecture has a major effect on energy absorption, damage propagation, damage resistance and damage tolerance of two different composite systems: UD cross-ply laminate and 3D woven composites. Among the 3D woven composites, four different weave architectures: layer-to-layer, angle interlock, twill angle interlock and modified angle interlock were studied.

It was observed that the maximum contact force, absorbed energy and damaged area increase approximately linearly with the force of the impact energy. The damaged area for the 3D woven composites is half that of the damaged area for UD cross-ply at the same impact energy, whereas the difference in the absorbed energy is not that significant. The damage propagates along the yarn direction in both the 3D woven and the UD cross-ply laminate. However, in woven composites it is more localized because the binder yarn restricts damage propagation at the binder cross-over point; whereas in the UD laminate the damage is predominantly intra-ply and spread in a circular shape up to the support fixture. Similarly, 3D woven composites have significantly higher damage resistance, therefore more energy is required to cause a unit area of damage compared to the UD laminate. Within the 3D woven structures,

the MAI structure displays better impact resistance in both the warp and weft direction.

The residual compressive strength of the impacted panels decreases with an increase in impact energy. The UD laminate has higher residual strength reduction than the 3D woven composites in both directions and a steep fall in the strength is observed at impact energies of 5 J & 10 J. The rate of change of CAI with respect to impact energy is similar for all 3D weaves. The CAI strength values are almost similar for 3D woven composites in both directions, except AI and MAI, showing the highest and lowest strength values in the weft direction, which depends on the percentage of straight yarns parallel to the loading direction. The normalized compressive strength value shows that the 3D woven structures are notch insensitive and more damage tolerant than the UD laminate at various impact energies and damage widths. However, AI shows higher damage tolerant properties along the weft direction, and it is presumed that the high stress concentration at the binder interlacement point precedes delamination damage at lower load levels, increasing the ultimate compressive strength of the impacted specimens by load redistribution. In contrast, the strength loss for open holes is higher than low velocity impacts, especially for UD laminate.

It is concluded that the 3D woven structures are more impact resistant and damage tolerant than the UD cross-ply laminate. The use of the binder yarn in a weft direction make the woven structure almost equally damage tolerant in both warp and weft directions, and when experiencing high impact energies (20-30 J). The next chapter presents the final conclusions of this research.

7   Conclusions and Recommendations

7.1   Introduction

Three dimensional woven composites are prime examples of advanced materials with potential application in the industrial, aerospace and military sectors. These materials possess sufficient high in-plane mechanical properties whilst retaining the benefits of integral through-thickness reinforcement, and the ability to produce near net-shape preforms for structural components. However, the mechanical characterization of 3D woven composites under different loading conditions has not been fully examined. Therefore, the aim of the proposed research was to investigate the effect of weft binder on damage tolerance as well as on in-plane tensile and compression properties in both the longitudinal and transverse directions. In addition to this, the modification of 3D weave architecture for improved mechanical properties was also investigated.

The research programme has involved the fabric and composites manufacturing of four different 3D woven structures, layer-to-layer (LTL), angle interlock (A.I), twill angle interlock (TAI) and modified angle interlock (MAI) using in-house weaving and resin infusion facilities. In order to compare the properties of 3D woven composites, UD cross-ply laminate was fabricated with a similar fibre density. In-plane as well as out-of-plane testing was performed to provide new insights into in-plane tensile properties, notch sensitivity, impact resistance and damage tolerance for weft bound, 3D woven composites. Further, the comparison of mechanical properties and the failure mechanism of 3D woven composites with UD cross-ply laminate in both warp and weft directions were identified and discussed. The following section gives a brief summary of all the findings and accomplishments.

7.2 Conclusions

Tensile properties

The tensile strength, modulus, strain-to-failure and failure mechanism of 3D woven and UD cross-ply laminate were studied experimentally, while Digital Image Correlation (DIC) was used to analyze the influence of weave architecture on local strain behaviour. The UD cross-ply laminate exhibited higher strength and stiffness properties due to the presence of non-crimp yarns in both directions (warp and weft). Among 3D woven structures, the weave architecture influenced strength and modulus properties. The influence of the weave pattern was the combined effect of crimp % in the fabric, stress concentration at the binder yarn points, resin-rich areas and number of binder yarns per unit, as discussed in chapter 4. The effect of weave architecture on the ultimate strength of the material was more prominent in the warp direction than in the weft direction, while the elastic modulus was less affected by the weave configuration. The high warp crimp and resin-rich areas induced by the binder yarn led to a lower AI strength along the warp yarns. Owing to binder path modification, the long TAI binder floats reduced the binder crimp, and increased the amount of aligned tows in the loading direction, giving superior modulus, with the same strength properties as the LTL structure in both (warp and weft) directions. However, it was the MAI that exhibited the highest tensile strength in the warp direction, while the lowest strength and stiffness in the weft direction was a consequence of a higher number of binder yarns parallel to the loading direction. It was found that tensile strength in the can be improved by reducing stress concentration arising from the pinching of the binder yarn.

Further, the analysis of surface-strain maps of the 3D woven composites found that maximum local strain occurs on the 3D laminate surface at the binder yarn crimp

location, and that the localized strain values were approximately two to three times higher than the specimen strain-to-failure. The localized stress and strain concentration at the binder interlacement point led to yarn splitting in the warp direction and localized specimen fracture in the weft direction.

Open hole tensile properties

It was concluded that the loading direction was influential to the notch sensitivity of 3D woven composites. When the notched specimens of 3D woven composites were loaded in tension, the undulation of the binder yarn allowed the damage to grow easily along the binder yarn, reducing the stress concentration by extensive matrix cracking, delamination and transverse cracking. Therefore, a high notched strength as well as notch insensitivity was achieved in the weft direction. However, in the warp direction specimen, the stress relieving and energy absorption mechanism was inhibited by the binder yarns, which restricted the crack propagation and delayed the splitting of the yarn. All the 3D woven composites exhibited the same notch insensitivity in the warp direction, whereas in the weft direction the AI was about 9% more notch sensitive than the LTL, TAI and MAI structures. The stress concentration and sharp curve of the binder yarn in AI affected the load carrying capability of the binder yarns, consequently reducing the ultimate notched strength. In comparison to UD cross-ply laminate, the 3D woven composites appeared more notch sensitive in the warp direction due to restrained damage propagation. UD cross-ply laminate appeared to exhibit better notch insensitivity in both warp and weft directions, whereas 3D woven composites showed less notch sensitivity along the binder yarns.

Impact resistance

The out-of plane damage behaviour of the 3D woven and UD cross-ply laminate was investigated using low velocity impact. It was concluded that through-thickness reinforcement (binder yarn) of 3D woven composites improved the impact resistance by crack arresting, thus suppressing delamination and crack propagation. Absorbed energy and damaged areas were seen to increase with the growth of impact energy. The analysis of ultrasonic c-scan and energy absorption data revealed that the 3D woven composites absorbed almost the same amount of energy to give a damaged area which was half that exhibited by the UD cross-ply experiencing the same impact energy. The damage propagated along the longer yarn floats, and this phenomenon was more prominent at the high impact energy levels in which the damage area of 3D woven composites was elliptical-shaped and diamond-shaped for warp and weft impacted specimens, respectively. However, damage was also more localized because binder yarn restricted the damage propagation, whereas in the UD laminate the damage appeared to be predominantly intra-ply and spread in a circular shape up to the support fixture. Similarly 3D woven composites have significantly higher damage resistance, therefore more energy is required to cause a unit area of damage compared to the UD laminate. Within the 3D weaves, the MAI exhibited better impact resistant, due to more binding between the binders and warp yarns reducing interfacial damage and absorbing energy in the form of fibre breakage.

Residual compressive strength properties

The small damaged areas across the 3D woven composites led to relatively small decreases in residual compressive strength. A gradual fall of residual compressive strength with an increase in impact energy showed the ductile behaviour and damage

tolerance of 3D woven composites. On the other hand, a sharp fall in residual strength with an increase in impact energy was an indication of the lower damage tolerance of the UD cross-ply laminate under compressive loads. Better impact resistance and damage tolerance for 3D woven composites was attributed to high interlaminar fracture toughness, which gave less extensive delamination within the impacted specimens and suppressed the further development of fracture under compression. The 3D weaves exhibited almost the same normalized compressive strength (σ_n/σ_{un}) in both warp and weft direction except for the AI structure which gave higher damage tolerant properties in the weft direction. It is proposed that the high AI damage tolerance was due to stress redistribution; whereby the yarn misalignment and the stress concentration at the interlacement point led to delamination damage at lower load levels, increasing the ultimate compressive strength of the impacted specimens. Furthermore, the comparison of normalized residual compressive strength properties for open hole "damage" and low velocity impact damage showed that the strength loss for an open hole was more than for an impact damaged specimen, even though the damaged area was double, when caused by an impact event.

7.3 Summary

The effect of the weft binder as well as weave optimization for improved damage tolerance and in-plane properties of 3D woven composites have been analysed in comparison to a UD cross-ply laminate. It was found that stress concentration due to the binder yarn caused lower in-plane mechanical properties compared with UD cross-ply laminate. Improved in-plane and damage tolerance properties of 3D woven composites in a specific direction can be achieved by modifying the weave architecture. The influence of binder direction and weave architecture is more prominent on in-plane and damage tolerance (notch sensitivity) under tensile loads, and 3D woven composites

achieved higher notch insensitivity along the binder yarns. However the influence of the weave architecture and binder yarn orientation on the normalized compressive strength properties of 3D woven composites is negligible. This observation supports the findings for notch insensitivity, damage resistance and damage tolerance in both longitudinal and transverse directions. The high fracture toughness and crack bridging phenomenon, occurring due to through-thickness reinforcement, led to significantly high damage resistance and also damage tolerance of 3D woven composites compared to UD cross-ply laminate.

This research is the first step as well as a basic guide for the scientific/ industrial community to understand the influence of weft binder on the in-plane and damage tolerance properties of 3D woven layer-to-layer and angle interlock structures. The following are the approximate design rules that are generated from this research. These design rules provide a comparison between the weave architectures in both warp and weft directions separately.

Weave Structures	Tensile Strength		Normalised Tensile Notched Strength		Impact/ Damage Resistance		Normalised Compressive Strength (CAI and OHC)	
	Warp	Weft	Warp	Weft	Warp	Weft	Warp	Weft
LTL	↑↑	↑↑↑	↑↑	↑↑↑	↑↑	↑↑↑	↑↑↑	↑↑
A.I	↑	↑↑	↑↑	↑↑	↑↑	↑↑↑	↑↑↑	↑↑↑
TAI	↑↑	↑↑↑	↑↑	↑↑↑	↑↑	↑↑↑	↑↑↑	↑↑
MAI	↑↑↑	↑	↑↑	↑↑↑	↑↑↑	↑↑↑	↑↑↑	↑↑

Strong = ↑↑↑   Medium = ↑↑   Weak = ↑

The mechanical properties for 3D woven architectures can be improved upon in the required direction, and under specific loads, by altering the binder path and fibre volume fraction in the specific direction.

7.4 Recommendations for further work

Recommendations that would be valuable extensions to the development of these materials include:

- A parallel comparison of similar 3D woven structures with warp binder would help to fully identify the influence of binder yarn direction on mechanical properties.

- Further mechanical tests such as fatigue, interlaminar toughness and interlaminar shear tests could provide a significant amount of information about the influence of binder path modification on durability and interlaminar properties and their comparison to standard 3D woven structures such as layer-to-layer and angle-interlock.

- FE analysis of the 3D woven composites used in the present study and their comparison with the experimental data would be useful in order to predict the failure mechanism of optimized 3D weave architectures under different loading conditions.

References

1.	A.Miravete, *3-D textile reinforcements in composite materials*. 1999: CRC PressI Llc.

2.	L.Tong, A.P.Mouritz., *3D Fibre reinforced polymer composites*. 2002: Elsevier Science.

3.	W.Fung, M.Hardcastle., *Textiles in automotive engineering*. 2001: Woodhead Publishing Limited.

4.	B.Griffiths, *Boeing sets pace for composites usage in large civil aircraft*, in *Composites World*. 2005.

5.	M.K.Bannister, *Development and application of advanced textile composites.* Proceedings of the Institution of Mechanical Engineers, Part L: Journal of Materials Design and Applications, 2004. **218**(3): p. 253-260.

6.	R.Kamiya, B.A.Cheeseman., P.Popper, T.W.Chou, , *Some recent advances in the fabrication and design of three-dimensional textile preforms: a review.* Composites Science and Technology, 2000. **60**(1): p. 33-47.

7.	G.A.Bibo, P.J.Hogg., R.Backhouse, A.Mills, , *Carbon-fibre non-crimp fabric laminates for cost-effective damage-tolerant structures.* Composites Science and Technology, 1998. **58**(1): p. 129-143.

8.	J.Brandt, K.Drechsler., F.J.Arendts, , *Approaches for improving the damage tolerance of composite structures*, in *Developments in the Science and Technology of Composite Materials*. 1990, Springer Netherlands. p. 509-516.

9.	A.P.Mouritz, M.K.Banister., P.J.Falzon, K.H.Leong, , *Review of applications for advanced three-dimensional fibre textile composites.* Composites Part A: Applied Science and Manufacturing, 1999. **30**(12): p. 1445-1461.

10.	B.N.Cox, M.S.Dadkhah., W.L.Morris, J.G.Flintoff,, *Failure mechanisms of 3D woven composites in tension, compression, and bending.* Acta Metallurgica et Materialia, 1994. **42**(12): p. 3967-3984.

11.	T.W.Chou, F.K.Ko., *Three-dimensional fabrics for composites* in *Textile structural composites*. 1989, Elsevier. p. 129-169.

12.   J.Brandt, K.Drechsler., F.J.Arendts, , *Mechanical performance of composites based on various three-dimensional woven-fibre preforms.* Composites Science and Technology, 1996. **56**(3): p. 381-386.

13.   V.A.Guénon, T.W.Chou., J.W.Gillespie, , *Toughness properties of a three-dimensional carbon-epoxy composite.* Journal of Materials Science, 1989. **24**(11): p. 4168-4175.

14.   F.Chen, J.M.Hodgkinson., *Impact behaviour of composites with different fibre architecture.* Proceedings of the Institution of Mechanical Engineers, Part G: Journal of Aerospace Engineering, 2009. **223**(7): p. 1009-1017.

15.   M.H.Mohamed, A.E.Bogdanovigh., L.C.Dikinson, *A new generation of 3D woven fabric preform and composites.* SAMPE Journal, 2001. **37**(3): p. 8-17.

16.   R.Jones, T.E.Tay, J.F.Williams, , *Assessment of the effect of impact damage in composites: Some problems and answers.* Theoretical and Applied Fracture Mechanics, 1988. **9**(2): p. 83-95.

17.   S.Abrate, *Impact on laminated composites: Recent advances.* Applied Mechanics Reviews, 1994. **47**(11): p. 28.

18.   K.Baliski, *Multiaxial three dimensional woven fabrics*, in *Advances in modern woven fabric technology*, S. Vassiliadis, Editor. 2011.

19.   A.P.Mouritz, B.N.Cox., *A mechanistic interpretation of the comparative in-plane mechanical properties of 3D woven, stitched and pinned composites.* Composites Part A: Applied Science and Manufacturing, 2010. **41**(6): p. 709-728.

20.   A.Miravete, *3-D Textile Reinforcements in Composite Materials*. 1999: CRC Press.

21.   S.Mazumdar, *Composites manufacturing: materials, product, and process engineering*. 2001: Taylor & Francis.

22.   Matthews, Z. *Fly rods + reel online http://www.flyrodreel.com/*. April 2011.

23.   S.Adanur, *Textile structural composites ,In :Wellington Sears handbook of industrial textiles*. 1995: Technomic Publishing Company.

24.   T.W.Chou, F.K.Ko., *Textile Structural Composites*. 1989: Elsevier Science & Technology Books.

25.   R.Marks, A.T.C.Robinson., *Principles of weaving*. 1976: Textile Institute.

26.   B.N.Cox, G.Flanagan., *Handbook of analytical methods for textile composites*. 1997, NASA Langley Technical Report Server.

27.   *http://juandejoya.tumblr.com*.

28.   C.K.Mullen, P.J.Roy., *Fabrication and properties description of AVCO 3D carbon-carbon cylindrical composites*, in *SAMPE Symposium*. 1972: Los Angeles.

29.   L.Tong, A.P.M., M.K.Bannister,, *Chapter 2 - Manufacture of 3D fibre preforms*, in *3D Fibre Reinforced Polymer Composites*. 2002, Elsevier Science: Oxford. p. 13-46.

30.   J.Quinn, R.McIlhagger., A.T.McIlhagger,, *A modified system for design and analysis of 3D woven preforms.* Composites Part A: Applied Science and Manufacturing, 2003. **34**(6): p. 503-509.

31.   X.Ding, H.L.Yi. *Parametric representation of 3D woven structures*. in *6th Asian Textile Conference*. 2001. Hong Kong.

32.   Ding Xin, Y.H.Lei., *Representation of 3D woven structures by parametric method.* Journal of Donghua University, 2005. **22**(1).

33.   L.Bersuch, R.Benson., S.Owens,, *Affordable composite structure for next generation fighters*, in *43rd International SAMPE Symposium and exhibition*. 1998. p. 56-65.

34.   H.L.Yi, X.Ding., *Conventional approach on manufacturing 3D woven preforms used for composites.* Journal of Industrial Textiles, July 2004. **34**(1): p. 39-50.

35.   J.A.Suarez, C.Buttitta., *Novel composites for wing and fuselage applications*, in *NASA Contractor Report*. September 1996. p. 90.

36.   M.De Freitas, L.Reis., *Failure mechanisms on composite specimens subjected to compression after impact.* Composite Structures, 1998. **42**(4): p. 365-373.

37. M.O.W.Richardson, M.J.Wisheart., *Review of low-velocity impact properties of composite materials.* Composites Part A: Applied Science and Manufacturing, 1996. **27**(12): p. 1123-1131.

38. G.A.Bibo, P.J.Hogg., *The role of reinforcement architecture on impact damage mechanisms and post-impact compression behaviour.* Journal of Materials Science, 1996. **31**(5): p. 1115-1137.

39. W.J.Cantwell, J.Morton., *The impact resistance of composite materials — a review.* Composites, 1991. **22**(5): p. 347-362.

40. S.P.Joshi, C.T.Sun., *Impact induced fracture in a laminated composite.* Journal of Composite Materials, 1985. **19**(1): p. 51-66.

41. D.Liu, L.E.Malvern., *Matrix cracking in impacted glass/epoxy plates.* Journal of Composite Materials, 1987. **21**(7): p. 594-609.

42. S.Lee, J.Cheon., Y.Im, , *Experimental and numerical study of the impact behavior of SMC plates.* Composite Structures, 1999. **47**(1–4): p. 551-561.

43. Y.P.Siow, V.P.W.Shim., *An experimental study of low velocity impact damage in woven fiber composites.* Journal of Composite Materials, 1998. **32**(12): p. 1178-1202.

44. F.J.Yang, W.J.Catwell., *Impact damage initiation in composite materials.* Composites Science and Technology, 2010. **70**(2): p. 336-342.

45. S.Hong, D.Liu., *On the relationship between impact energy and delamination area.* Experimental Mechanics, 1989. **29**(2): p. 115-120.

46. W.J.Cantwell, J.Morton., *Geometrical effects in the low velocity impact response of CFRP.* Composite Structures, 1989. **12**(1): p. 39-59.

47. W.J.Cantwell, J.Morton., *Impact perforation of carbon fibre reinforced plastic.* Composites Science and Technology, 1990. **38**(2): p. 119-141.

48. E.Demuts, R.S.Whitehead., R.B.Deo, *Assessment of damage tolerance in composites.* Composite Structures, 1985. **4**(1): p. 45-58.

49. W.J.Cantwell, J.Morton., *Comparison of the low and high velocity impact response of cfrp.* Composites, 1989. **20**(6): p. 545-551.

50.   W.J.Cantwell, J.Morton., *Detection of impact damage in CFRP laminates.* Composite Structures, 1985. **3**(3–4): p. 241-257.

51.   J.Morton, E.W.Godwin, *Impact response of tough carbon fibre composites.* Composite Structures, 1989. **13**(1): p. 1-19.

52.   F.Mili, B.Necib., *Impact behavior of cross-ply laminated composite plates under low velocities.* Composite Structures, 2001. **51**(3): p. 237-244.

53.   P.Robinson, G.A.O.Daies., *Impactor mass and specimen geometry effects in low velocity impact of laminated composites.* International Journal of Impact Engineering, 1992. **12**(2): p. 189-207.

54.   V.P.Shim, L.M.Yang., *Characterization of the residual mechanical properties of woven fabric reinforced composites after low-velocity impact.* International Journal of Mechanical Sciences, 2005. **47**(4–5): p. 647-665.

55.   A.P.Christoforou, *Impact dynamics and damage in composite structures.* Composite Structures, 2001. **52**(2): p. 181-188.

56.   Z.Aslan, R.Karakuzu, B.Okutan, , *The response of laminated composite plates under low-velocity impact loading.* Composite Structures, 2003. **59**(1): p. 119-127.

57.   W.J.Cantwell, *The influence of target geometry on the high velocity impact response of CFRP.* Composite Structures, 1988. **10**(3): p. 247-265.

58.   P.H.Thornton, *Energy absorption in composite structures.* Journal of Composite Materials, 1979. **13**(3): p. 247-262.

59.   G.L.Farley, *Energy absorption of composite materials.* Journal of Composite Materials, 1983. **17**(3): p. 267-279.

60.   D.Liu, *Delamination resistance in stitched and unstitched composite plates subjected to impact loading.* Journal of Reinforced Plastics and Composites, 1990. **9**(1): p. 59-69.

61.   L.H.Strait, M.L.Karasek., M.F.Amateau, , *Effects of stacking sequence on the impact resistance of carbon fiber reinforced thermoplastic toughened epoxy laminates.* Journal of Composite Materials, 1992. **26**(12): p. 1725-1740.

62. C.K.Davies, K.H.Williamson, *Flexed plate impact testing of carbon fibre-reinforced polymer composites.* Composites, 1985. **16**(4): p. 279-285.

63. P.O.Sjoblom, J.T.Hartness, T.M.Cordell, *On low-velocity impact testing of composite materials.* Journal of Composite Materials, 1988. **22**(1): p. 30-52.

64. W.J.Cantwell, J.Morton, *Post-impact fatigue performance of carbon fibre laminates with non-woven and mixed-woven layers.* Composites, 1983. **14**(3): p. 301-305.

65. W.J.Cantwell, P.T.Curtis, J.Morton, *Impact and subsequent fatigue damage growth in carbon fibre laminates.* International Journal of Fatigue, 1984. **6**(2): p. 113-118.

66. P.T.Curtis, S.M.Bishop, *An assessment of the potential of woven carbon fibre-reinforced plastics for high performance applications.* Composites, 1984. **15**(4): p. 259-265.

67. N.K.Naik, Y.C.Sekhar, *Damage in laminated composites due to low velocity impact.* Journal of Reinforced Plastics and Composites, 1998. **17**(14): p. 1232-1263.

68. F.K.Ko, D.Hartman, *Impact behaviorof 2-D and 3-D Glass/Epoxy composites.* SAMPE Journal, 1986. **22**(4): p. 26-30.

69. S.Chou, H.-C.Chen, and H.-E.Chen, *Effect of weave structure on mechanical fracture behavior of three-dimensional carbon fiber fabric reinforced epoxy resin composites.* Composites Science and Technology, 1992. **45**(1): p. 23-35.

70. M.N.Ghasemi Nejhad, A.P.-Majidi, *Impact behaviour and damage tolerance of woven carbon fibre-reinforced thermoplastic composites.* Composites, 1990. **21**(2): p. 155-168.

71. J.K.Kim, and M.-L.Sham, *Impact and delamination failure of woven-fabric composites.* Composites Science and Technology, 2000. **60**(5): p. 745-761.

72. G.A.Schoeppner, S.Abrate, *Delamination threshold loads for low velocity impact on composite laminates.* Composites Part A: Applied Science and Manufacturing, 2000. **31**(9): p. 903-915.

73.   G.Belingardi, R.Vadori., *Low velocity impact tests of laminate glass-fiber-epoxy matrix composite material plates.* International Journal of Impact Engineering, 2002. **27**(2): p. 213-229.

74.   G.A.O.Davies, D.Hitchings, G.Zhou, , *Impact damage and residual strengths of woven fabric glass/polyester laminates.* Composites Part A: Applied Science and Manufacturing, 1996. **27**(12): p. 1147-1156.

75.   G.Zhou, *Effect of impact damage on residual compressive strength of glass-fibre reinforced polyester (GFRP) laminates.* Composite Structures, 1996. **35**(2): p. 171-181.

76.   C.Atas, D.Liu, *Impact response of woven composites with small weaving angles.* International Journal of Impact Engineering, 2008. **35**(2): p. 80-97.

77.   C.Atas, O.Sayman, *An overall view on impact response of woven fabric composite plates.* Composite Structures, 2008. **82**(3): p. 336-345.

78.   M.Quaresimin et al., *Energy absorption in composite laminates under impact loading.* Composites Part B: Engineering, 2013. **44**(1): p. 133-140.

79.   R.Park,and J.Jang, *Impact behavior of aramid fiber/glass fiber hybrid composite: evaluation of impact behavior using delamination area.* Journal of Composite Materials, 2000. **34**(13): p. 1117-1135.

80.   M.V.Hosur, M.Abdullah, S.Jeelani, *Studies on the low-velocity impact response of woven hybrid composites.* Composite Structures, 2005. **67**(3): p. 253-262.

81.   A.Enfedaque, J.M.Molina, F.Gálvez, C.González, J.LLorca, , *Effect of glass fiber hybridization on the behavior under impact of woven carbon fiber/epoxy laminates.* Journal of Composite Materials, 2010. **44**(25): p. 3051-3068.

82.   L.Tong, A.P.Mouritz., M.K.Bannister, *Chapter 5 - 3D woven composites*, in *3D Fibre Reinforced Polymer Composites*, A.P.M. L.Tong, M.K.Bannister, , Editor. 2002, Elsevier Science: Oxford. p. 107-136.

83.   J. Brandt, K.Drechsler, M.Mohamed, *Manufacture and performance of carbon/epoxy 3-D woven composites*, in *37th International SAMPE symposium.* 1992.

84.   S.Adanur, Y.P.Tsao, C.W.Tam, *Improving fracture resistance of laminar textile composites by third direction reinforcement.* Composites Engineering, 1995. **5**(9): p. 1149-1158.

85.   J.N.Baucom, M.A.Zikry, *Evolution of failure mechanisms in 2D and 3D woven composite systems under quasi-static perforation.* Journal of Composite Materials, 2003. **37**(18): p. 1651-1674.

86.   J.N.Baucom, M.A.Zikry, *Low-velocity impact damage progression in woven E-glass composite systems.* Composites Part A: Applied Science and Manufacturing, 2005. **36**(5): p. 658-664.

87.   Y.A.Bahei-El-Din, M.A.Zikry, *Impact-induced deformation fields in 2D and 3D woven composites.* Composites Science and Technology, 2003. **63**(7): p. 923-942.

88.   Y.Luo, B.Sun, Y.Qiu, B.Gu, *Transverse impact behavior and energy absorption of three-dimensional orthogonal hybrid woven composites.* Composite Structures, 2007. **81**(2): p. 202-209.

89.   L.Lv, B.Sun, Y.Qiu, B.Gu, *Energy absorptions and failure modes of 3D orthogonal hybrid woven composite struck by flat-ended rod.* Polymer Composites, 2006. **27**(4): p. 410-416.

90.   T.R.Walter, G.Subhash, B.V.Sankar, C.F.Yen, *Damage modes in 3D glass fiber epoxy woven composites under high rate of impact loading.* Composites Part B: Engineering, 2009. **40**(6): p. 584-589.

91.   R.Gerlach, C.R.Siviour, J.Wiegand, N.Petrinic, *In-plane and through-thickness properties, failure modes, damage and delamination in 3D woven carbon fibre composites subjected to impact loading.* Composites Science and Technology, 2012. **72**(3): p. 397-411.

92.   R.S.King, G.Stewart, A.T.Mcilhagger,and J.P.Quinn, *The influence of through-the-thickness binder yarn count on fibre volume fraction ,crimp, and damage tolerance within 3D woven carbon fibre composites.* polymer and Polymer composites, 2009. **17**(5): p. 303-312.

93.   N.V.Padaki et al., *Influence of preform interlacement on the low velocity impact behavior of multilayer textile composites.* Journal of Industrial Textiles, 2010. **40**(2): p. 171-185.

94.   P.Potluri, P.Hogg, M.Arshad, D.Jetavat, P.Jamshidi, *Influence of fibre architecture on impact damage tolerance in 3D woven composites.* Applied Composite Materials, 2012. **19**(5): p. 799-812.

95.   H.T.Wu, G.S.Springer, *Impact induced stresses, strains, and delaminations in composite plates.* Journal of Composite Materials, 1988. **22**(6): p. 533-560.

96.   O.Ishai, A.Shragai., *Effect of impact loading on damage and Residual Compressive Strength of CFRP laminated beams.* Composite Structures, 1990. **14**(4): p. 319-337.

97.   S.A.Hitchen, R.M.Kemp, *The effect of stacking sequence on impact damage in a carbon fibre/epoxy composite.* Composites, 1995. **26**(3): p. 207-214.

98.   W.J.Cantwell, P.T.Curtis., J.Morton, *An assessment of the impact performance of CFRP reinforced with high-strain carbon fibres.* Composites Science and Technology, 1986. **25**(2): p. 133-148.

99.   A.Mehmet, K.Ramazan, A.Yusuf, *Compression-after impact behavior of laminated composite plates subjected to low velocity impact in high temperatures.* Composite Structures, 2009. **89**(1): p. 77-82.

100.   D.Ghelli, G.Minak., *Low velocity impact and compression after impact tests on thin carbon/epoxy laminates.* Composites Part B: Engineering, 2011. **42**(7): p. 2067-2079.

101.   D.A.Wyrick, D.F.Adams, *Residual strength of a carbon/epoxy composite material subjected to repeated impact.* Journal of Composite Materials, 1988. **22**(8): p. 749-765.

102.   De Carvalho, S.T. Pinho, and P. Robinson, *An experimental study of failure initiation and propagation in 2D woven composites under compression.* Composites Science and Technology, 2011. **71**(10): p. 1316-1325.

103.   B.N.Cox, M.S.Dadakhah, R.V.Inman, W.L.Morris, J.Zupon, *Mechanisms of compressive failure in 3D composites.* Acta Metallurgica et Materialia, 1992. **40**(12): p. 3285-3298.

104.   G.L.Farley, *A mechanism responsible for reducing compression strength of through-the-thickness reinforced composite material.* Journal of Composite Materials, 1992. **26**(12): p. 1784-1795.

105. Y.Wang, D.Zhao, *Effect of fabric structures on the mechanical properties of 3-D textile composites.* Journal of Industrial Textiles, 2006. **35**(3): p. 239-256.

106. Y.Mahadik, S.R.Hallett, *Effect of fabric compaction and yarn waviness on 3D woven composite compressive properties.* Composites Part A: Applied Science and Manufacturing, 2011. **42**(11): p. 1592-1600.

107. S.Kari, M.Kumar, A.C.Long and N.A.Warrior, *Effect of yarn cross-sectional shapes and crimp on the mechanical properties of 3D woven composites*. in *ICCM -17*. 2009. Scotland.

108. D.Rudov-Clark, *Experimenta Investigation of the Tensile Properties of Three-Dimensional Woven Composites*, in *School of Aerospace*. RMIT

109. E.R.Kaswell, *Wellington Sears handbook of industrial textiles*. 1968: Textile Book Service.

110. M.Mohamaed, L.Dikinson, Alexander Bogdanovich. *3D Weaving: What, How and Where*. in *44th International SAMPE Symposium*. 1999. Long Beach , CA, USA.

111. ASTM D2584, *Standard test method for ignition loss of cured reinforced resin.* 2011.

112. ASTM D792, *Standard test methods for density and specific gravity (relative density) of plastics by displacement.* 2008.

113. T.R.Guess , E.D.Reedy, *Comparison of interlocked fabric and laminated fabric Kevlar 49/epoxy composites.* Journal of Composite , Technology and research, 1985. **7**(4).

114. M.Bannister, I.Herszberg, A.Nicolaidis, F.Coman, K.H.Leong, *The manufacture of glass/epoxy composites with multilayer woven architectures.* Composites Part A: Applied Science and Manufacturing, 1998. **29**(3): p. 293-300.

115. B.N.Cox, G.Flanagan, M.S.Dadkhah, W.L.Morris, *On the tensile failure of 3D woven composites.* Composites Part A: Applied Science and Manufacturing, 1996. **27**(6): p. 447-458.

116. P.J.Callus, A.P.Mouritz, M.K.Bannister, K.H.Leong, *Tensile properties and failure mechanisms of 3D woven GRP composites.* Composites Part A: Applied Science and Manufacturing, 1999. **30**(11): p. 1277-1287.

117.   J.P.Quinn, A.T. McIlhagger, and R. McIlhagger, *Examination of the failure of 3D woven composites.* Composites Part A: Applied Science and Manufacturing, 2008. **39**(2): p. 273-283.

118.   K.Pochiraju, T.W.Chou, *Three-dimensionally woven and braided composites. II: An experimental characterization.* Polymer Composites, 1999. **20**(6): p. 733-747.

119.   H.Gu, Z.Zhili, *Tensile behavior of 3D woven composites by using different fabric structures.* Materials & Design, 2002. **23**(7): p. 671-674.

120.   L.Tong, A.P. Mouritz, and M.K. Bannister, *Chapter 5 - 3D Woven Composites*, in *3D Fibre Reinforced Polymer Composites*. 2002, Elsevier Science: Oxford. p. 107-136.

121.   L.Lee, A.P.Mouritz, M.K.Bannister, I.Herszberg, *Effect of weaving damage on the tensile properties of three-dimensional woven composites.* Composite Structures, 2002. **57**(1–4): p. 405-413.

122.   B.Lee, K.H.Leong, I.Herszberg, *Effect of weaving on the tensile properties of carbon fibre tows and woven composites.* Journal of Reinforced Plastics and Composites, 2001. **20**(8): p. 652-670.

123.   S.V.Lomov, D.S.Ivanov, T.C.Truong, I.Verpoest, F.Baudry, K.B.Vanden, H.Xie, , *Experimental methodology of study of damage initiation and development in textile composites in uniaxial tensile test.* Composites Science and Technology, 2008. **68**(12): p. 2340-2349.

124.   S.Lomov, D.Ivanov, I.Verpoest, M.Zako, T.Kurashiki, H.Nakai, J.Molimard, A.Vautrin, *Full-field strain measurements for validation of meso-FE analysis of textile composites.* Composites Part A: Applied Science and Manufacturing, 2008. **39**(8): p. 1218-1231.

125.   D.Ivanov, S.Ivanov, S.Lomov, I.Verpoest, *Strain mapping analysis of textile composites.* Optics and Lasers in Engineering, 2009. **47**(3â€"4): p. 360-370.

126.   L.Stepan, A.E.Bogdanovich, D.S.Ivanov, D.Mungalov, K. Mehmet, I.Verpoest, *A comparative study of tensile properties of non-crimp 3D orthogonal weave and multi-layer plain weave E-glass composites. Part 1: Materials, methods and principal results.* Composites Part A: Applied Science and Manufacturing, 2009. **40**(8): p. 1134-1143.

127. D.S.Ivanov, L.Stephan, A.Bogdanovich, K. Mehmet, I.Verpoest, *A comparative study of tensile properties of non-crimp 3D orthogonal weave and multi-layer plain weave E-glass composites. Part 2: Comprehensive experimental results.* Composites Part A: Applied Science and Manufacturing, 2009. **40**(8): p. 1144-1157.

128. K.H.Leong, B.Lee, I.Herszberg, M.K.Bannister, *The effect of binder path on the tensile properties and failure of multilayer woven CFRP composites.* Composites Science and Technology, 2000. **60**(1): p. 149-156.

129. R.D.Hale, *An experimental investigation into strain distribution in 2D and 3D textile composites.* Composites Science and Technology, 2003. **63**(15): p. 2171-2185.

130. P.A.Lagace, *Notch sensitivity of graphite/epoxy fabric laminates.* Composites Science and Technology, 1986. **26**(2): p. 95-117.

131. S.P.Ng, P.C.Tse, K.J.Lau, *Progressive failure analysis of 2/2 twill weave fabric composites with moulded-in circular hole.* Composites Part B: Engineering, 2001. **32**(2): p. 139-152.

132. L.W.Chang, S.S.Yau, T.W.Chou, *Notched strength of woven fabric composites with moulded-in holes.* Composites, 1987. **18**(3): p. 233-241.

133. J.Awerbuch, M.S.Madhukar, *Notched strength of composite laminates: Predictions and Experiments—A Review.* Journal of Reinforced Plastics and Composites, 1985. **4**(1): p. 3-159.

134. N.K.Naik, P.S.Shembekar, M.K.Verma, *On the influence of stacking sequence on notch sensitivity of fabric laminates.* Journal of Composite Materials, 1990. **24**(8): p. 838-852.

135. Y.K.Boey, Y.W.Kwon, *Progressive damage and failure strength of notched woven fabric composites under axial loading with varying strain rates.* Composite Structures, 2013. **96**(0): p. 824-832.

136. H.A.Haery, R.Zahari, W.Kuntjoro, M.T.Yakub, *Tensile strength of notched woven fabric hybrid glass, carbon/epoxy composite laminates.* Journal of Industrial Textiles, 2012.

137. B.G.Green, M.R.Winson, S. R.Hallett, *An experimental investigation into the tensile strength scaling of notched composites.* Composites Part A: Applied Science and Manufacturing, 2007. **38**(3): p. 867-878.

138. P.Chen, Z. Shen, and J.Y. Wang, *Prediction of the strength of notched fiber-dominated composite laminates.* Composites Science and Technology, 2001. **61**(9): p. 1311-1321.

139. G.H.Erçin et al., *Size effects on the tensile and compressive failure of notched composite laminates.* Composite Structures, 2013. **96**(0): p. 736-744.

140. P.S.Shembekar, N.K.Naik, *Notched strength of fabric laminates. II: Effect of stacking sequence.* Composites Science and Technology, 1992. **44**(1): p. 13-20.

141. N.K.Naik, P.S.Shembekar, *Notched strength of fabric laminates I: Prediction.* Composites Science and Technology, 1992. **44**(1): p. 1-12.

142. K.H.Tsai, C.H.Cou, T. H.Wu, *Fatigue behavior of 3D multi-layer angle interlock woven composite plates.* Composites Science and Technology, 2000. **60**(2): p. 241-248.

143. K.Ko, T.W.Chou, *Three-Dimensional fabrics for composites. Composite Materials Series 3,Textile structural composites. 1989: 129-172*

144. ASTM D5766, *Standard test method for open hole tensile strength of ploymer matrix composite laminates*. 2002.

145. P.J.Callus, *The effects of hole-size and enviroment on the mechanical behaviour of a quasi-isotropic AS4/3501-6 laminate in tension, compression and bending*. 2007, Australian Goverment, Deparment of defence.

146. A.E.Bogdanovich, *Advancements in manufacturing and applications of 3-D woven preforms and composites*, in *16th International conference on composite materials*. 2007: Japan.

147. J.C.Prichard, P.J.Hogg, *The role of impact damage in post-impact compression testing.* Composites, 1990. **21**(6): p. 503-511.

148. K.T.Tan, N.Watanabe, Y.Iwahori, *Impact damage resistance, response, and mechanisms of laminated composites reinforced by through-thickness stitching.* International Journal of Damage Mechanics, 2012. **21**(1): p. 51-80.

149. N.Rajiv, L.Charles, *Damage resistant materials for aero-engine applications*, in *40th Structures, Structural Dynamics, and Materials Conference and Exhibit*. 1999, American Institute of Aeronautics and Astronautics.